NASA CR- 152, 255

A Reproduced Copy

OF

Reproduced for NASA

by the

NASA Scientific and Technical Information Facility

CR-152255

10

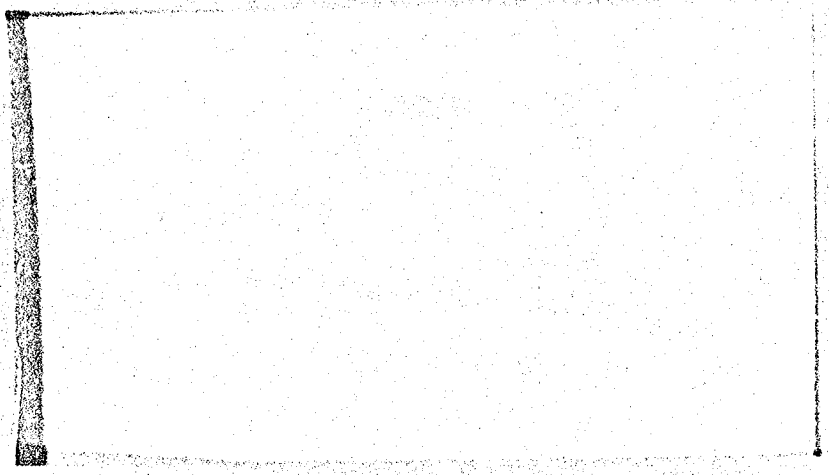

(NASA-CR-152255) PHASE 1 WIND TUNNEL TESTS OF THE J-97 POWERED, EXTERNAL AUGMENTOR V/STOL MODEL (De Havilland Aircraft Co. Ltd.) 101 p HC A06/MF A01 CSCL 01A

N80-28303

Unclas
G3/02 26015

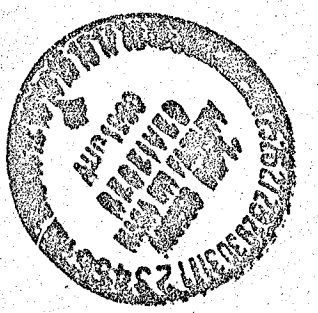

THE DE HAVILLAND AIRCRAFT OF CANADA LIMITED

NASA CR 152255

DHC-DND 79-4

PHASE 1 WIND TUNNEL TESTS OF THE J-97 POWERED, EXTERNAL AUGMENTOR V/STOL MODEL

JULY, 1980

THE DE HAVILLAND AIRCRAFT OF CANADA LIMITED

DOWNSVIEW, ONTARIO, CANADA M3K IY5

DHC-DND 79-4

PHASE 1 WIND TUNNEL TESTS OF THE J-97 POWERED, EXTERNAL AUGMENTOR V/STOL MODEL

SEPTEMBER 1979

THE DE HAVILLAND AIRCRAFT OF CANADA LIMITED

DHC-DND 79-4

PHASE 1 WIND TUNNEL TESTS OF THE J-97 POWERED, EXTERNAL AUGMENTOR V/STOL MODEL

NASA Contract No. NASW 2797
DSS Contract Serial No. 2SR77-00008

Prepared by.... D.B. Garland .....
D.B. Garland

Approved by.... D.C. Whittley .....
D.C. Whittley

SEPTEMBER 1979

1. SUMMARY

Test results, with some analysis, are presented for a large-scale, external augmentor V/STOL model in the 40- by 80-Foot Wind Tunnel at the Ames Research Center, NASA. The model was powered by a GE J97 engine and featured longitudinal ejectors alongside and external to the fuselage together with an augmentor-flap on the low aspect ratio, double-delta wing.

A static thrust augmentation ratio of 1.60 was measured for the fuselage augmentor at a nozzle pressure ratio of 3.0 and a nozzle exhaust gas temperature of 700°C.

At forward speed the model showed a strong positive lift interference, due to the augmentor flap, and a marked absence of negative lift interference due to the fuselage augmentor jet system. The nose-up moment of the fuselage augmentor inlet flow was approximately cancelled by a 60° deflection of the augmentor-flap. An assessment of the thrust and drag components, especially the momentum drag of the fuselage augmentor inlet flow, was made which will allow the prediction of transition performance of a wide range of aircraft designs based on the present conceptual model.

A brief series of lateral tests showed strong but well-ordered effects of power.

2. TABLE OF CONTENTS

3. INTRODUCTION

A large-scale model of a De Havilland V/STOL concept was tested in the NASA, Ames 40- by 80- Foot Wind Tunnel in a preliminary investigation of general aerodynamic characteristics. The model, shown diagrammatically in Figure 1, applies ejector-type thrust augmentor principles with minimal adverse interference between the lifting jets and the wing during transition. In addition, the bulk of the fuselage augmentor diffuser is formed external to the normal aircraft contour by doors which fold out from the fuselage sides; this avoids using aircraft volume and minimizes frontal area at high speed. Approximately 80% of the installed engine thrust issues from the chordwise fuselage augmentors and 20% from the wing augmentor flap. The flap is deflected to 90° for take-off and is used for thrust vectoring to achieve transition from hover to wing-borne flight. Transfer of thrust from the fuselage augmentors to a standard propulsion nozzle provides the other main means for transition. Further discussion regarding the concept may be found in Reference 1.

The research work described here was proposed by De Havilland Aircraft of Canada (DHC) and conducted in cooperation with NASA, Ames Research Center who jointly funded the work with the Canadian Department of National Defence.

The basic aerodynamic data of the large-scale wind tunnel investigation are presented in Reference 2.

4. DESCRIPTION OF MODEL AND TESTS

4.1 Geometry

The model is powered by a single J-97 engine as shown in the three-view drawing in Figure 1. Photographs of the model mounted in the Ames 40- by 80- Foot Wind Tunnel are given in Figure 2. Sections through the fuselage and wing augmentor are given in Figures 3 and 4. The wing has a NACA 16-008 section modified in the region of the fuselage augmentor inlet to give constant inlet geometry. The tail surfaces are based on the NACA 0012 section. Table 1 lists the major geometric parameters of the airframe and Table 2 provides details of fuselage augmentor geometry.

Provision was made to partially close the fuselage augmentor doors, from a diffuser area ratio of 1.6 to 1.0, to reduce inlet flow momentum drag during transition. Again, to effect transition, individual fuselage augmentor nozzles were blanked off with small plates inserted in the supply ducting and an appropriate compensating nozzle was provided at the rear end of the fuselage duct for each case, (Figure 5). Tests were conducted with one quarter and one half of the fuselage nozzles blanked-off. A small 'trim' nozzle, also at the rear of the fuselage duct, was required to achieve the optimum running line for the J-97 engine. Therefore, when thrust was transferred to the rear nozzle, it was sized to include the trim area.

The complete sugmentor flap rotated as a unit with the air supply duct and nozzle assembly. Flap deflection

angles of 0^{o}, 30^{o}, 60^{o} and 90^{o} were used during tests. Table 3 gives details of wing geometry.

Standard support struts were used to mount the model in the centre of the 40' x 80' working section, well clear of ground effect statically.

Instrumentation for these preliminary tests included duct static pressures (Figure 5) , some nozzle exit total pressures and the standard engine instruments. Also, for one half of the test runs, a large multi-tube rake (shown in Figure 6) was fitted to the left hand fuselage augmentor. It was used to determine exit velocity distributions and mass flow and thrust by integration.

4.2 Thrust Loading

The J-97 engine is rated at an exhaust gas pressure ratio EPR of 3.5, approximately, on a standard day. The fuselage and wing augmentors, their nozzles and ducting, were designed on the basis of this pressure ratio. The wing area of the model was chosen to give an augmented thrust loading of 60 lb/ft^2 with the J-97 operating at its rated, standard day, maximum thrust. As a result, the model is quite representative of a high speed aircraft with respect to the volume occupied by the ejector lift system, the geometry of the augmentor, the inlet flow momentum drag during transition and the aircraft frontal area when the augmentor doors are closed.

At the elevated temperatures often encountered in the 40 x 80 foot wind tunnel ($120^{o}F$, for example) the practical

maximum EPR was about 2.5. The corresponding reference pressure ratio, measured at a static tap in the fuselage ducting and used to set engine thrust, was RPR = 2.30 (Figure 7). The majority of tests was made at this value of RPR, producing an augmented thrust loading of 35 lb/ft^2.

Since it can be shown and demonstrated that the performance of the model is a function of its jet coefficient and is essentially independent of the operating EPR in the tunnel, then the effective 'full-scale' forward speed dynamic head is greater than the tunnel 'q' by the ratio

Full-scale thrust loading/Model thrust loading.

Hence, comparing an aircraft design operating at a thrust loading of, say, 70 lb/ft^2, with the model under test at RPR = 2.30, the equivalent full-scale q would be twice the tunnel q.

4.3 Data Reduction

For all force and moment data, the thrust of the small trim nozzle area in the rear fuselage was subtracted from the balance values. The inlet momentum drag of the J97 engine was not subtracted.

Wind tunnel boundary corrections were based on the aerodynamic or effective lift coefficient computed as follows:

$$C_{L_{EFF}} = C_L - C_{J_{AUG_F}} \cos\alpha_u - C_{J_{AUG_W}} \sin(\alpha_u + \delta_F) - C_{J_{NR}} \sin\alpha_u = C_{L_{aero}}$$

The following boundary corrections were then made:

$$\alpha = \alpha_u + 0.3538\, C_{L_{aero}}$$

$$C_D = C_{D_u} + .0062\, C_{L_{aero}}^2$$

$$C_M = C_{M_u} + .0200\, C_{L_{aero}} \quad \text{(tail on only)}$$

All coefficients are based on gross wing area, S, which includes the projection of the complete wing across the fuselage. For reference purposes only, the net wing area, the projection of the outer wing panels to the fuselage centre-line, is 68.8% of the gross wing area (see Table 1).

Pitching moments are given with respect to the moment reference centre at $0.472\bar{c}$.

5. STATIC TEST RESULTS

Tests results for various configurations at zero forward speed were obtained in the 40 x 80 foot wind tunnel with the large overhead doors open. Previously, the model had been tested statically at the de Havilland plant where some important component tests had taken place. In the following, reference is made to static tests at NASA, Ames and at DHC.

The static performance of the fuselage and wing augmentors is defined by the gross thrust augmentation ratio in each case. This is the ratio of measured augmented thrust to measured nozzle thrust at the same nozzle pressure ratio and for the same nozzle flow rate. Internal nozzle losses are thereby separated from strictly augmentor performance.

Since thrust of the bare nozzles cannot be measured directly on the complete model, some prior static tests were performed at DHC. The first was a full-scale, cold flow test of a reduced length, single, fuselage augmentor. Twelve augmentor nozzles were supplied with air at a stagnation temperature near ambient. The test apparatus permitted direct measurement of isolated nozzle thrust and mass flow and a measurement of the influence of the augmentor inlet and fuselage side wall on thrust force and mass flow (that is, with the outer wall of the ejector diffuser missing). These structural components were not removable from the wind tunnel model, but it was shown by the cold flow tests that they caused an augmentation of thrust of approximately 10%, as shown in

Figure 8. Also shown in Figure 8 is the performance of the model complete with shrouds when powered with a cold air supply: at the design pressure ratio of 3.0, the gross thrust augmentation ratio ϕ_G was 1.66.

The second series of prior tests was of the wind tunnel model on an outdoor balance (Reference 3), the model having a ground clearance of 7.5 feet, sufficient to raise it out of ground effect, on the basis of data from previous work with a similar model. These tests were made to demonstrate the structural integrity of the hot ducting and to determine the thrust augmentation with hot gas primary flow. Force measurements were made with and without fuselage augmentor doors, before the wing augmentor was installed. (The appropriate J-97 running line conditions were maintained by variation of the area of the rear fuselage trimming nozzle.) With both fuselage augmentors running, the base area between them experienced a slight negative pressure. A single measurement at the mid-base location indicated a base thrust of about -0.5% of the augmentor thrust. Using the cold flow test data (Figure 8) to determine the bare nozzle thrust efficiency (and making due allowance for the slight increase of nozzle mass flow at sub-critical pressure ratios with the augmentor doors on) the bare nozzle thrust and the gross thrust augmentation ratio were determined for the hot gas tests. The comparison between the hot and cold test data obtained in Canada is shown in Figure 9. The reduction in ϕ_G from 1.66 to 1.60 is believed

to be due to primary gas temperature but there were several minor geometrical differences between the two augmentors.

In the wind tunnel, for static tests, the model was mounted on the standard struts, giving a ground clearance of about 18 feet, the overhead tunnel doors were wide open and run times were kept to a minimum to prevent build-up of tunnel q. There was nevertheless some evidence of re-circulation of warm augmentor efflux - at a fixed throttle position the exhaust gas pressure would sometimes decrease with time, particularly at high power settings. The lift force would also fall a little below the value measured on the outdoor test stand. A comparison of static test data from DHC and ARC is shown in Figures 10 and 11 with augmentor doors off and on, respectively. The wing augmentor flap was set at $\delta_F = 0^\circ$ for these tests. Agreement between the DHC and ARC tests is very good up to a reference pressure ratio of about 2.0 when re-circulation effects apparently intrude to a small degree.

The wing augmentor thrust was obtained from the difference in lift force between $\delta_F = 0^\circ$ and $\delta_F = 90^\circ$. Wing augmentor nozzle thrust was not measured separately and had to be estimated from a knowledge of geometric nozzle area, wing duct stagnation pressure and previous experience of likely discharge coefficient and thrust efficiency. The gross thrust augmentation ratio was then calculated to be 1.55, at test NPR's, comparing with a cold flow result of 1.60 for a similar augmentor tested at DHC.

A summary plot of the static lift of the complete model at all flap angles tested is given in Figure 12 and is compared with the computed values used in analysis of test data for the purpose of isolating the aerodynamic characteristics of the model. Note that analysis of the forward speed test data (to obtain 'effective' force coefficients) does not depend upon on assessment of thrust augmentation ratio but only on the measured forces on the model at zero wind speed.

6. LONGITUDINAL PERFORMANCE

6.1 Power-off, Clean Configuration

The fuselage augmentor shrouds and end-plates were removed and augmentor inlets and exits were closed and faired (for example, see Figure 3). Force data in coefficient form are shown in Figures 13(a) and (b) for $\delta_F = 0^\circ$ and 30° respectively. The C_L versus α curve shows some evidence of vortex lift with flap angle set at zero. The outer-wing leading edge stalled above $\alpha = 10^\circ$ with $\delta_F = 30^\circ$ giving rise to a nose-up pitching moment.

6.2 Power-on Characteristics: Basic Configuration

Longitudinal performance tests consisted of polars at a fixed thrust setting at various values of dynamic pressure (q) ranging from 3 psf to 40 psf. Flap angles of 0°, 30°, 60° and 90° were tested. The basic configuration was as follows:

All fuselage nozzles operative.
Diffuser area ratio equal to 1.6.
Nozzle pressure ratio equal to 2.52.
Horizontal tail removed.

Longitudinal characteristics are shown in standard coefficient form for each flap angle in Figures 14a to 14d. (Note that the data in Figures 14b and 14d are presented with the augmentor exit rake installed, rake-off data not being available. The rake had some effect on lift and drag, as described in Section 9.2.) The same data can be displayed in an alternative form if the forces for all flap angles are normalized by the static augmented thrust of the fuselage

augmentor plus wing augmentor for the $\delta_F = 90^\circ$ case; the sum being the hover thrust, T_H, (Figures 15a to 15d). This form of presentation is of particular value for analysis of transition performance. Pitching moments are normalized by $T_H\bar{c}$ so that $M/_{T_H\bar{c}}$ is the out of balance arm as a fraction of the m.a.c. when $T_H = W$. The moment reference centre is at $0.472\bar{c}$, which corresponds to the predicted static balance point with the wing augmentor flap deflected to 90°.

From the data presented in coefficient form it can be seen that stalling angle of the wing increases as flap angle is reduced but that the outer wing panel continues to suffer from premature stall as was the case power-off. The large components of jet lift tend to mask the aerodynamic performance when plotted in this form but the data become more meaningful in the normalized form (Figure 15). It can be seen that the augmentor flap provides a very powerful means of increasing aerodynamic lift at zero α as speed increases: therefore flap angle could be reduced very early in the transition to provide forward thrust. For flap 30° the curves for all values of q collapse and pass approximately through the point $L/_{T_H} \approx 1$, $D/_{T_H} \approx 0$ so that insufficient thrust is available to achieve horizontal acceleration in this configuration for the case with $T_{H/_W} = 1.0$. For $\delta_F = 60^\circ$ a positive acceleration is indicated ($D/_{T_H}$ negative) although at rather large negative angles of attack.

Some margin of hover thrust over weight is necessary for operational purposes so that $T_{H/_W}$ might be 1.1 (say).

Thus in transition, with L = W, $L/T_H = W/T_H \approx 0.91$ and a positive acceleration ($= -D/W = -1.10\ (D/T_H)$) would be achieved more easily. Figure 16 shows D/T_H vs q for $L/T_H = 1$ and 0.91 for the basic configuration.

6.3 Augmentor Configurations for Transition

In the transitional flight regime it becomes necessary to transfer thrust from the fuselage augmentor to the conventional propulsion nozzle (and vice versa) and to retract (or deploy) the augmentor shrouds. This sequence would be performed in such a way as to minimize the time for an accelerating transition or to give maximum control over the descent gradient for a decelerating transition.

Consider first the accelerating transition which will require a combination of the following as forward speed increases:

- rotation of augmentor flap for thrust vectoring
- use of small nose-down attitude for thrust vectoring
- transfer of thrust from fuselage augmentor to propulsion nozzle, possibly with after-burning
- build-up of wing lift to replace jet lift
- closure of fuselage augmentor shrouds to throttle augmentor and reduce momentum drag, (i.e. change to diffuser area ratio).

With this in mind tests were conducted to investigate the effect of change in diffuser area ratio of the fuselage augmentor and of thrust transfer.

6.3.1 Effect of Reduced Diffuser Area Ratio

The model was designed to accept a reduction from DAR = 1.6 to 1.0. Static tests performed in the wind tunnel showed a corresponding reduction in ϕ_G from 1.61 to 1.47, at RPR = 2.3. Laboratory tests with a single similar augmentor had indicated a greater reduction was likely, to about 1.37 at DAR = 1.0. The reduction in secondary mass flow on the large scale model was also quite small, about 8% according to augmentor exit rake integrations.

The measured longitudinal force data are shown in Figure 17 for δ_F = 30° and 60° where the normalizing parameter T_H remains as for the basic configuration. Comparisons in Figure 18 show the effects at forward speed are approximately compatible with a lift loss due to static augmentor thrust reduction and a drag reduction due to the combination of momentum drag decrease and reduced drag component of augmentor thrust at positive angle of attack. However, the ratio of lift loss to drag reduction was poorer than that obtained by simply reducing angle of attack so the net effect of this degree of augmentor throttling was not beneficial to transition. This is indicated by cross-plots of D/T_H at constant L/T_H in Figure 19.

It is possible that further reduction in DAR might have given a favourable result. This was not available during the first test series and is to be explored in further tests.

6.3.2 Effect of Thrust Transfer

Thrust transfer from fuselage augmentor nozzles to the rear fuselage propulsion nozzle was accomplished by inserting small blanking plates between the attachment flanges of alternate fuselage augmentor nozzles. An equivalent area of propulsion nozzle was provided by increasing the diameter of the orifice plate used for this purpose. Blanking-off was done in two stages, first, approximately 1/4 of the fuselage nozzles were blanked-off (7 out of 27 nozzles per side, even numbered nozzles, counting from the front) and then approximately 1/2 of the nozzles (13 out of 27), extending the alternate nozzle sequence along the whole augmentor). The diffuser area ratio remained at 1.0 for these tests and the measured static thrust augmentation ratio dropped slightly, from 1.47 to 1.43 and 1.40 for 1/4 and 1/2 thrust transfers, respectively.

Recorded test data are shown in Figures 20 and 21 and various comparative plots in Figure 22 for the $\delta_F = 60^\circ$ configuration. A summary plot of D/T_H VS L/T_H at $\alpha = 0^\circ$, Figure 23, shows evidence of a benefit at the higher speeds tested. Similar plots for $\delta_F = 30^\circ$, Figures 24 and 25, show a definite benefit above q = 20 psf, although still not sufficient to provide acceleration for $L/T_H = 1.0$ with DAR = 1.0. The data suggest that DAR = 1.6 would have performed better, but tests were carried

out with DAR = 1.6 only with a complete set of nozzles. The reduction in augmentor exit flow due to blanking-off 1/2 of the nozzles was only about 12% according to exit rake data (Figure 26) and the corresponding reduction in momentum drag was quite small therefore.

6.3.3 Steep Gradient Approach

For transition from wing-borne flight to a vertical landing it is desirable to achieve a steep gradient approach, say $\gamma = -10^{\circ}$ to -15°. In aerodynamic terms this means D/T_H needs to be in the range 0.15 to 0.25 approximately. Inspection of the force data for the standard configuration shows that this is conveniently achieved with small flap deflection and modest angle of attack.

6.4 Effect of Jet Flow on Aerodynamic Characteristics

Wind tunnel force data do not provide separate measurements of jet and aerodynamic force components. Therefore there are two parameters of interest which remain unknown:

(i) the aerodynamic characteristics as a function of jet strength

and (ii) the variation of jet thrust with speed.

However, it has been found useful in other similar cases to define the thrust in an arbitrary fashion and then find the effective aerodynamics force by difference directly from the measured forces. In this case, the jet forces

and moments acting on the model are assumed equal to static values for the configuration under consideration (with resolution of forces according to model attitude). Thus these effective forces reflect the sum of true aerodynamic force plus changes in jet thrust and similarly for moments.

The analysis is complicated further by the fact that the jet is deployed in two distinct ways, that is, partly through the augmentor flap and partly through the fuselage augmentor so that two forms of interference are present. It is possible to conduct tests on the model with only the augmentor flap operative but such tests were not performed in this series. However, tests with $\delta_F = 0^\circ$ were performed for a range of power settings and these help to define the interference due to the fuselage jet.

6.4.1 Lift

The definition of effective lift coefficient is given by:-

$$C_{L_{effective}} = C_L - C_{J_{AUG_F}} \cos \alpha_u - C_{J_{AUG_W}} \sin (\alpha_u + \delta_F) - C_{J_{N_R}} \sin \alpha_u$$

where $C_{J_{AUG_F}}$ and $C_{J_{AUG_W}}$ are based on the static augmented thrust of the respective augmentors.

When looking for the effect of forward speed (i.e. C_J) on lift, for example, one might expect to find the following:

(i) a substantial increase in lift due to the augmentor flap

(ii) possibly a serious negative lift due to interference between the fuselage lifting jet and the wing

(iii) some increase in lift due to turning of the secondary flow of the fuselage augmentor

(iv) some loss in thrust of the fuselage augmentor on account of inlet loss.

Figure 27(a) shows $C_{L_{eff}}$ vs α over a range of C_J for zero flap deflection so as to indicate the interaction between the fuselage jet and the wing. It can be seen that the net interference is quite small. Since effects (iii) and (iv) above are not thought to be large and are of opposite sign it is concluded that (ii) is relatively small. This finding is of some interest because wing/jet interference effects are known to be quite large for many V/STOL configurations (Reference 4).

Figures 27(b) and (c) show $C_{L_{eff}}$ vs α with C_J as parameter for $\delta_F = 30^\circ$ and 60°. It can be seen that, as expected, the augmentor flap provides a powerful means of generating lift at zero α. Since the net lift interference due to the fuselage jet has been shown to be small, the effect on lift of flap deflection may be reasonably attributed solely to the flap. Thus the jet flap effect can be illustrated in terms of $C_{L_{eff}}$ vs C_J and flap angle as shown in Figure 28.

Variations in fuselage augmentor configurations (i.e. reducing DAR or blanking-off nozzles) had only small effects on lift interference as shown in Figure 29.

6.4.2 Drag

The corresponding equation for effective drag coefficient is:-

$$C_{D_{eff}} = C_D - C_{J_{AUG_F}} \sin\alpha + C_{J_{AUG_W}} \cos(\alpha + \delta_F) + C_{J_{N_R}} \cos\alpha$$

Note that this equation assumes zero thrust recovery of the deflected wing augmentor flap thrust.

$C_{D_{eff}}$ is shown versus $(C_{L_{eff}})^2$ for each q tested in Figures 30(a), (b) and (c) for $\delta_F = 0^\circ$, 30° and 60°, respectively. The components of $C_{D_{eff}}$ will include

(1) profile drag

(2) drag due to lift

(3) J-97 inlet flow momentum drag

(4) fuselage augmentor inlet flow momentum drag

(5) augmentor exit rake drag, if installed

(6) thrust lapse of the wing augmentor

(7) thrust recovery of the wing augmentor thrust, when deflected

(8) interference effects due to the fuselage augmentor efflux.

A comparison of the $C_{D_{eff}}$ data at each flap angle (Figure 31) shows that δ_F is not a major influence. However, by inspection it can be seen that lift dependent drag and momentum drag of the fuselage augmentor represent the two major components of $C_{D_{eff}}$. Some of the obviously

smaller components (contained in the list above) can be estimated fairly closely, thereby permitting the momentum drag component to be determined. Figure 32 shows the variation of drag force components versus forward speed (at zero C_L) so as to isolate the momentum drag contribution (assuming no interference drag).

The inlet mass flow derived from the fuselage momentum drag component is compared with exit rake results in Figures 33 and 34. (Note that the rake data are corrected for turbulence effects as described in Section 9.3 and that primary nozzle flow is subtracted to get inlet flow rate.) Agreement between the drag and rake data is quite reasonable, indicating that any interference effects on drag are probably small.

6.4.3 Pitching Moment

The effective pitching moment coefficient, on the same basis as for lift and drag, is:-

$$C_{m_{eff}} = C_m - C_{J_{AUG_F}} \cdot \frac{x_F}{\bar{c}} - C_{J_{AUG_W}} \cdot \frac{x_W}{\bar{c}} \sin \delta_F - C_{J_{N_R}} \cdot \frac{x_N}{\bar{c}}$$

Again, for the case of $\delta_F = 0^\circ$, $\alpha = 0^\circ$ the anticipated components would be

(i) the moment due to the fuselage augmentor inlet flow

(ii) an interference moment due to the fuselage augmentor efflux, including effect of change of exit thrust with forward speed

(iii) the power-off C_{m_o}

If (ii) is assumed to be negligible, then (i) can be calculated. Figure 35 shows $C_{m_{eff}}$ versus C_{D_m}, the fuselage augmentor inlet momentum drag coefficient, based on data from the exit rake.

For cases where δ_F and α are not zero, there will be additional components of $C_{m_{eff}}$, i.e.

(iv) moment due to δ_F at constant α and $C_{J_{AUG_W}}$

(v) moment due to α at constant δ_F and $C_{J_{AUG_W}}$

(vi) moment due to J-97 inlet flow

These components are illustrated in Figures 36 and 37. The moment due to J-97 inlet flow is calculated assuming zero upwash due to lift at the engine inlet face (see Figure 37(a)).

The effect of blanking-off some of the fuselage augmentor nozzles is shown on total moment in Figures 38 and 39. The differences are almost equal to the static moments, implying only small changes in secondary inlet flow.

7. LONGITUDINAL STABILITY AND CONTROL

The primary function of the tail with a delta wing is to allow use of flap angle to increase lift, as in high speed manoeuvring or steep gradient approach. At the low speeds of V/STOL transition, the tail contribution to pitching moment is not large and it is assumed that complementary reaction control methods would be used, including fuselage augmentor nozzles.

With a volume coefficient of 0.126, the present horizontal tail produced the power-off moment shown in Figure 40 for tail angles of 5° and 15° at a flap angle of 30°. The derived lift curve slope was .044 per degree (assuming $q_T/q = 1.0$) and the downwash is shown in Figure 41. In the range $-10 \leq \alpha \leq 16^\circ$, $\partial\epsilon/\partial\alpha$ was about 0.55. The change in stability due to the tail was from $\partial C_M/\partial C_L = .045$, tail off, to -.050, tail on.

Power-on, with $\delta_F = 60^\circ$, the effect of adding the tail at $i_T = 15^\circ$ is shown in Figure 42. The pitching moment data show some suspicious variations which may not be of aerodynamic origin but the apparent trend indicates a downwash as shown in Figure 43. The tail provides a stabilizing moment but not of sufficient magnitude to make $\partial C_M/\partial C_L$ negative with the present reference centre.

8. LATERAL/DIRECTIONAL STABILITY

Figure 44 shows the effect of sideslip on the directional derivatives. Power-off, the model had neutral weather-cock stability due to the unrepresentatively long nose housing the J-97 powerplant. The engine inlet flow is de-stabilizing and, together with a similar effect of the fuselage augmentor inlet flow, contributes a large portion of the directional instability.

The side force is very linear and is strongly affected by power, partly due to inlet momentum drag components.

The rolling moment shows a rather large asymmetry but the scatter and accuracy of the data is partly to blame. There is a strong positive dihedral effect due to application of power.

The effect of flap angle on directional derivatives is very small (Figure 45).

9. AUGMENTOR EXIT RAKE

9.1 Description

The fuselage augmentor exit rake comprised fourteen individual rakes spanning the exit width, thirteen carrying seventeen total head tubes and one static tube, the last rake carrying seventeen static tubes. The latter was mounted at the mid-point along the augmentor; the pitot rakes were spaced alternately under and between augmentor nozzles in the exit plane of the diffuser. Six thermocouples were also mounted on the rake structure to measure efflux temperature. Figure 6 shows the layout of the rake. The 238 pressures were recorded via Scanivalves by the data acquisition system. About one half of the test runs were done with the rake installed.

9.2 Effect on Force Data

Measurements were made of the effect of the rake on balance data. None could be discerned statically but at forward speed addition of the rake caused a small decrease in lift and a small increase in drag (see Figure 46). There was no effect on pitching moment.

The lift and drag effects should be taken into account when making fine comparisons between data with and without rake.

9.3 Rake Thrust and Mass Flow

A direct indication of rake thrust integration accuracy is obtained by comparing computed rake thrust with static balance lift force, with $\delta_F = 0^\circ$. Figure 47 shows

the rake over-estimated thrust by about 13½%. This is not a surprising result for internally chamfered pitot tubes in a turbulent flow, (see Reference 5). The corresponding discrepancy in integrated mass flow would be approximately one half of the thrust error, i.e. 7%.

The chordwise distribution of exit thrust is shown for the static case in Figure 48. The fall-off in thrust level near the front end-plate was discovered after the test period and is believed to be due to excessive clearance between the adjacent nozzle and the end-plates, caused by a smaller thrust expansion of the nozzle ducting than anticipated. The effect of forward speed is similarly shown in Figure 49, at $\alpha = 0^{\circ}$. Further light is shed on these effects by examination of the exit isovels, (contours of constant velocity) in Figure 50. The forward low velocity region becomes an outboard low velocity region extending aft from the front end-plate for several feet as speed is increased. At present, the origin of this effect is not known. The integrated thrust values (Figure 51) show a complex but small variation with forward speed and with angle of attack (Figure 52). The isovels (Figure 53) show an aggravation of the outboard disturbance with angle of attack.

With DAR reduced from 1.6 to 1.0 the exit thrust was reduced, as expected, the longitudinal distribution was much smoother (Figure 54) and there was no separated region at the front end-plate. However, a low velocity region was observed at forward speed in the front outboard location, perhaps again signifying an inlet flow separation (Figure 55).

10. CONCLUSIONS

(i) A static thrust augmentation ratio of 1.60 was measured for the fuselage augmentor at a nozzle pressure ratio of 3.0 and a nozzle exhaust gas temperature of 700°C.

(ii) With the wing augmentor flap deflected, the model showed a strong, positive lift interference at forward speed.

(iii) The nose-up moment at forward speed due to the fuselage augmentor inlet flow was approximately cancelled by a 60° deflection of the wing augmentor flap.

(iv) A positive longitudinal acceleration capability was not achieved at the high speed end of the transition speed range. In retrospect, the half-nozzles configuration (50% thrust transferred to rear nozzle) should have been tested at DAR = 1.6 to yield some improvement. It should also be noted that a deflection of the fuselage augmentor nozzles by, say, 15° would provide a significant improvement in acceleration at all transition speeds.

(v) Augmentor throttling, with a full set of nozzles, from DAR = 1.60 to 1.0, did not produce a significant change in acceleration capability; transfer of up to 50% of fuselage augmentor nozzle thrust to the rear propulsion nozzle showed some benefit at higher speeds.

10. CONCLUSIONS (Cont'd.)

(vi) An augmentor exit rake showed relatively small changes in efflux thrust and mass flow with forward speed. Some degradation occurred at higher speeds (test $q > 20$ psf) aggravated by high angle of attack.

(vii) A horizontal tail provided a static margin increment of about $0.1\bar{c}$, power-off and a somewhat smaller increment power-on.

(viii) The lateral directional derivatives are strongly affected by power, destablizing in yaw but stable in side force and roll.

11. REFERENCES

1. Whittley, D.C. — Some Experimental Research on a New Aircraft Configuration Incorporating Ejector-Type Thrust Augmentation for VTOL. ICAS Paper No. 70-56, Rome, September 1970.

2. Aoyagi, K. Aiken, T.N. — Wind Tunnel Investigation of a Large-Scale VTOL Aircraft Model with Wing Root and Wing Thrust Augmentors. NASA TM 78589, September 1979.

3. Garland, D.B. — Static Tests of the J-97 Powered External Augmentor V/STOL Wind Tunnel Model. DHC Report No.DHC-DND 77-4, February 1978.

4. Hickey, D.H. Kirk, J.V. — Studies of Forces Induced on V/STOL Aircraft by Propulsion Flows. "Prediction Methods for Jet V/STOL Propulsion Aerodynamics", Volume 1, 1975. Naval Air Systems Command, Research and Technology Group.

5. Becker, H.A. Brown, A.P.G. — Response of Pitot Probes in Turbulent Streams. J. Fluid Mech. (1974) Volume 62, Part 1, p.p. 84-114.

6. Quinn, B. — Ejector Performance at High Temperatures and Pressures. Journal of Aircraft, December 1976.

12. SYMBOLS

A	=	Aspect ratio
ARC	=	Ames Research Center, NASA
$\bar{c}$	=	Mean aerodynamic chord (m.a.c.)
C_D	=	balance drag coefficient
C_{D_m}	=	fuselage augmentor inlet momentum drag coefficient
$C_{J_{AUG}}$	=	T_H/qS
$C_{J_{AUG_F}}$	=	X_{AUG_F}/qS
$C_{J_{AUG_W}}$	=	X_{AUG_W}/qS
$C_{J_{N_F}}$	=	X_{N_F}/qS
$C_{J_{N_R}}$	=	X_{N_R}/qS
$C_{J_{N_W}}$	=	X_{N_W}/qS
C_L	=	lift coefficient
C_l	=	rolling moment coefficient
C_m	=	pitching moment coefficient
C_{m_o}	=	C_m at $\alpha = 0^o$, $\delta_F = 0^o$, power off
C_n	=	yawing moment coefficient
C_y	=	side force coefficient
D	=	balance drag force
D_m	=	fuselage augmentor inlet flow momentum drag
DAR	=	diffuser area ratio of fuselage augmentor
DHC	=	The De Havilland Aircraft of Canada, Ltd.
EGT	=	exhaust gas temperature

12. SYMBOLS (Cont'd.)

EPR	=	exhaust gas pressure ratio = P_N/p_a
ETR	=	exhaust gas temperature ratio, EGT/Ta
i_T	=	horizontal tail incidence
L	=	lift force
$\dot{m}_F$	=	fuselage augmentor inlet flow rate
NPR	=	fuselage augmentor nozzle pressure ratio, $= P_{T_N}/p_a$
p_a	=	ambient pressure
P_{F_1}	=	J-97 exhaust duct reference static pressure
P_N	=	exhaust gas stagnation pressure at rear nozzle
P_{T_N}	=	total pressure at fuselage augmentor nozzles
q	=	wind tunnel dynamic head
q_t	=	dynamic head at tail location
RPR	=	J-97 exhaust reference pressure ratio, $= P_{F_1}/p_a$
S	=	gross wing area
T_a	=	ambient temperature
T_H	=	$\left(X_{AUG_F} + X_{AUG_W}\right)_{q = 0}$, the hovering thrust at DAR = 1.6
V_i	=	fuselage augmentor throat velocity of secondary air
V_∞	=	tunnel velocity
W	=	aircraft weight
X_{AUG_F}	=	$X_{N_F} \cdot \phi_{G_F}$, augmented static thrust of the fuselage augmentor
X_{AUG_W}	=	$X_{N_W} \cdot \phi_{G_W}$, augmented static thrust of the wing augmentor

12. SYMBOLS (Cont'd.)

X_{N_F}	=	nozzle thrust of fuselage augmentor
X_{N_R}	=	rear fuselage propulsive nozzle thrust
X_{N_W}	=	nozzle thrust of the wing augmentor
x_F	=	moment arm of fuselage augmentor thrust (1.292 ft.)
x_N	=	moment arm of rear fuselage nozzle thrust (0.333 ft.)
x_W	=	moment arm of wing augmentor thrust (4.667 ft.)
α	=	angle of attack, corrected for tunnel wall constraint
α_u	=	uncorrected angle of attack
β	=	sideslip angle
γ	=	glide path angle
δ	=	p_a/Sea Level standard atmospheric pressure
δ_F	=	wing augmentor deflection angle (flap angle)
ϵ	=	downwash angle
η_N	=	nozzle thrust efficiency
θ	=	T_a/Sea Level standard temperature
ϕ_{G_F}	=	gross thrust augmentation ratio of fuselage augmentor $\left(= X_{AUG_F} / X_{N_F}\right)$ at q = 0
ϕ_{G_W}	=	gross thrust augmentation ratio of wing augmentor $\left(= X_{AUG_W} / X_{N_W}\right)$ at q = 0

TABLE 1 GEOMETRY OF J-97 POWERED, EXTERNAL AUGMENTOR V/STOL MODEL

Wing	
Area, gross	141 ft^2
Area, net	97 ft^2
Span	15.25 ft.
Aspect ratio	1.65
t/c	6%
m.a.c.	12.68 ft.
Chord on fuselage ℄	16.92 ft.
Fuselage	
Overall length	approx. 28 ft.
Fin	
Area	22.4 ft^2
Span (above fuselage top)	4.33 ft.
Aspect ratio	0.84
Tailplane	
Area	20.4 ft^2
Span	7.67 ft.
Aspect ratio	2.88
Tail volume coefficient	0.126

Moment reference centre (wing leading edge joint, on wing chord datum)
Distance ahead of rear strut location $\bar{x}$ = 44.0"
(also equal to 47.2% of m.a.c.)

TABLE 2 GEOMETRY OF FUSELAGE AUGMENTOR

Augmentor	
Chordwise length	= 98 in.
Throat width (L_T)	= 10.5 in.
Exit width (L_E)	= 16.8, 10.5 in.
Diffuser area ratio (L_E/L_T)	= 1.60, 1.00
Length (min) (L)	= 34 in.
Mean nozzle width ($\bar{t}$)	= 0.457 in.
Augmentor length ratio ($L/\bar{t}$)	= 74
Nozzles	
Total geometric exit area (per side)	= 45.7 $in.^2$
Number of nozzles (per side)	= 27
Area (per nozzle)	= 1.693 $in.^2$
Aspect ratio (AR)	= 60
Span (b_N)	= 10.12 in.
Thickness at exit (t_N)	= 0.167 in.
Pitch (p)	= 3.68 in.
Pitch ratio ($p/\bar{t}$)	= 8.0

Note: Clearance between end nozzles and augmentor end-walls is 1/4p when hot.

TABLE 3 GEOMETRY OF WING AUGMENTOR

Span (per wing)			= 69.5 in.
Total nozzle area (per wing)			= 11.5 in.^{2}
Bay spans	24.25	22.75	22.5 in.
Nozzle area/bay	4.88	3.73	2.88 in.^{2}
$\bar{t}$	0.201	0.164	0.128 in.
Number of nozzles (N)	15	17	22
Area per nozzle (A_N)	0.325	0.219	0.131 in.^{2}
Pitch (p)	1.60	1.32	1.01 in.
Nozzle span (b)	3.61	2.96	2.29 in.
Nozzle thickness (t)	,090	.074	.057 in.
Nozzle aspect ratio (AR)	40	40	40
Throat (mid span) (L_T)	4.17	3.40	2.65 in.
Exit (mid span) (L_E)	6.67	5.44	4.24 in.
Diffuser area ratio L_E/L_T	1.60	1.60	1.60 in.
Nozzle inlet area/exit area	5.0	5.0	5.0
Augmentor length (mid span) (L)	17.3	14.7	12.1 in.
$L/\bar{t}$	86	90	95

RUN HISTORY

Sheet 1

RUN NO.	MODEL			J97 RPR	TUNNEL			RAKE	REMARKS
	δ_F	i_T	DAR		q	α	β		
1	0	OFF	—	~	0	0	0	OFF	Aug. doors off; 2.8" dia. trim nozzle.
2			—	~					
3			1.6	~					Aug. doors on.
4	90	OFF	1.6	~	0	0	0	OFF	Static thrust of wing augmentor.
5				~	1.3		180		
6				0	0	~	0		Weight tare.
7				~		0			Wing/duct fairings installed.
8				2.5	5	~			
9				2.4	10	~			
10				2.35	3	~			Bad balance data.
11				~	0	0			Trim nozzle increased to 4.8" dia.
12				2.4	3	~			Repeat of Run 10.
13				~	5	0			
14				~	10				
15				2.3			~		
16					5		~		
17	30	OFF	1.6	0	0	~	~	OFF	Weight tares.

RUN HISTORY

Sheet 2

RUN NO.	MODEL			J97 RPR	TUNNEL			RAKE	REMARKS
	δ_F	i_T	DAR		q	α	β		
18	30	OFF	1.6	~	0	0	0	OFF	Static thrust.
19				2.3	5	~			
20					10	~			
21					15	~			
22	30	OFF	1.6	~	0	0	0	ON	Static thrust: exit rake installed.
23				2.3	5	~			
24					10	~			
25					15	~			
26					25	~			
27				~	10	0			
28				~	25				
29				1.5	10		~		
30							~		Continuation of Run 29.
31				2.3			~		
32	60	OFF	1.6	~	0	0	0	ON	Static thrust.
33				2.3	5	~			
34					10	~			

RUN HISTORY

Sheet 3

RUN NO.	MODEL			J97 RPR	TUNNEL			RAKE	REMARKS
	δ_F	i_T	DAR		q	α	β		
35	60	OFF	1.6	2.3	15	~	0	ON	
36				~	10	0			
37				1.5			~		
38				2.3			~		
39	60	+ 15°	1.6	1.0	0	~	0	ON	Weight tare with tail on.
40				2.3	5	~			
41					10	~			
42					15	~			
43	0	+ 15	1.6	2.3	10	~	0	ON	
44					15	~			
45					25	~			
46	0	OFF	1.6	~	0	0	0	ON	Static thrust c.f. Run 3.
47				2.3	5	~			
48					10	~			
49				~		0			
50				1.5			~		
51				-	-	-	-		Not run.

RUN HISTORY

Sheet 4

RUN NO.	MODEL			J97 RPR	TUNNEL			RAKE	REMARKS
	δ_F	i_T	DAR		q	α	β		
52	0	OFF	1.6	2.3	10	0	~	ON	
53					15	~	0		
54				~	25	0			
55				2.3		~			
56	30	OFF	1.0	-	-	-	-	OFF	No transducer data: rake removed.
57				2.3	10	~	0		
58				-	-	-	-		No balance data.
59				~	0	0	0		Repeat of Run 56.
60				2.3	25	~			
61					25	~			
62				~		0			
63				~	10				
64				1.5			~		
65				2.3	40	~	0		
66	60	OFF	1.0	~	0	0	0	ON	Static thrust: rake installed.
67				2.3	5	~			
68					10	~			

RUN HISTORY

Sheet 5

RUN NO.	MODEL			J97 RPR	TUNNEL			RAKE	REMARKS
	δ_F	i_T	DAR		q	α	β		
69	60	OFF	1.0	2.3	15	~	0	ON	
70					25	~			
71	60	OFF	1.0	~	0	0	0	ON	¼ nozzles blanked; 7.5" dia. trim nozzle installed
72				2.3	15	~			
73					25	~			
74					40	~			
75	60	OFF	1.0	~	0	0	0	ON	½ nozzle blanked; 8.75" dia.trim nozzle installed
76				2.3	10	~			
77					15	~			
78					25	~			
79	30	OFF	1.0	~	10	0	0	ON	
80				~	25				
81				2.3		~			
82	30	OFF	1.0	~	0	0	0	OFF	Exit rake removed.
83				2.3	40	~			
84					25	~			
85					15	~			

RUN HISTORY

Sheet 6

RUN NO.	MODEL			J97 RPR	TUNNEL			RAKE	REMARKS
	δ_F	i_T	DAR		q	α	β		
86	30	OFF	1.0	1.0	25	~	0	OFF	Aug. open; power-off run.
87	0	OFF	1.0	~	0	0	0	OFF	
88				~	5				
89				2.3	15	~			
90					25	~			
91					40	~			
92	0	OFF	1.0	~	5	0	0	OFF	Rear nozzle fairing off.
93	0	OFF	-	-	0	~	0	OFF	Clean' conf.; weight tare fuselage aug. closed.
94					15	~			Power off runs.
95	30	OFF	-	-	15	~	0	OFF	Power off runs; fuselage aug. closed.
96						0	~		
97			-	-	15	12	~		
98	30	5°	-	-	0	~	0		Weight tare.
99					15	~			
100		15°				~			

DHC EXTERNAL AUGMENTOR V/STOL CONCEPT

G.A. OF J-97 POWERED MODEL

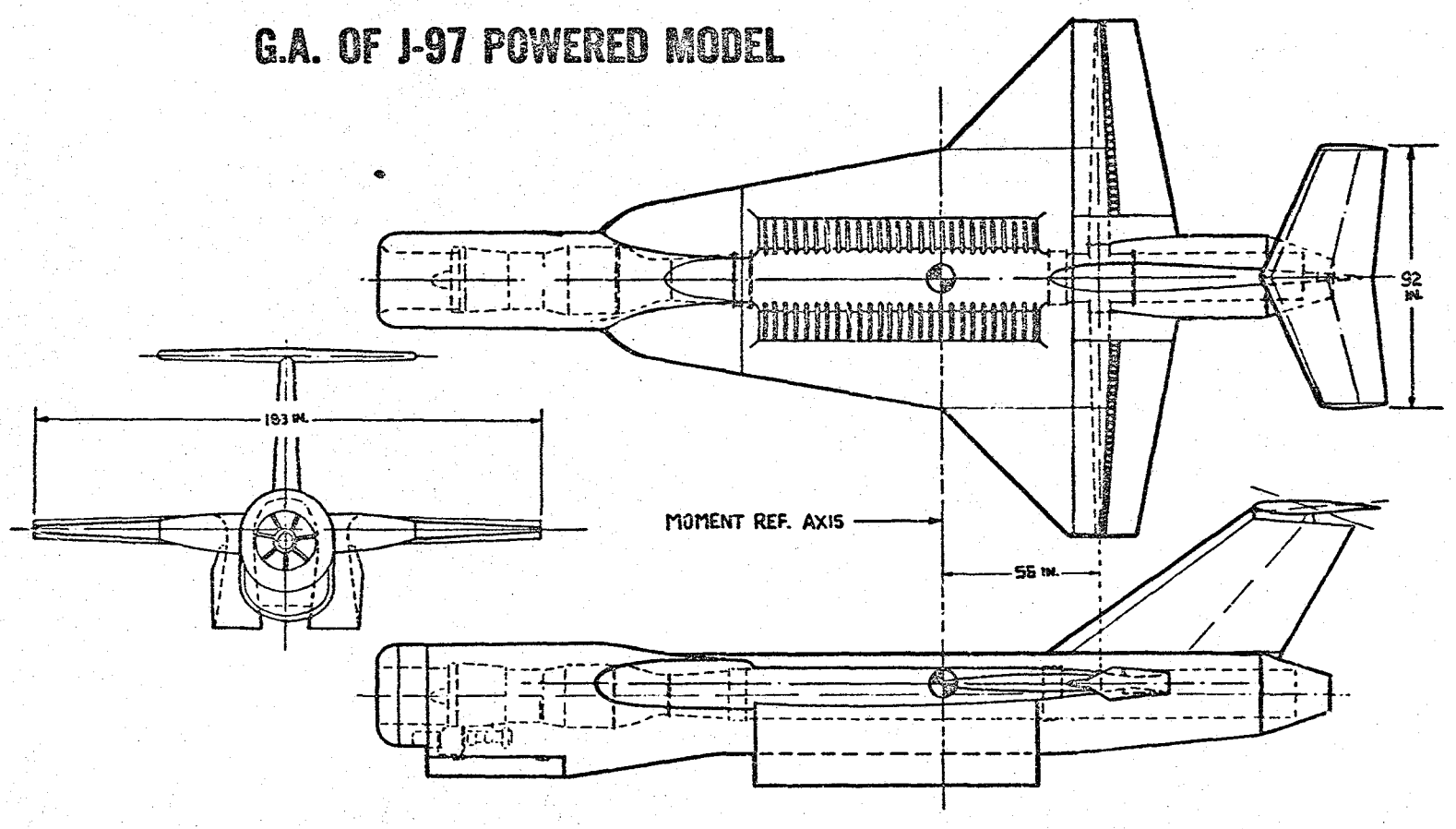

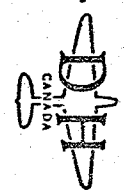

Fig. 1

Fig. 2 intentionally left blank.

Fig. 3

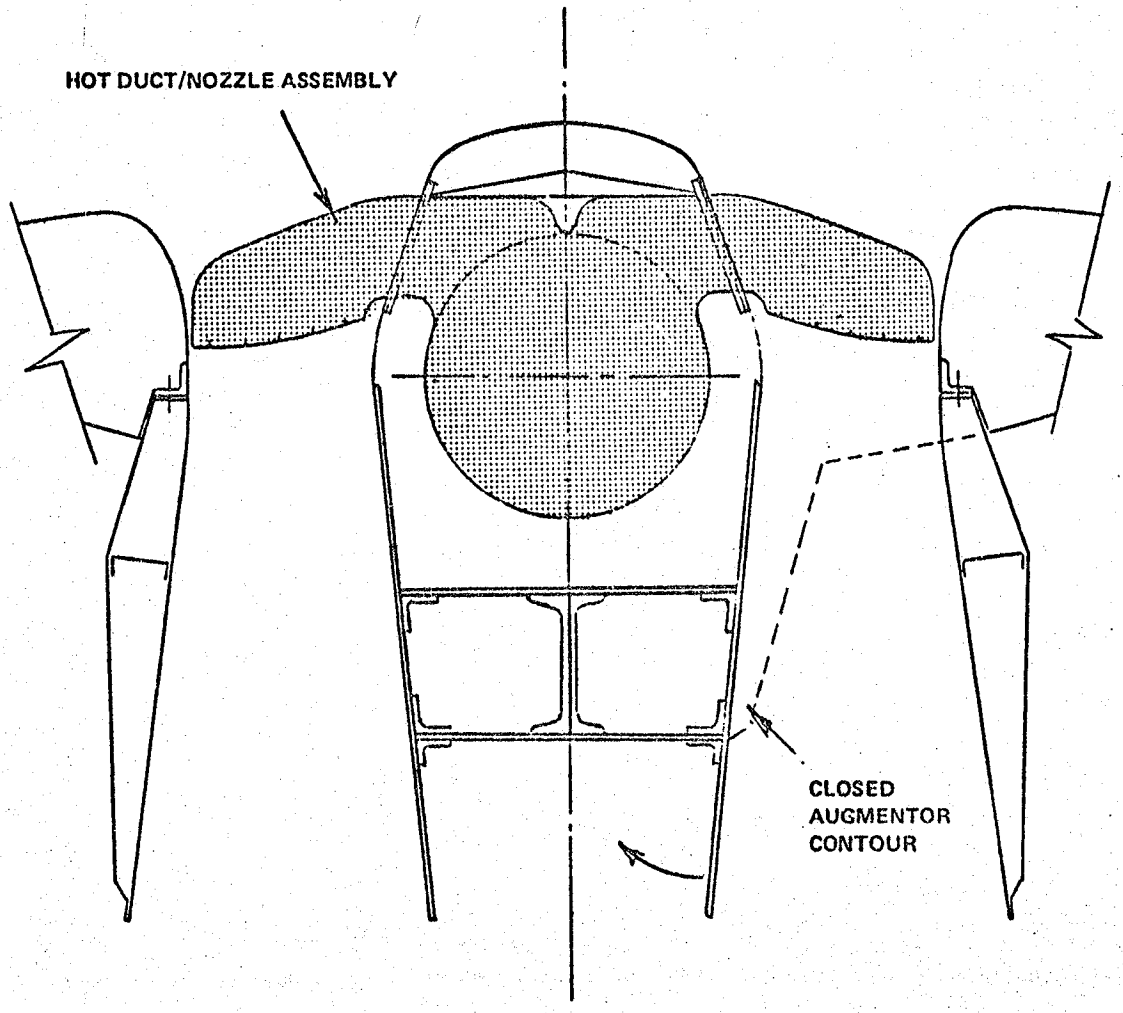

PRECEDING PAGE MISSING (FIG. 3)

SECTION THROUGH FUSELAGE AUGMENTOR

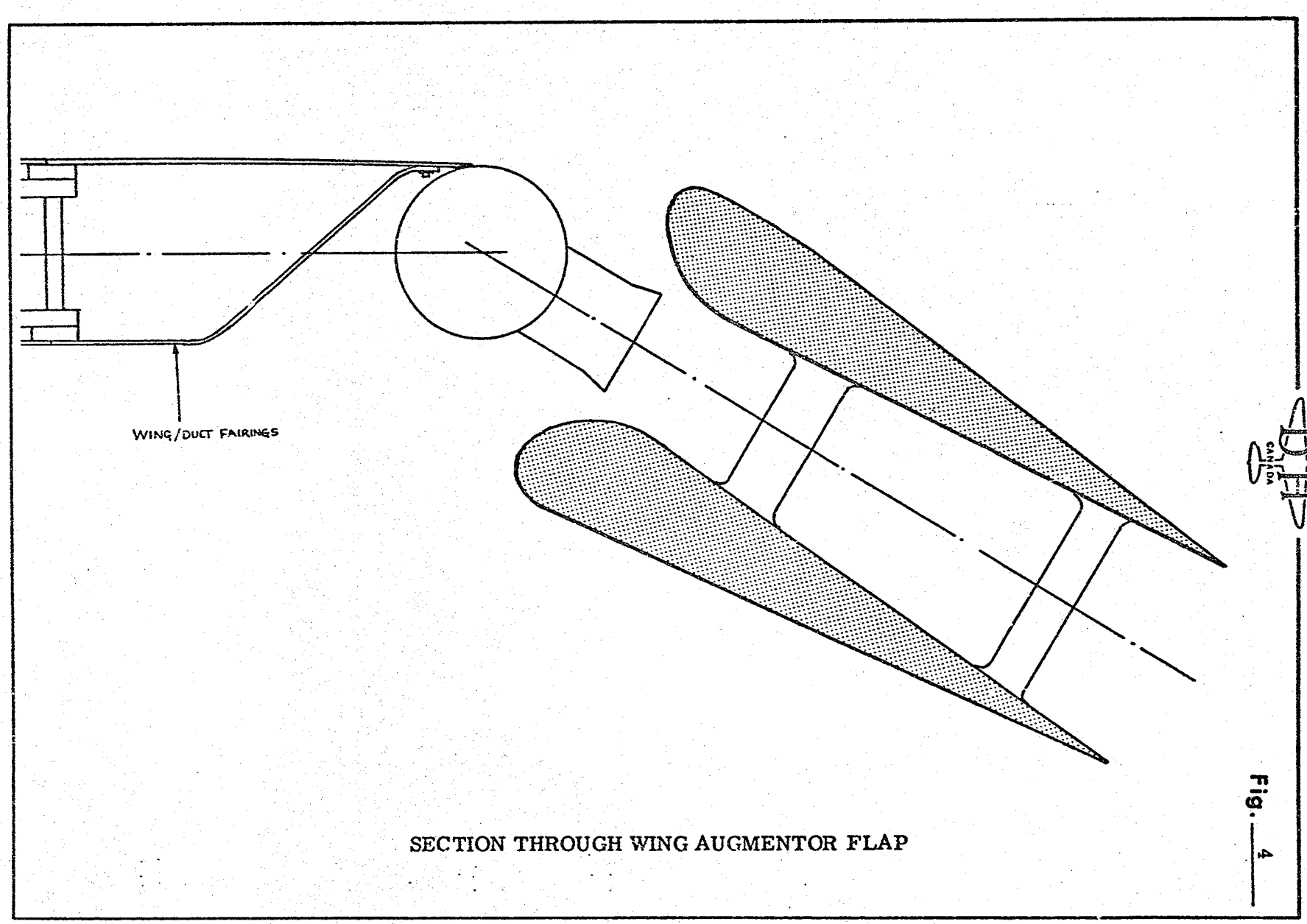

SECTION THROUGH WING AUGMENTOR FLAP

Fig. 4

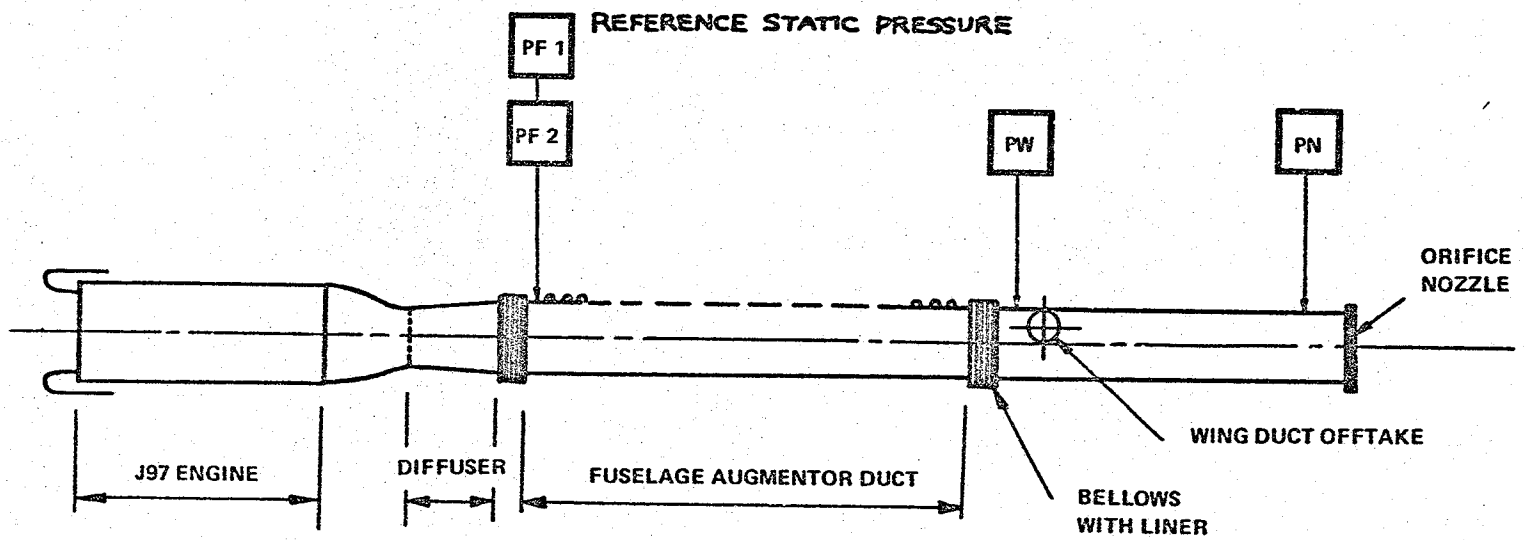

LOCATION OF DUCT STATIC PRESSURE TAPS

Fig. 5

CANADA

Fig. 6

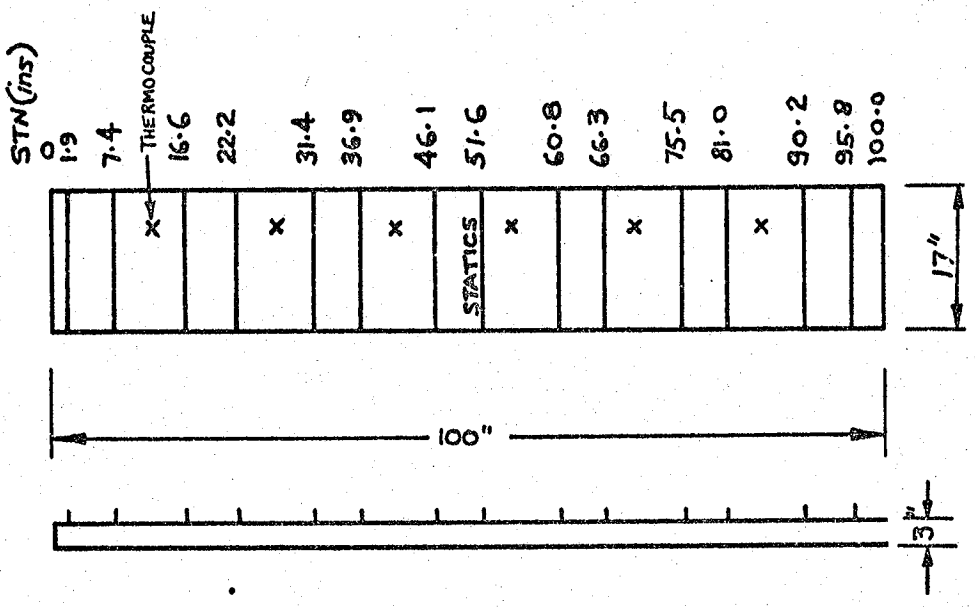

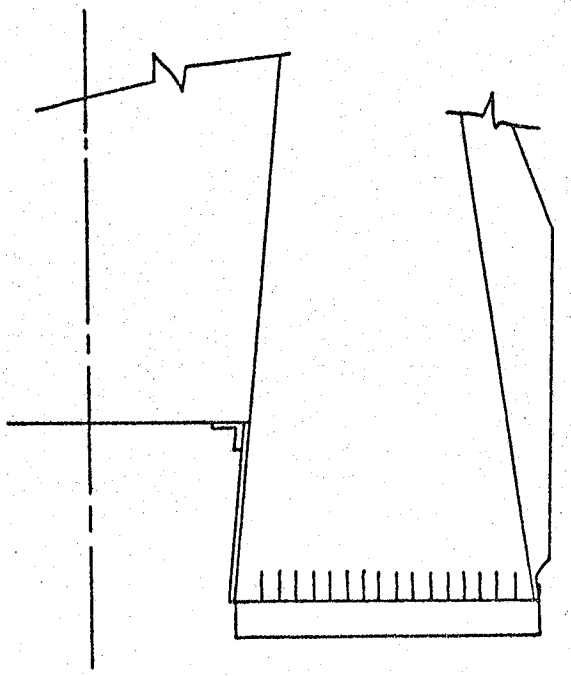

FUSELAGE AUGMENTOR EXIT RAKE

Fig. 7

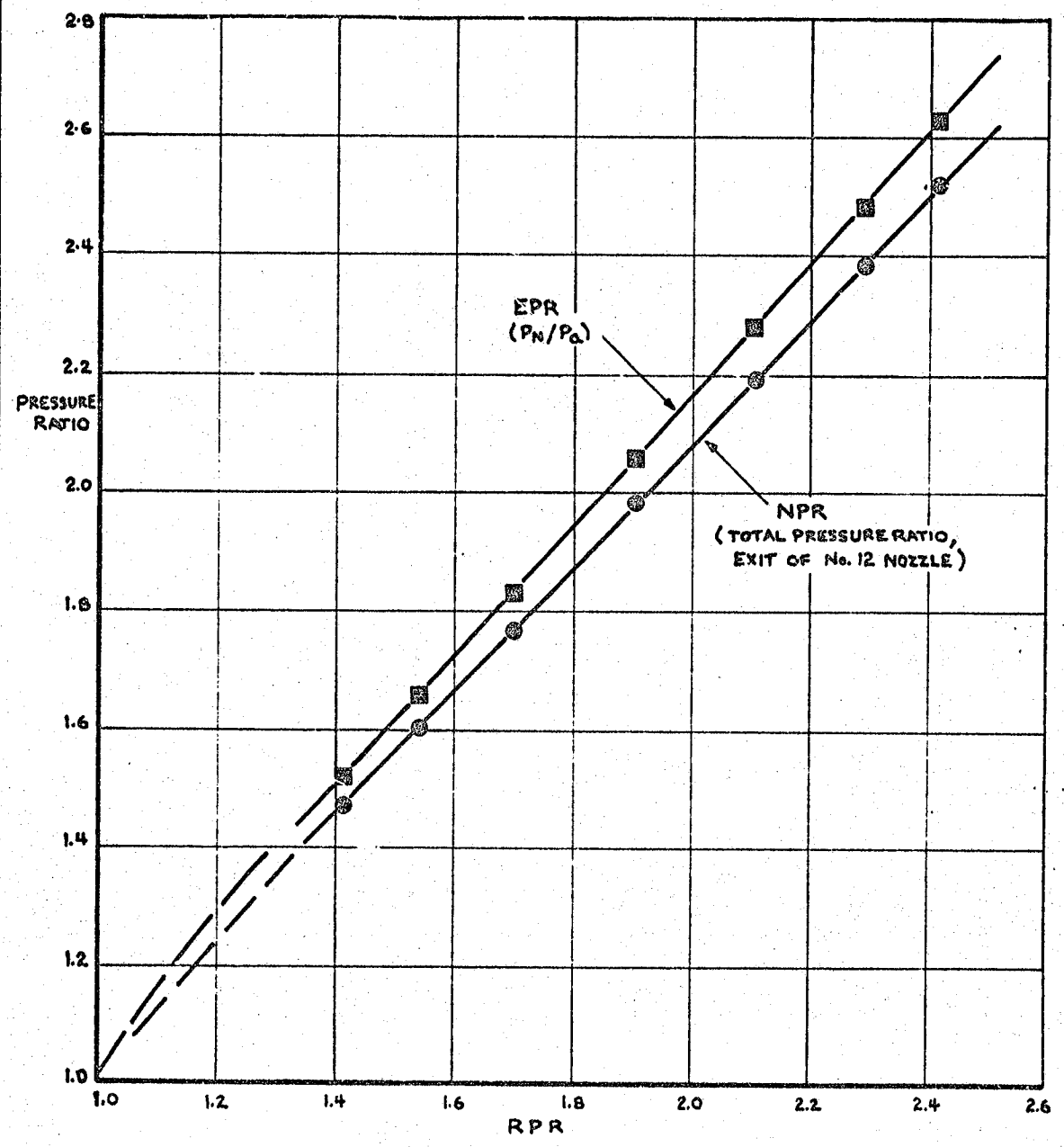

DUCT PRESSURES (RUN 7)

Fig. 8

COLD FLOW VTOL MODEL TEST RESULTS

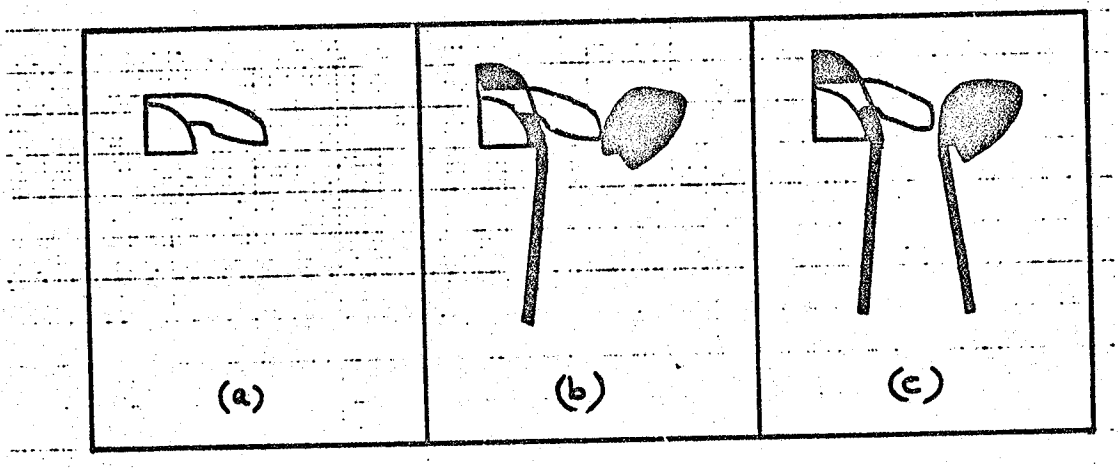

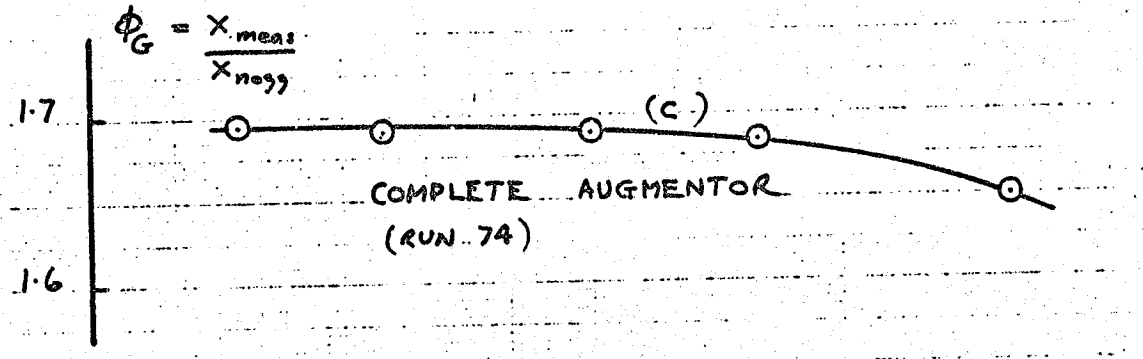

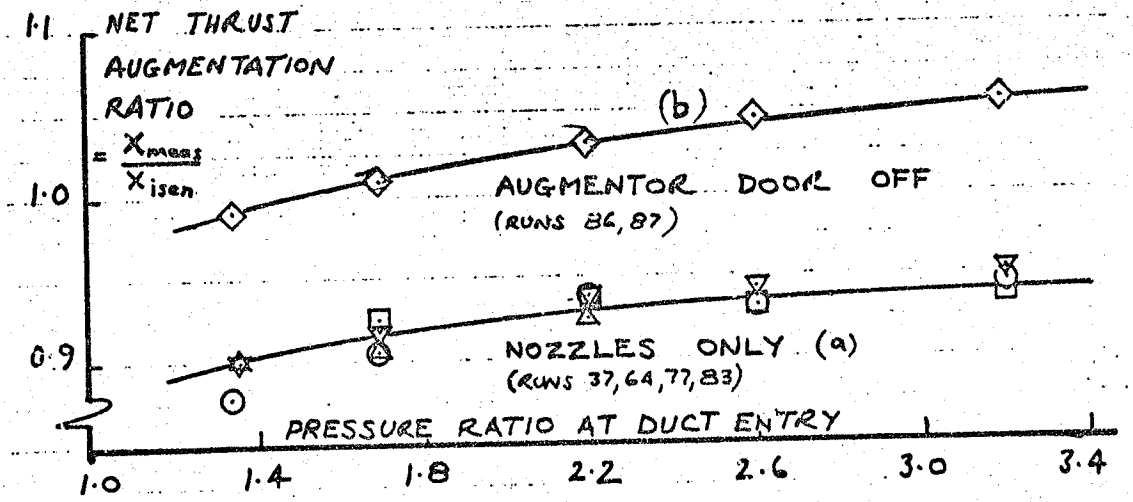

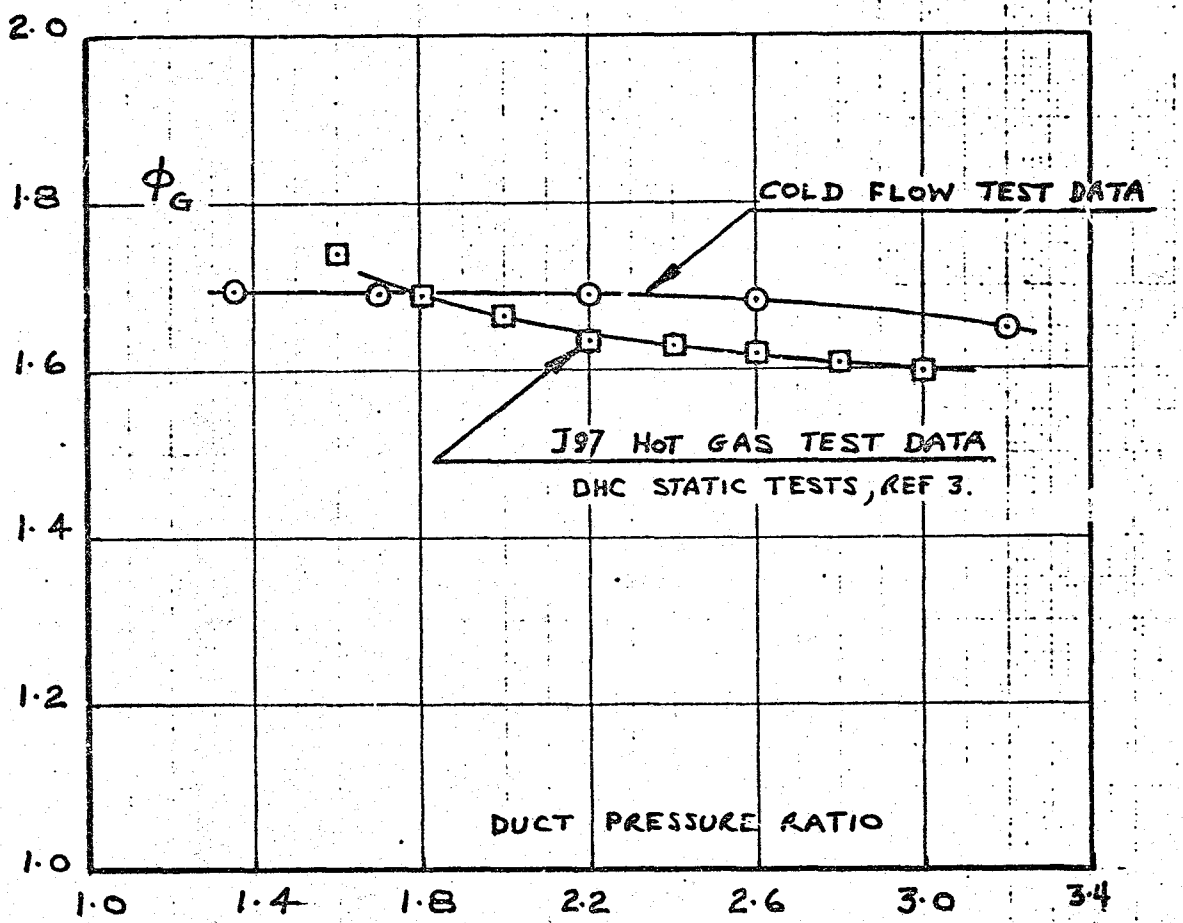

GROSS THRUST AUGMENTATION RATIO OF FUSELAGE AUGMENTOR

Fig. 9

Fig. 10

COMPARISON BETWEEN STATIC THRUST DATA,

AUGMENTOR DOORS OFF

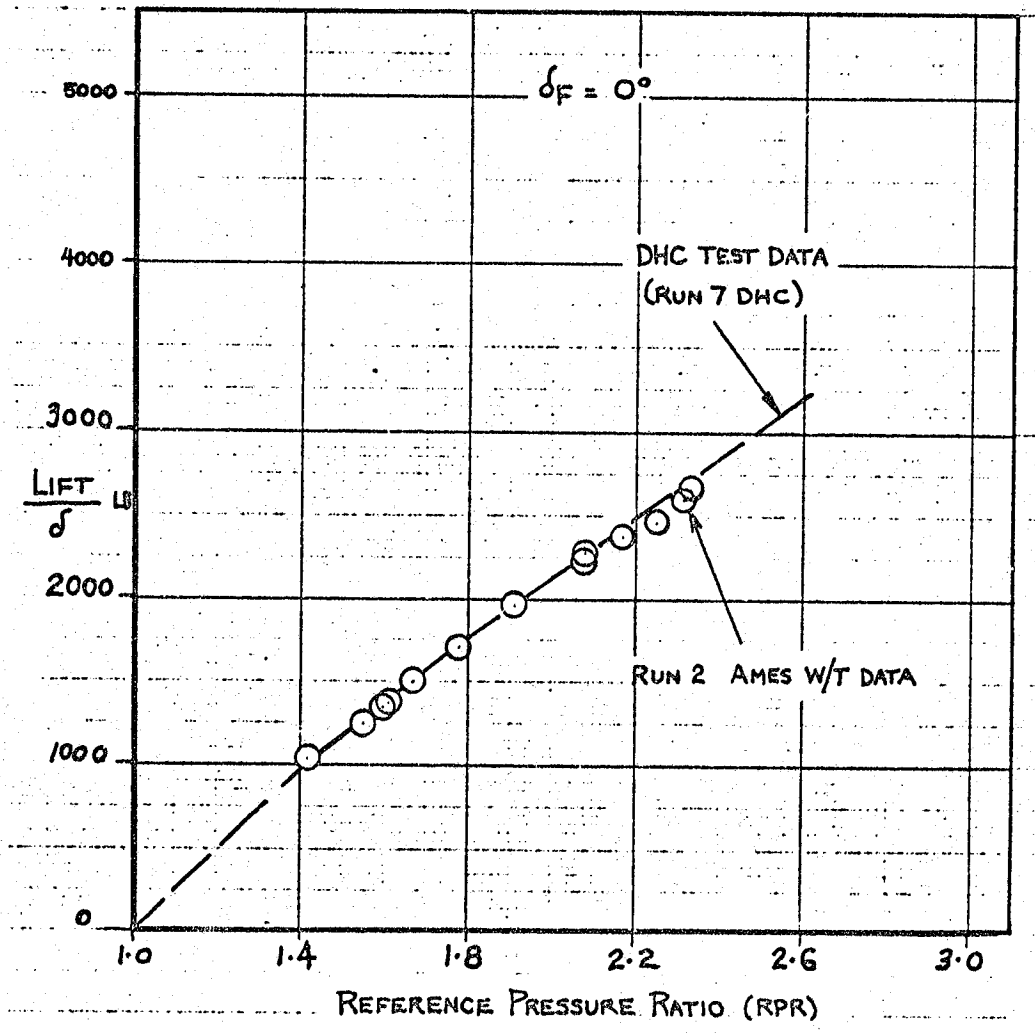

Fig. 11

COMPARISON BETWEEN STATIC THRUST DATA,

AUGMENTOR DOORS ON

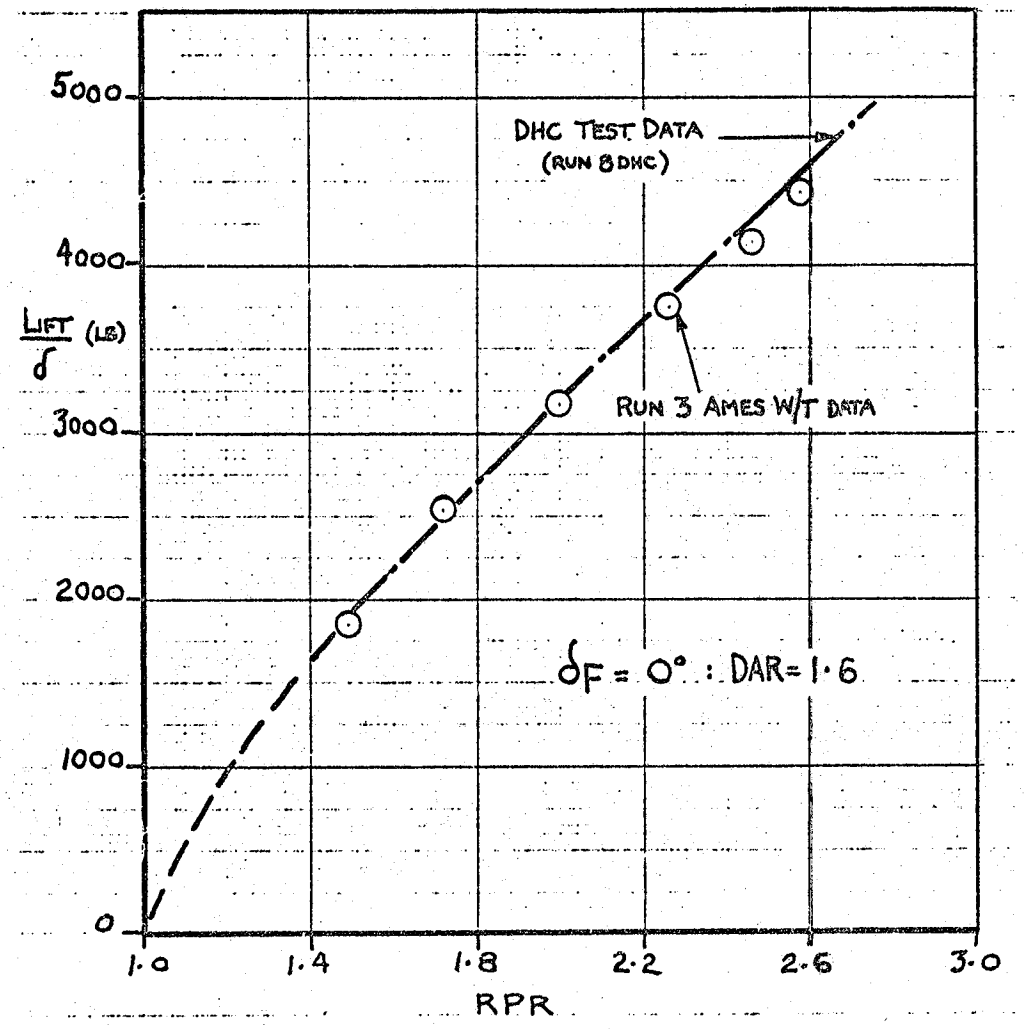

Fig. 12

BALANCE LIFT FORCE vs FLAP ANGLE

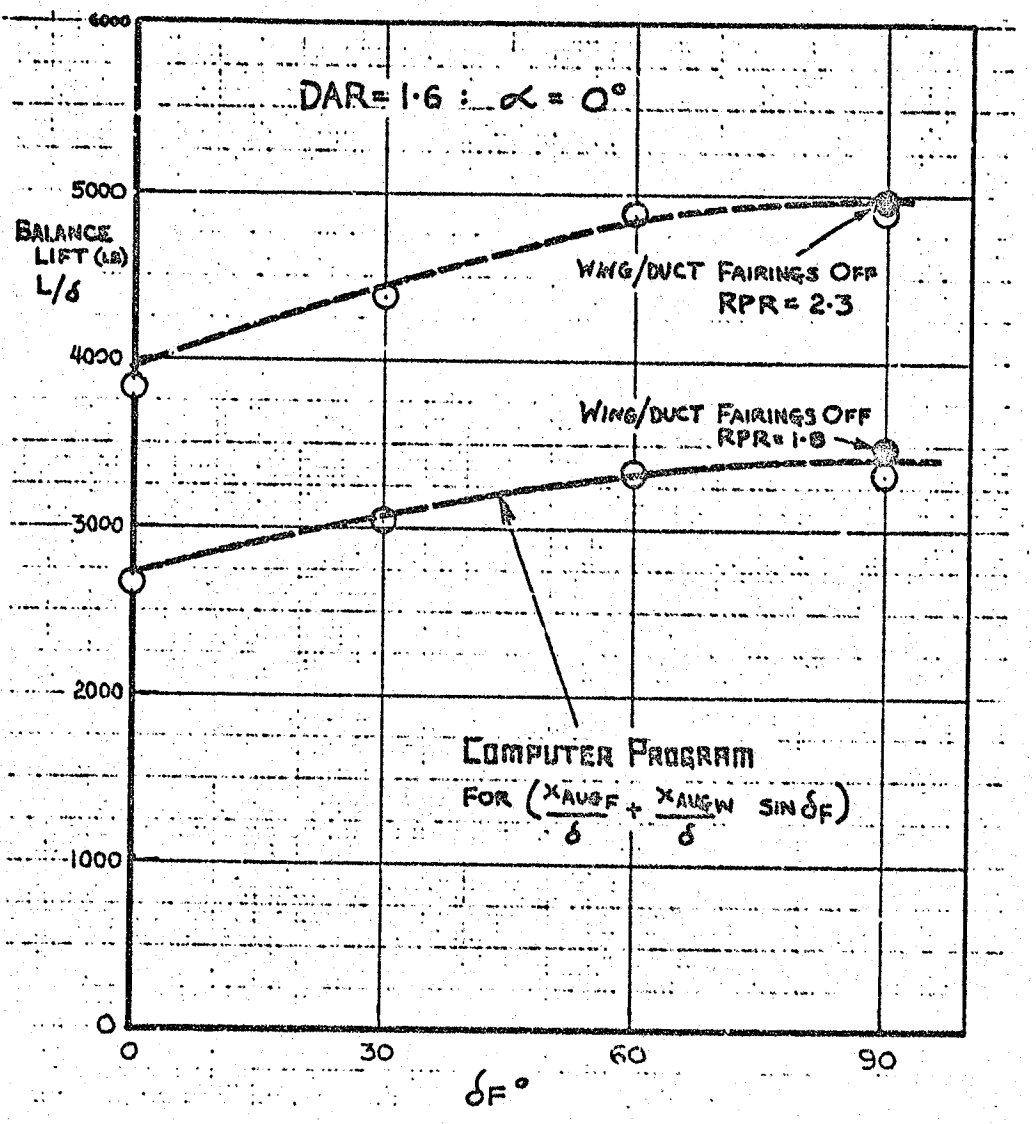

POWER-OFF, CLEAN CONFIGURATION;

$\delta_F = 0^\circ$; TAIL OFF

(RUN 94)

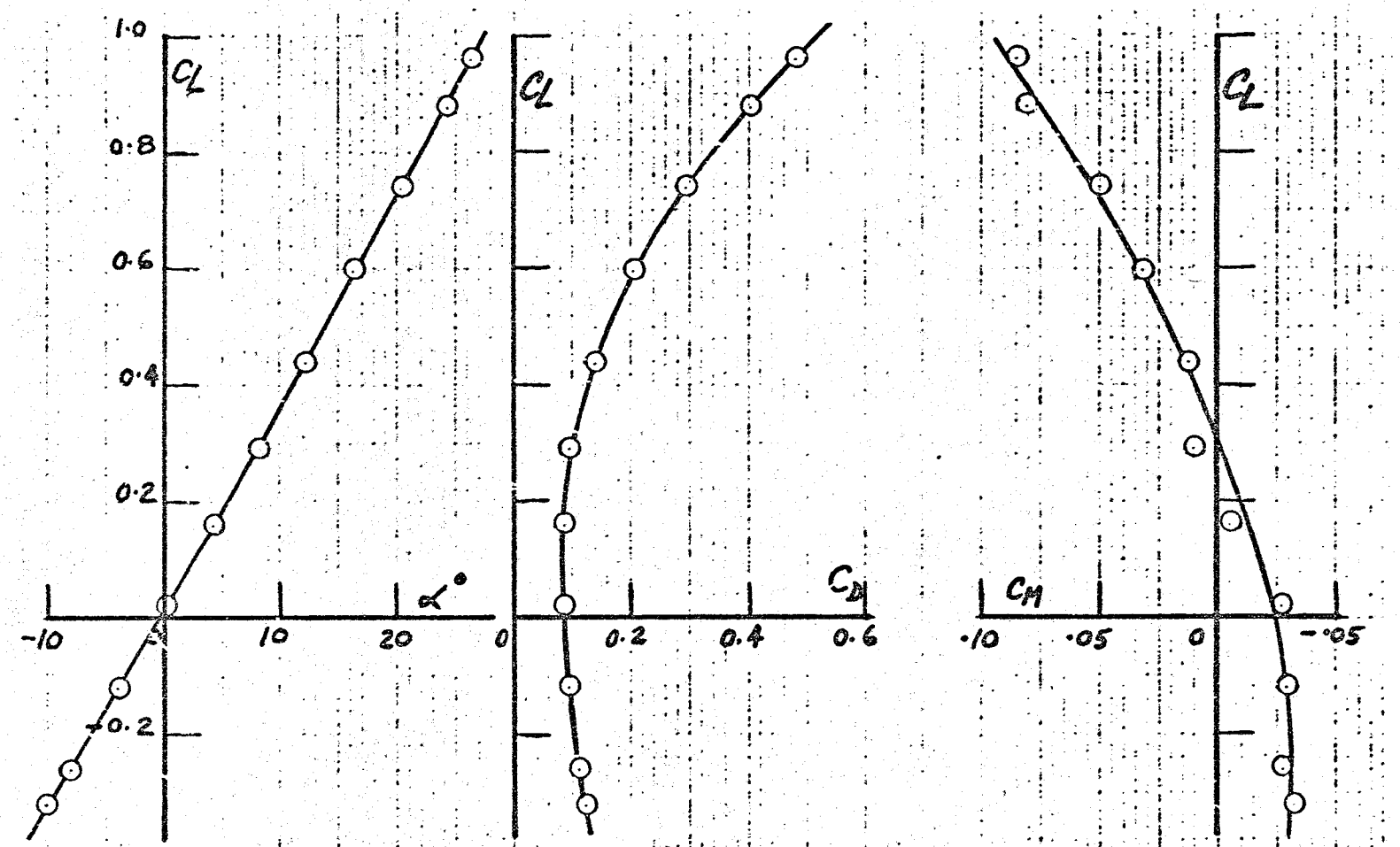

Fig. 13a

POWER-OFF, CLEAN CONFIGURATION;

$\delta_F = 30^\circ$; TAIL OFF

(RUN 95)

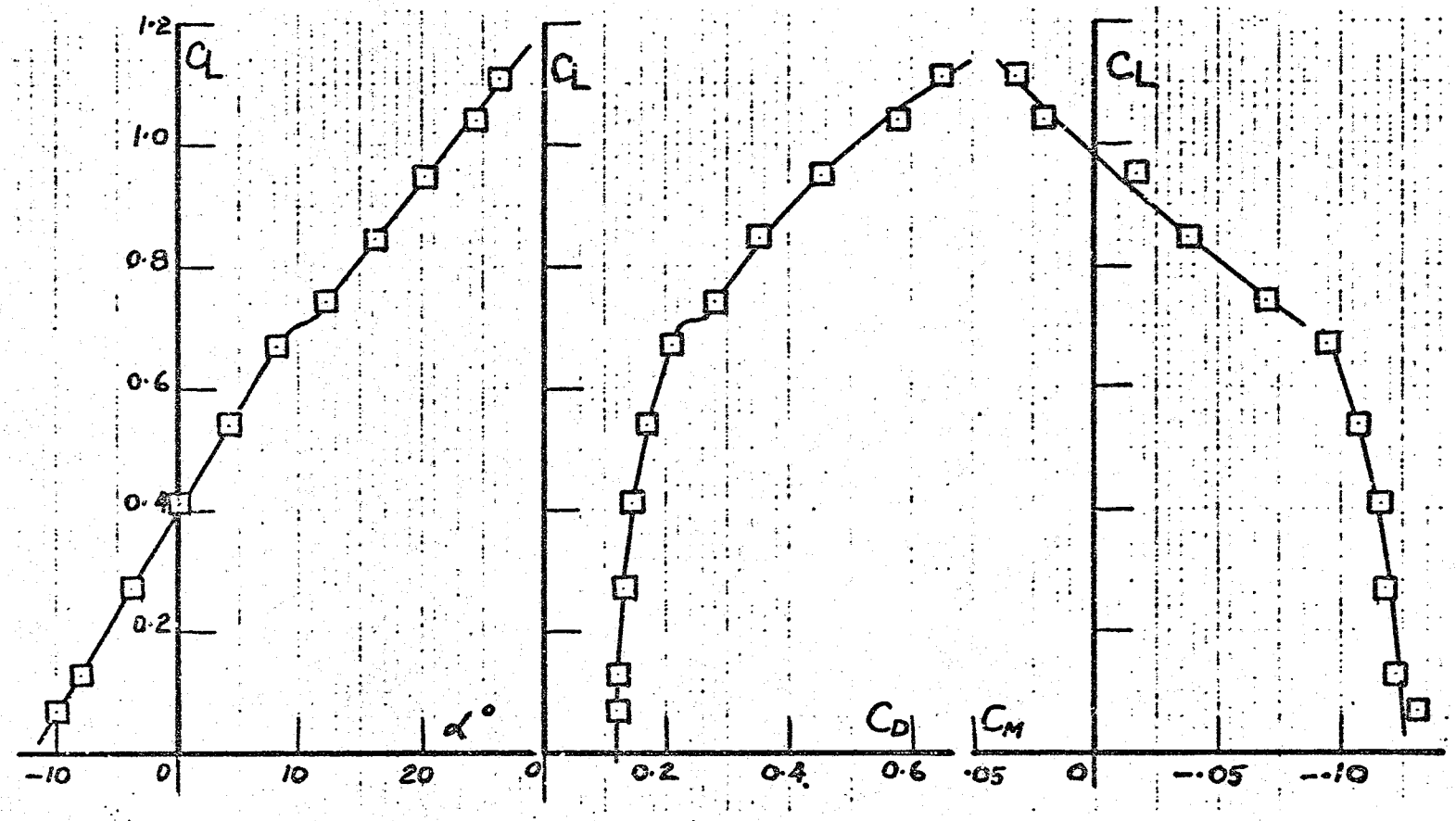

Fig. 13b

δ_F=90°: TAIL OFF: DAR = 1.6: RPR=2.4: RAKE OFF

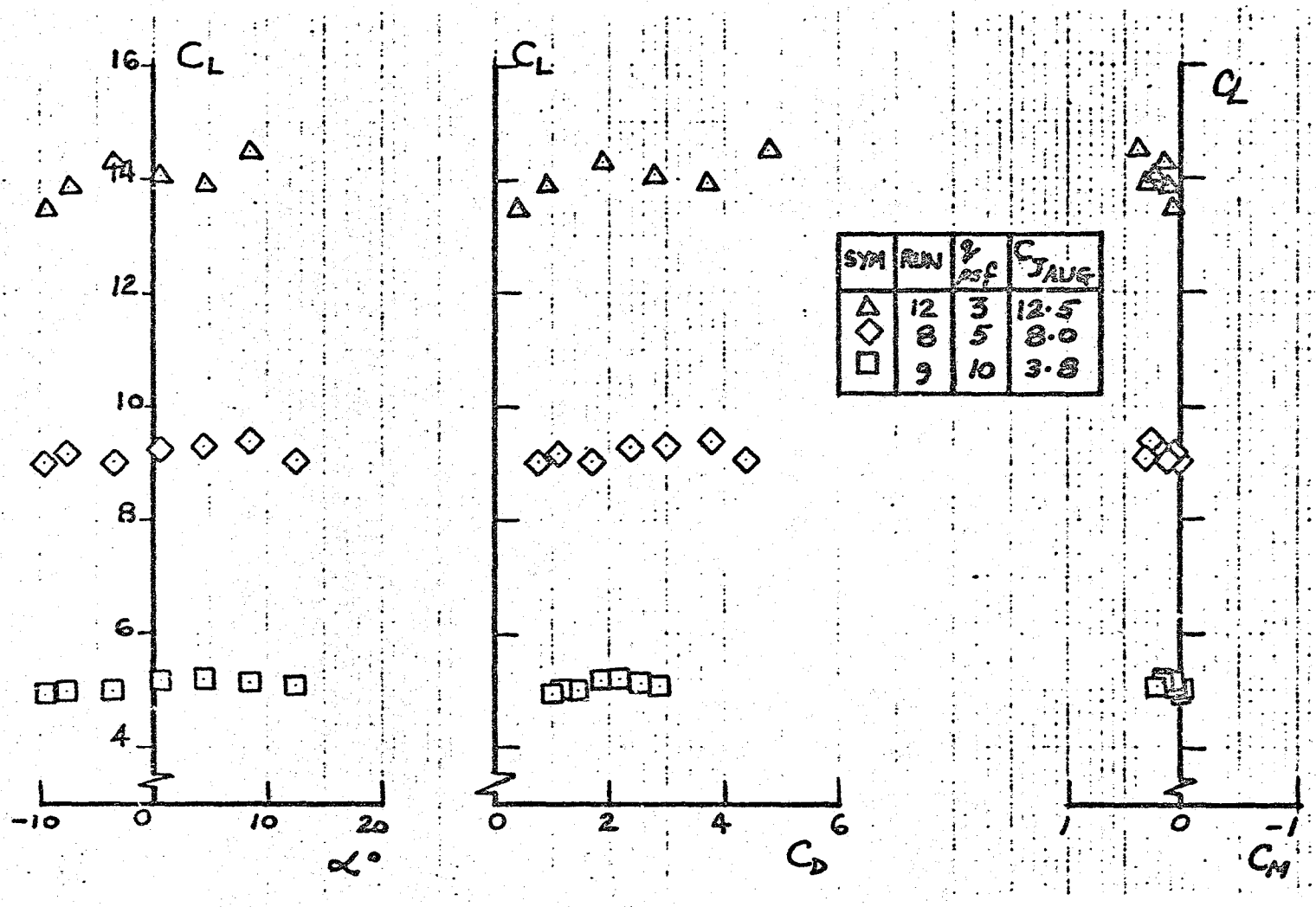

Fig. 14

δ_F=60°: TAIL OFF: DAR = 1.6: RPR = 2.3: RAKE ON

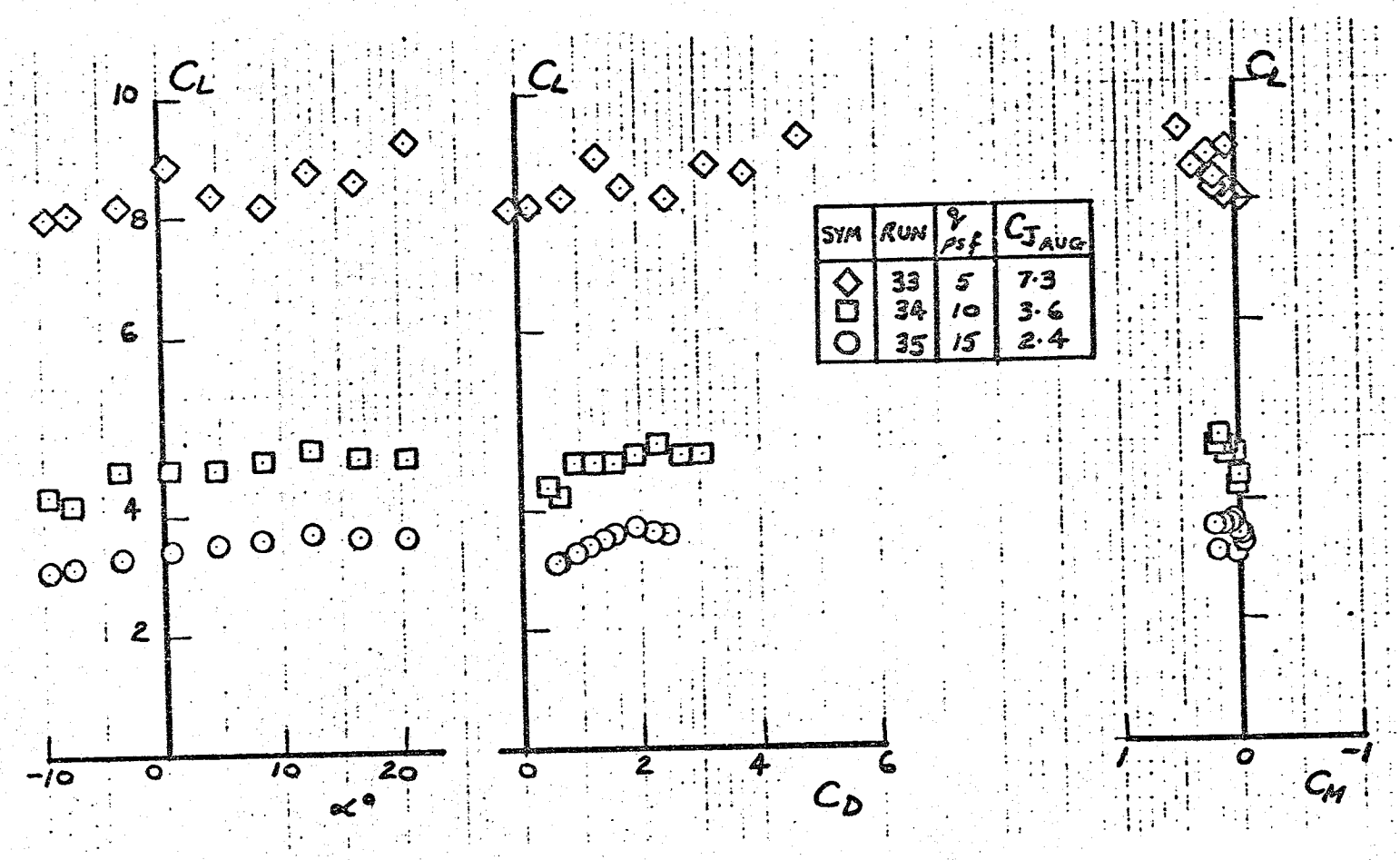

Fig. 14a

$\delta_F = 30^\circ$: TAIL OFF: DAR = 1.6: RPR = 2.3: RAKE OFF

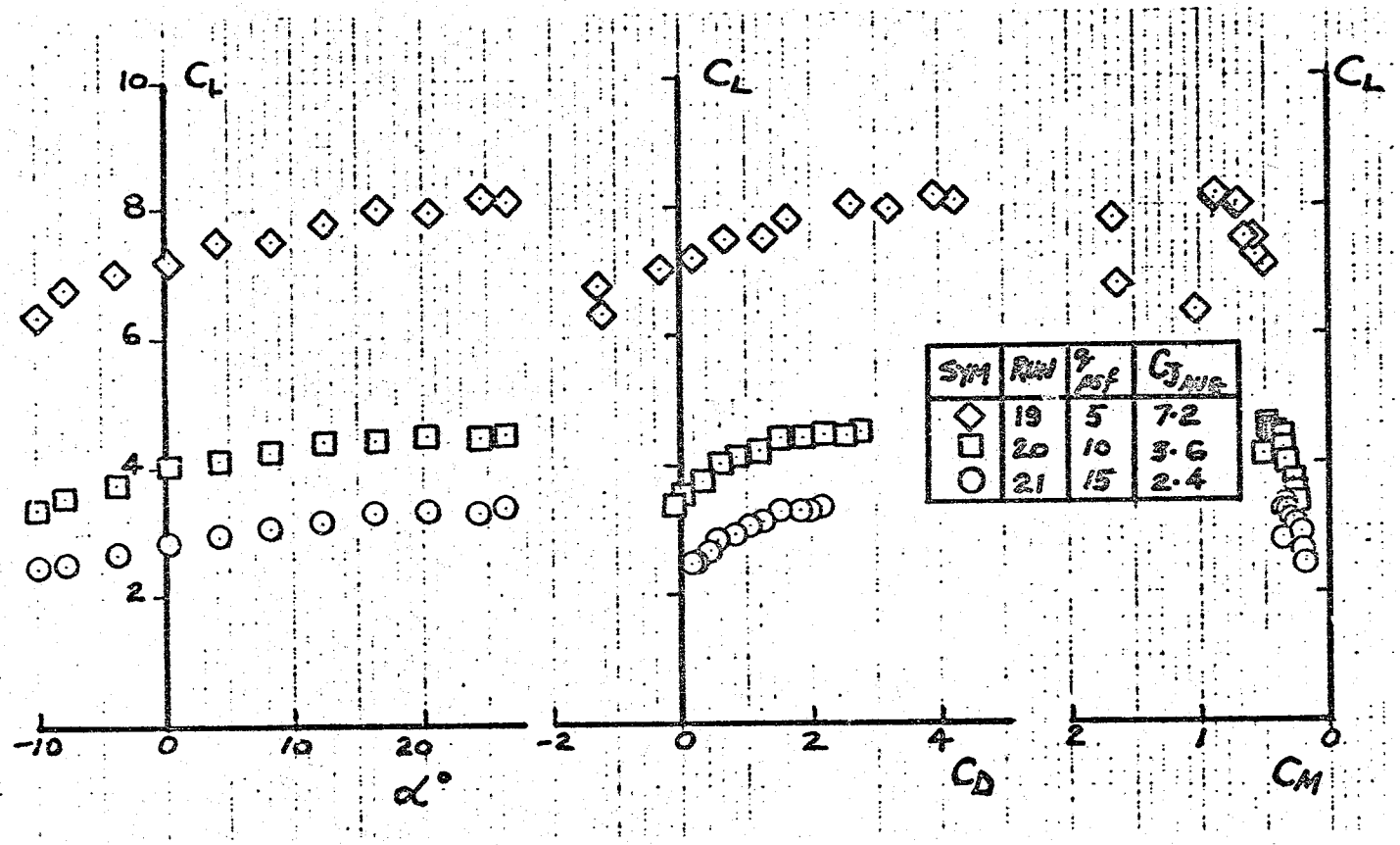

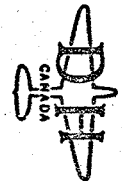

Fig. 14b

$\delta_F = 0^0$: TAIL OFF: DAR = 1.6: RPR = 2.3: RAKE ON

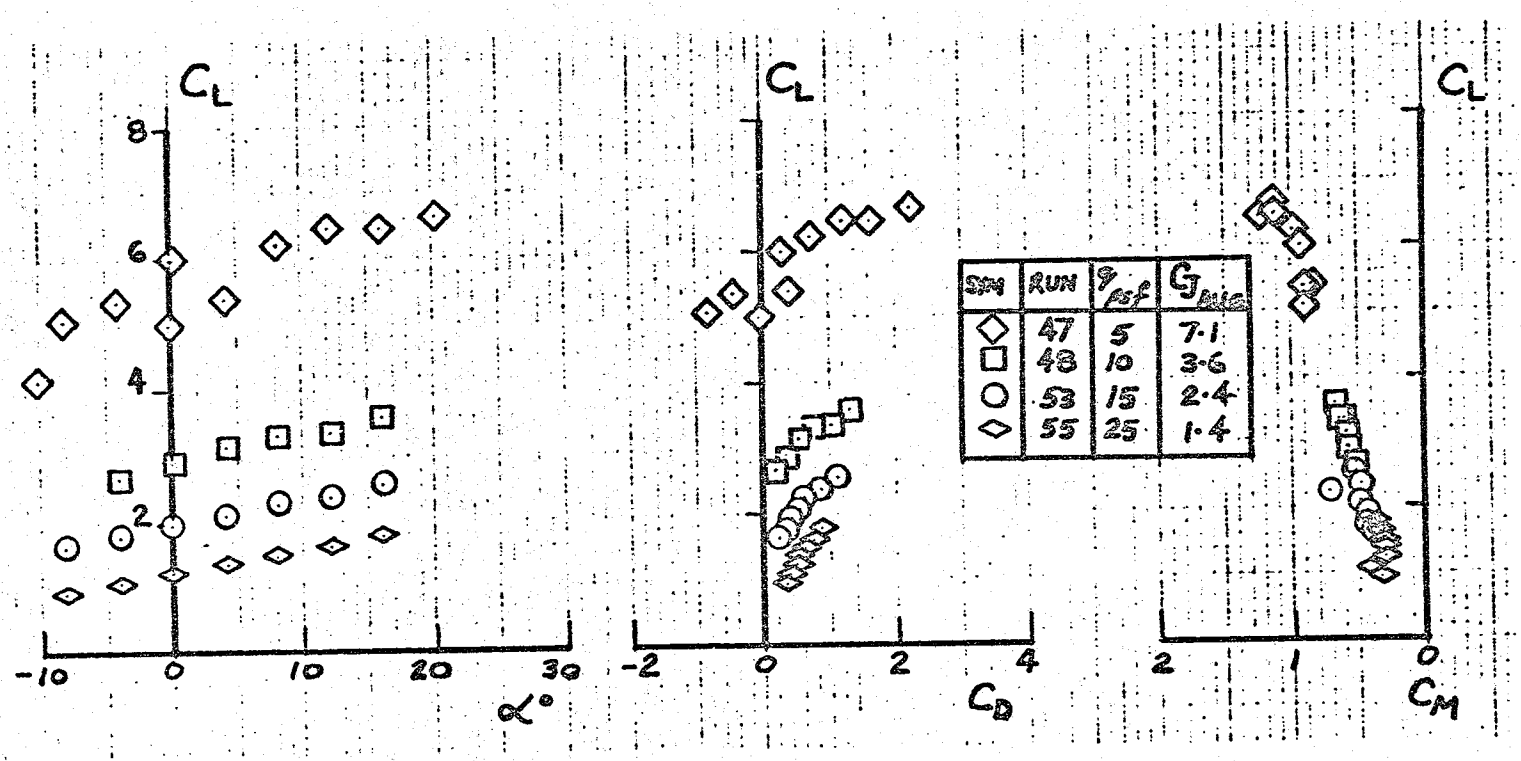

Fig. 14c

$\delta_F = 90^\circ$: TAIL OFF: DAR = 1.6: RRR = 2.4: RAKE OFF

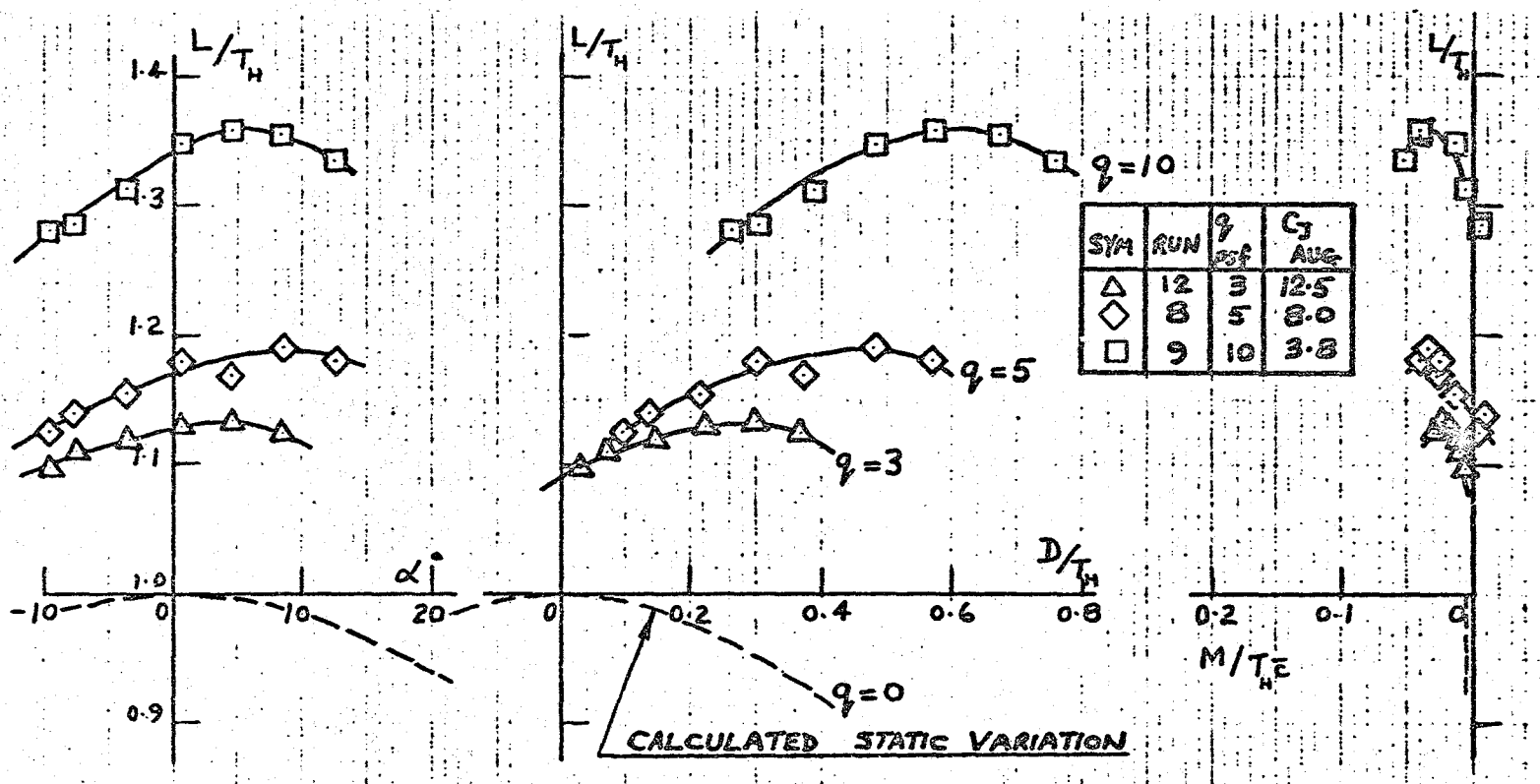

Fig. 15

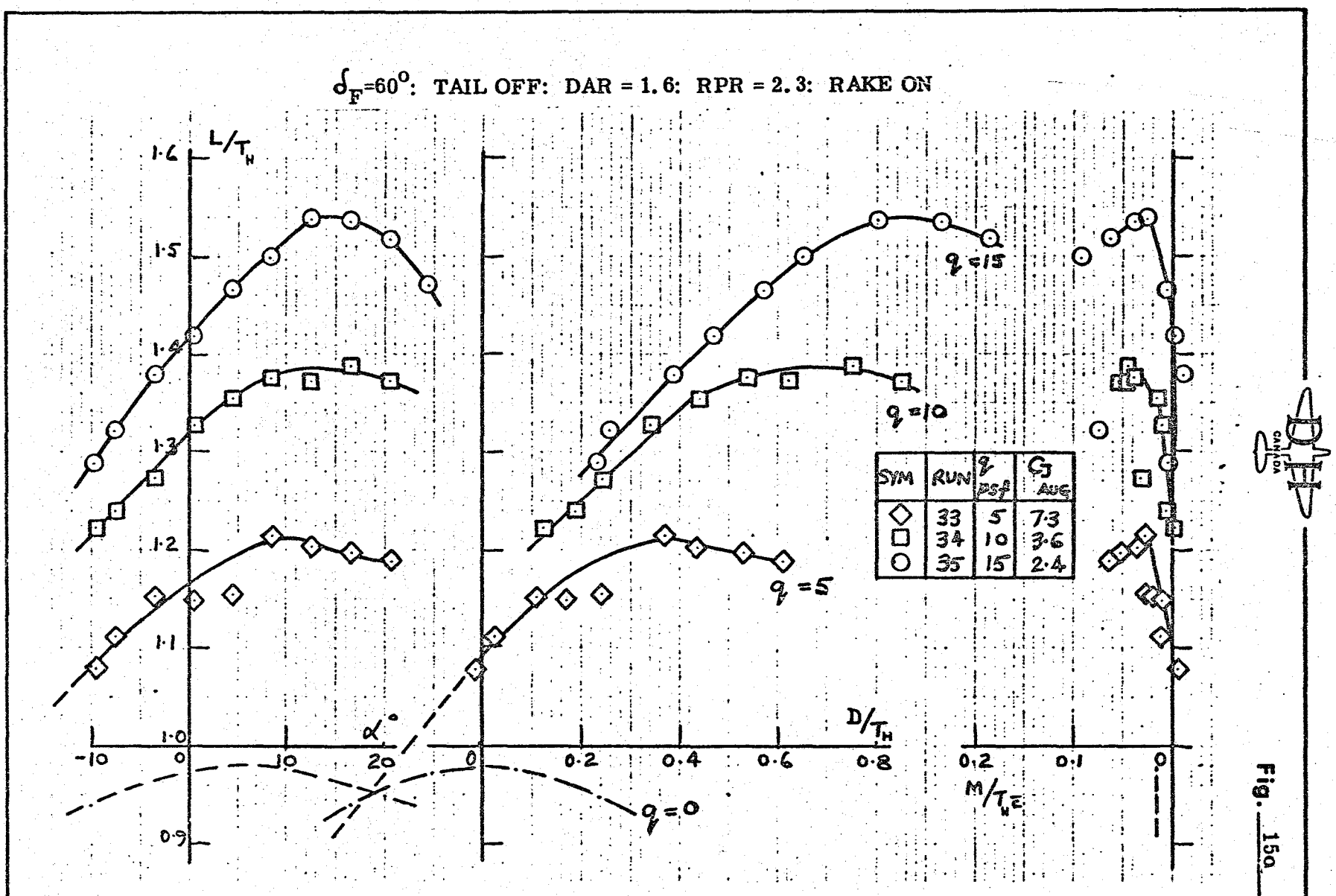
δ_F=60°: TAIL OFF: DAR = 1.6: RPR = 2.3: RAKE ON
L/T_H
1.6
1.5
1.4
1.3
1.2
1.1
1.0
0.9
α°
-10
0
10
20
q=15
q=10
q=5
q=0
SYM
RUN
q PSF
CJ AUG
33
5
7.3
34
10
3.6
35
15
2.4
D/T_H
0
0.2
0.4
0.6
0.8
M/T_H
0.2
0.1
0
CANARD

Fig. 15a

$\delta_F = 30^\circ$: TAIL OFF: DAR = 1.6: RPR = 2.3: RAKE OFF

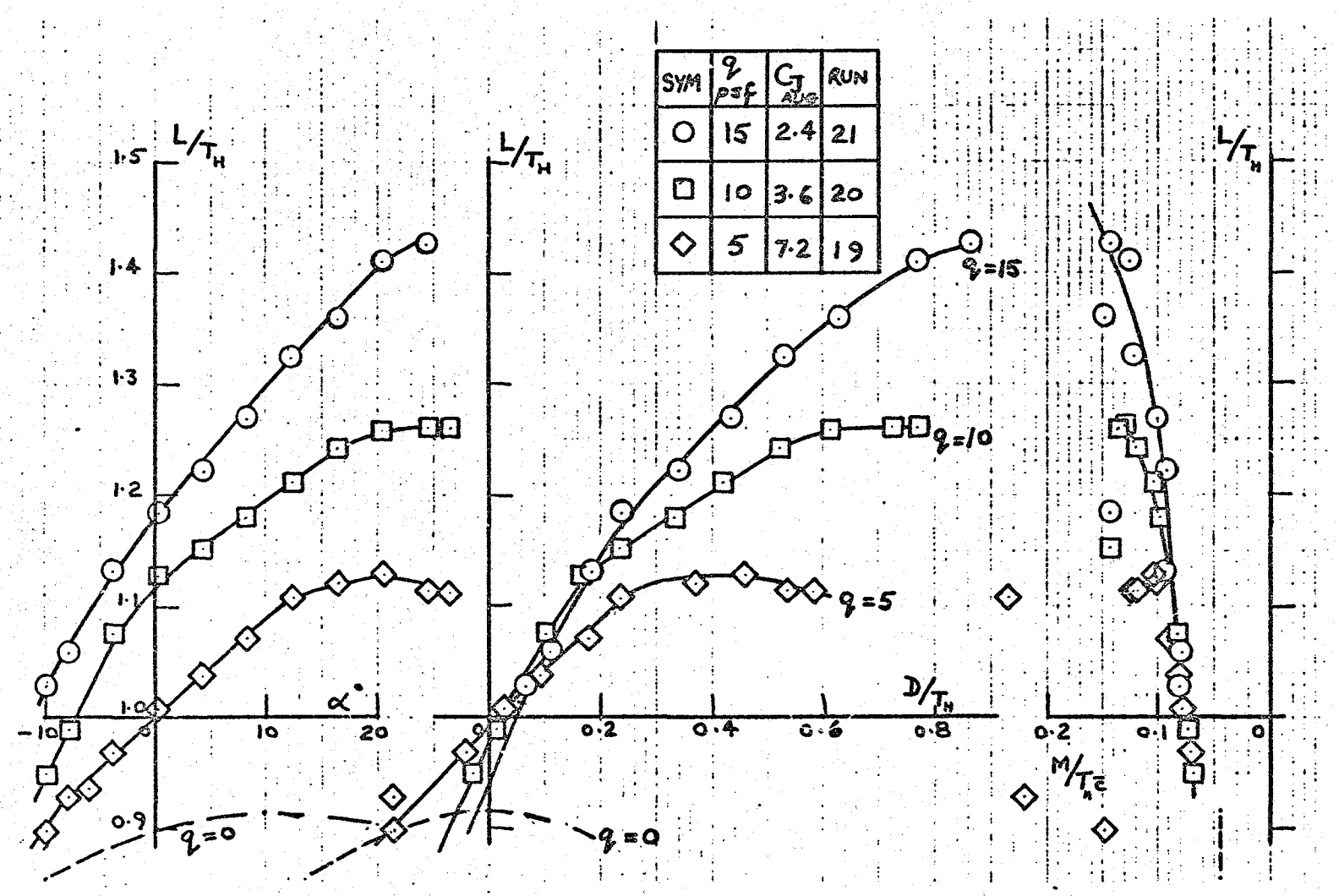

Fig. 15b

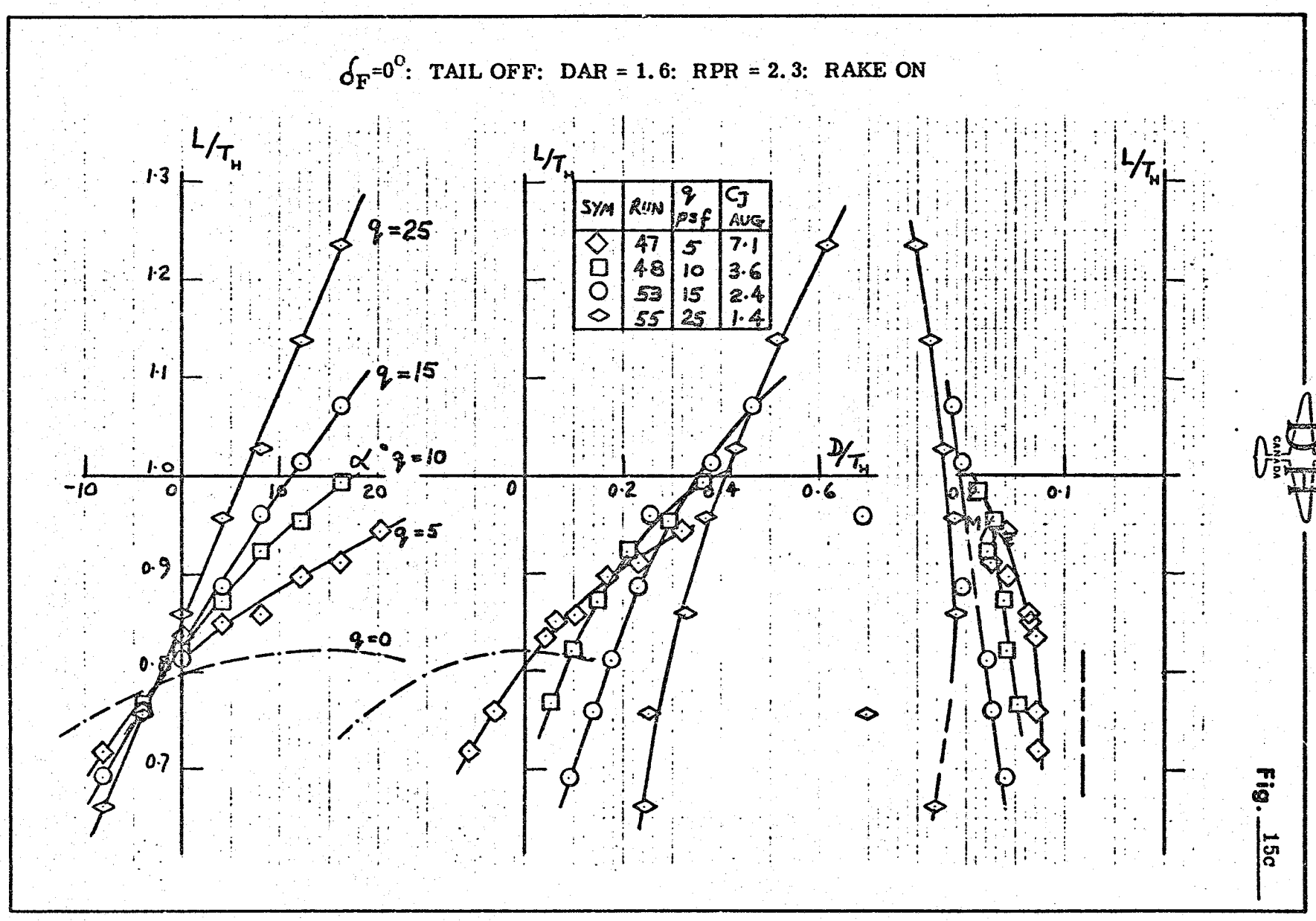
$\delta_F=0^\circ$: TAIL OFF: DAR = 1.6: RPR = 2.3: RAKE ON
L/T_H
1·3
1·2
1·1
1·0
0·9
0·8
0·7
q=25
q=15
q=10
q=5
q=0
α°
-10
0
10
20
SYM | RUN | q psf | CJ AUG
47 | 5 | 7·1
48 | 10 | 3·6
53 | 15 | 2·4
55 | 25 | 1·4
D/T_H
0·2
0·4
0·6
0·1

Fig. 15c

DRAG AT L/TH = 1.0 & 0.91

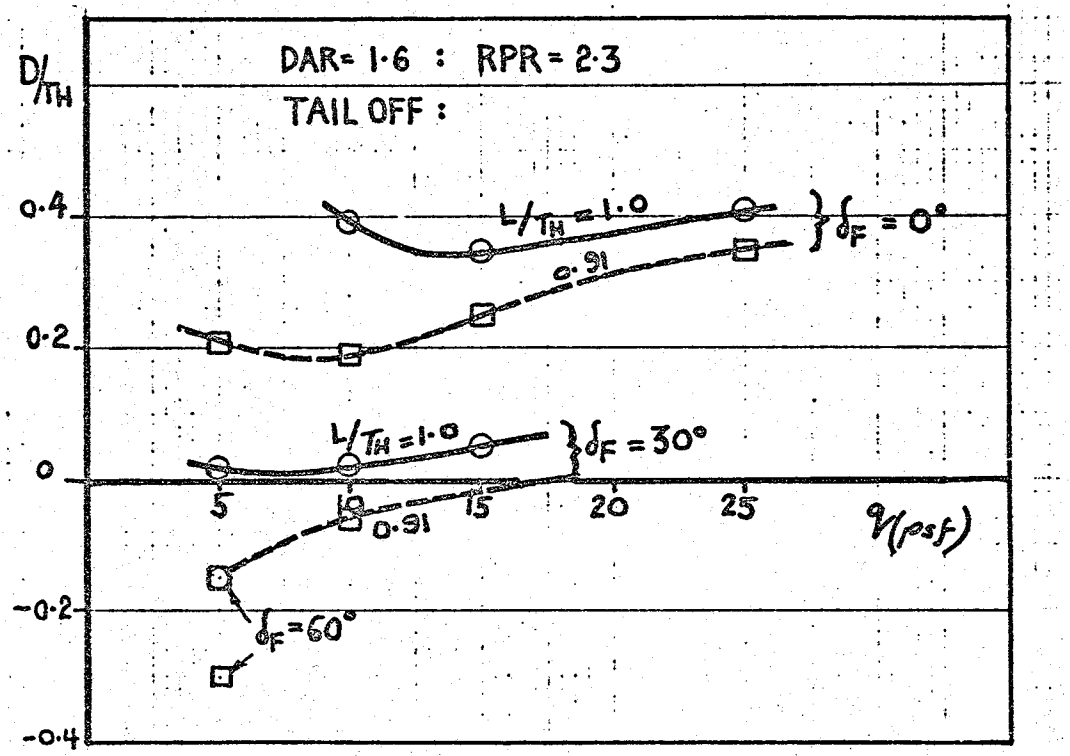

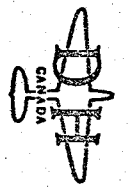

Fig. 16

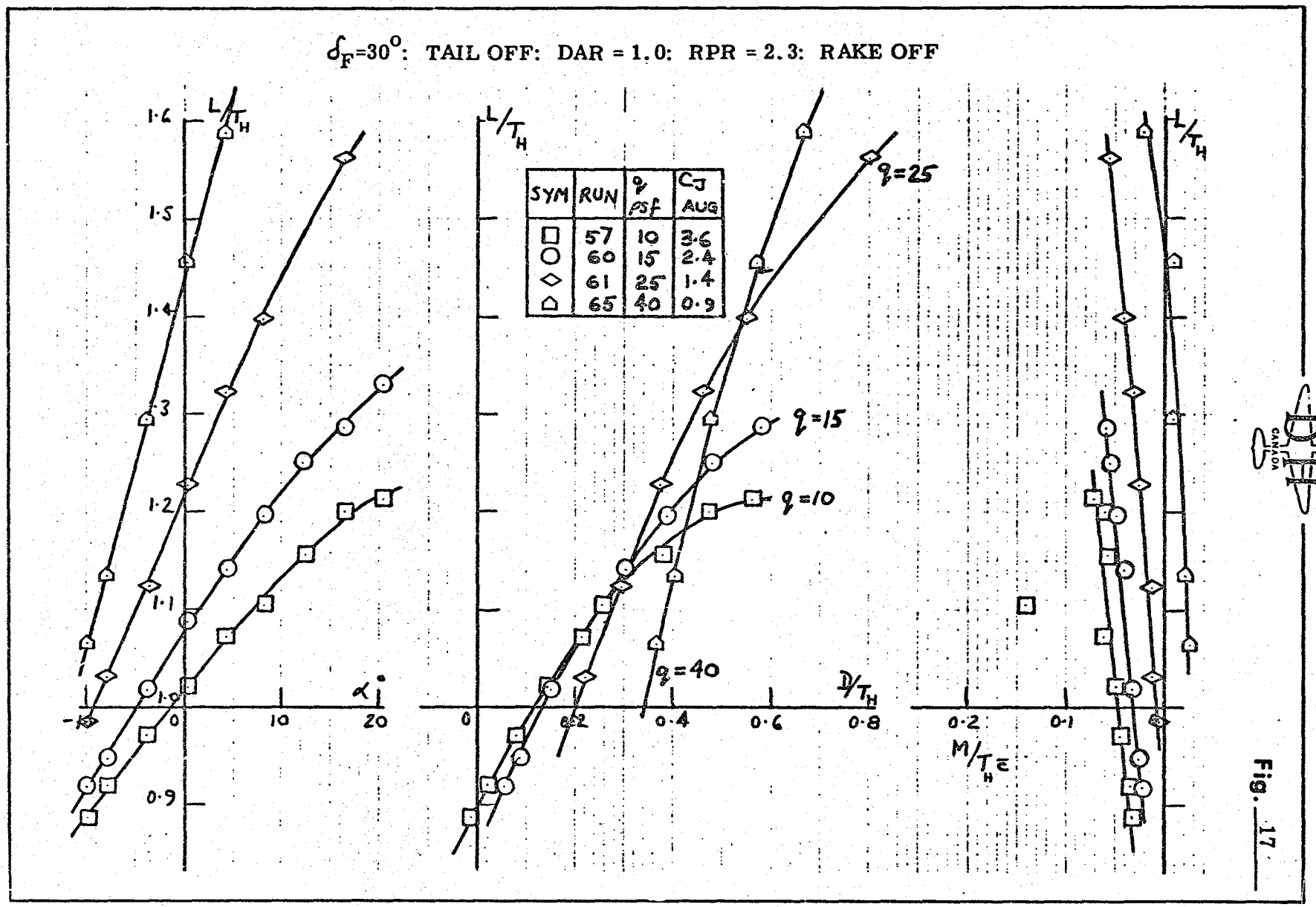
δ_F=30°: TAIL OFF: DAR = 1.0: RPR = 2.3: RAKE OFF
L/T_H
α°
D/T_H
M/T_H ε
SYM | RUN | q psf | C_J AUG
57 | 10 | 3.6
60 | 15 | 2.4
61 | 25 | 1.4
65 | 40 | 0.9
q=25
q=15
q=10
q=40
CANADA

Fig. 17

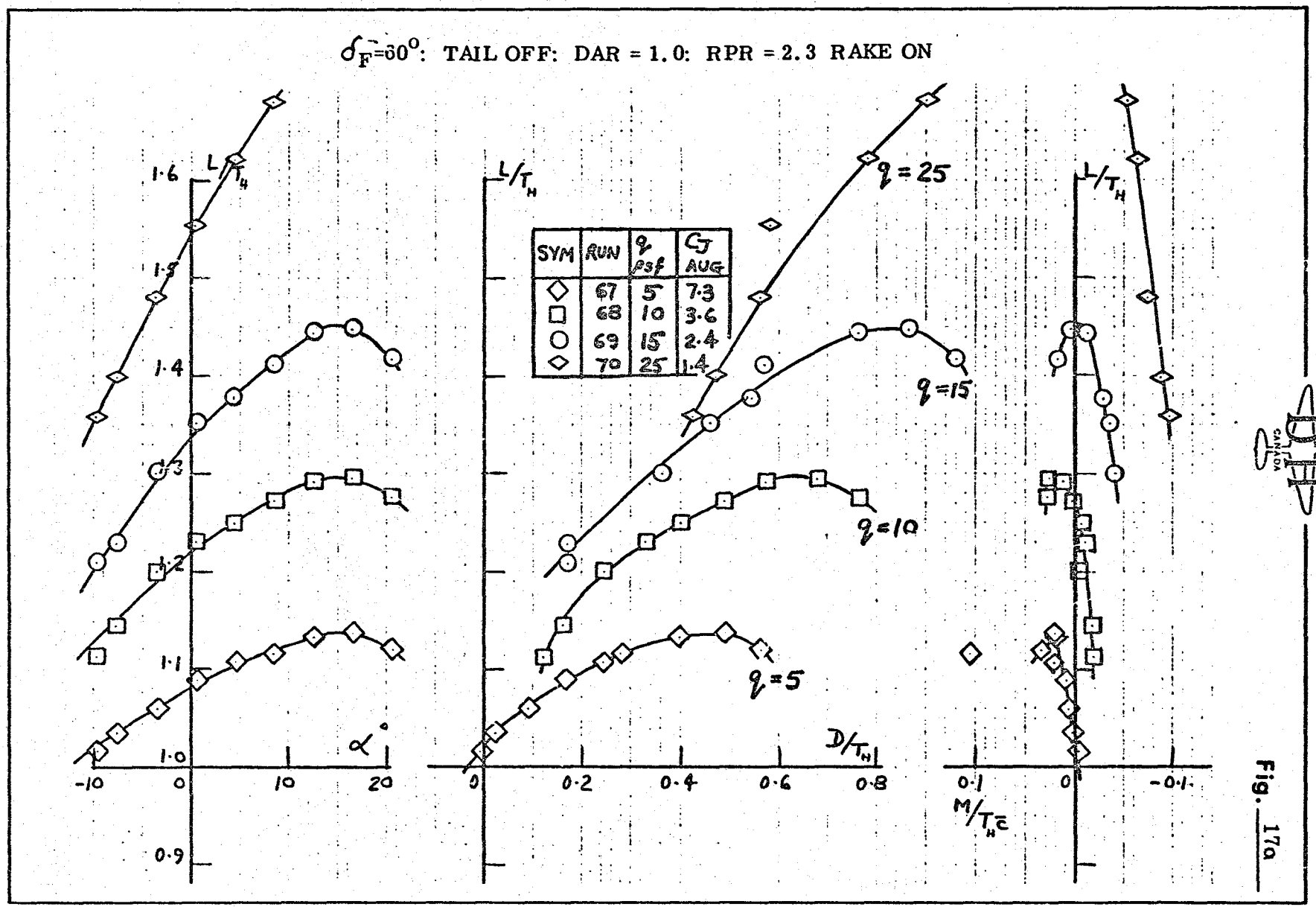
δ_F=60°: TAIL OFF: DAR = 1.0: RPR = 2.3 RAKE ON
L/T_H
α°
1.6
1.5
1.4
1.3
1.2
1.1
1.0
0.9
-10
0
10
20
SYM | RUN | q psf | CJ AUG
67 | 5 | 7.3
68 | 10 | 3.6
69 | 15 | 2.4
70 | 25 | 1.4
q=25
q=15
q=10
q=5
D/T_H
0
0.2
0.4
0.6
0.8
M/T_Hc
0.1
0
-0.1

Fig. 17a

Fig. 18

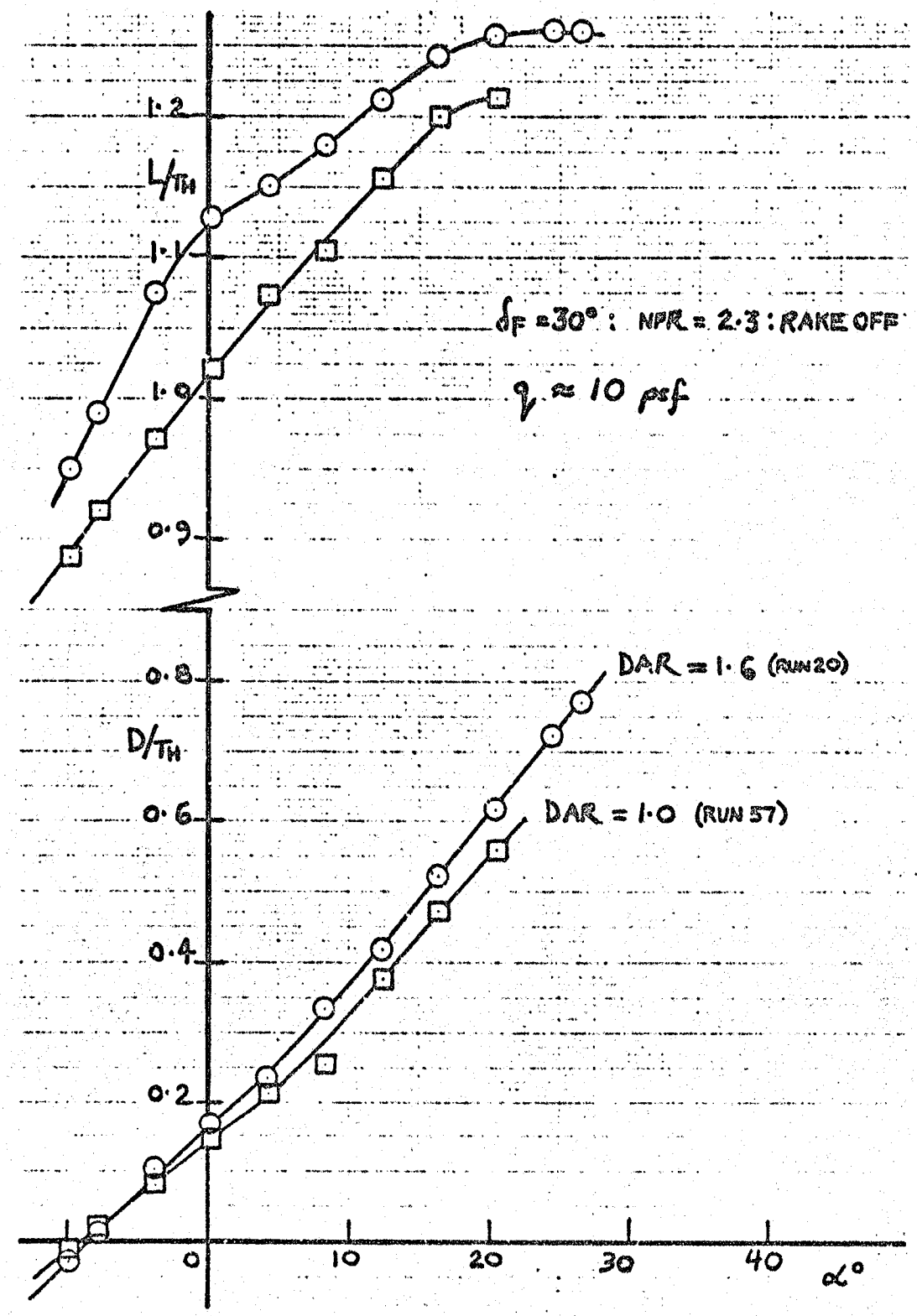

EFFECT OF AUGMENTOR THROTTLE ON L/T_H, D/T_H

Fig. 18a

$\delta_F = 30^\circ$: NPR = 2.3 $q_\infty = 15$ psf

TAIL OFF: RAKE OFF

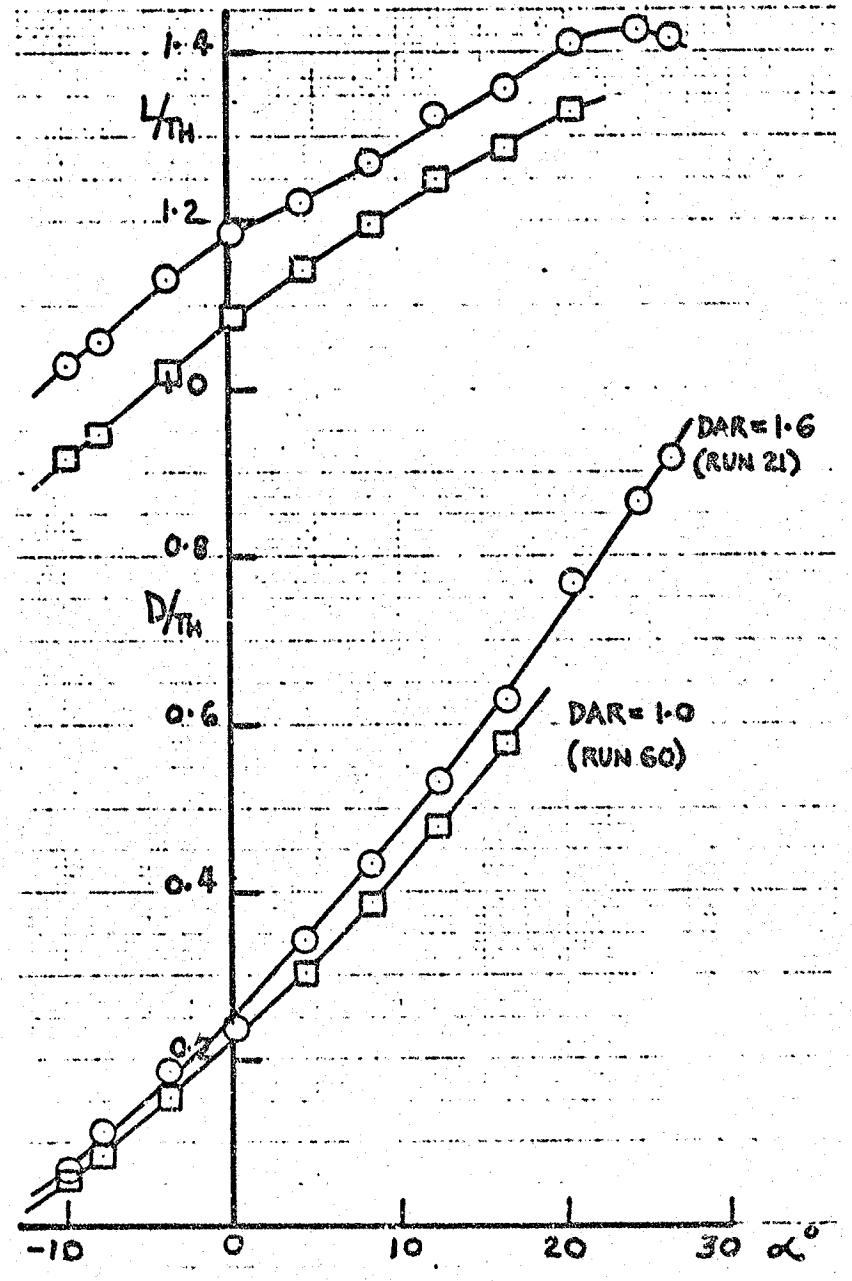

Fig. 19

EFFECT OF AUGMENTOR THROTTLING ON DRAG

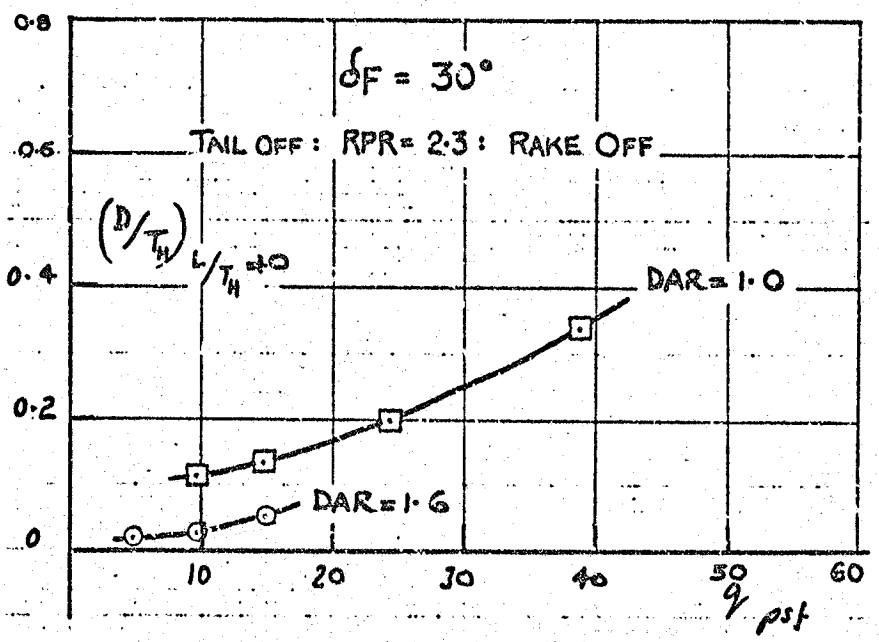

Fig. 19a

EFFECT OF AUGMENTOR THROTTLING ON DRAG

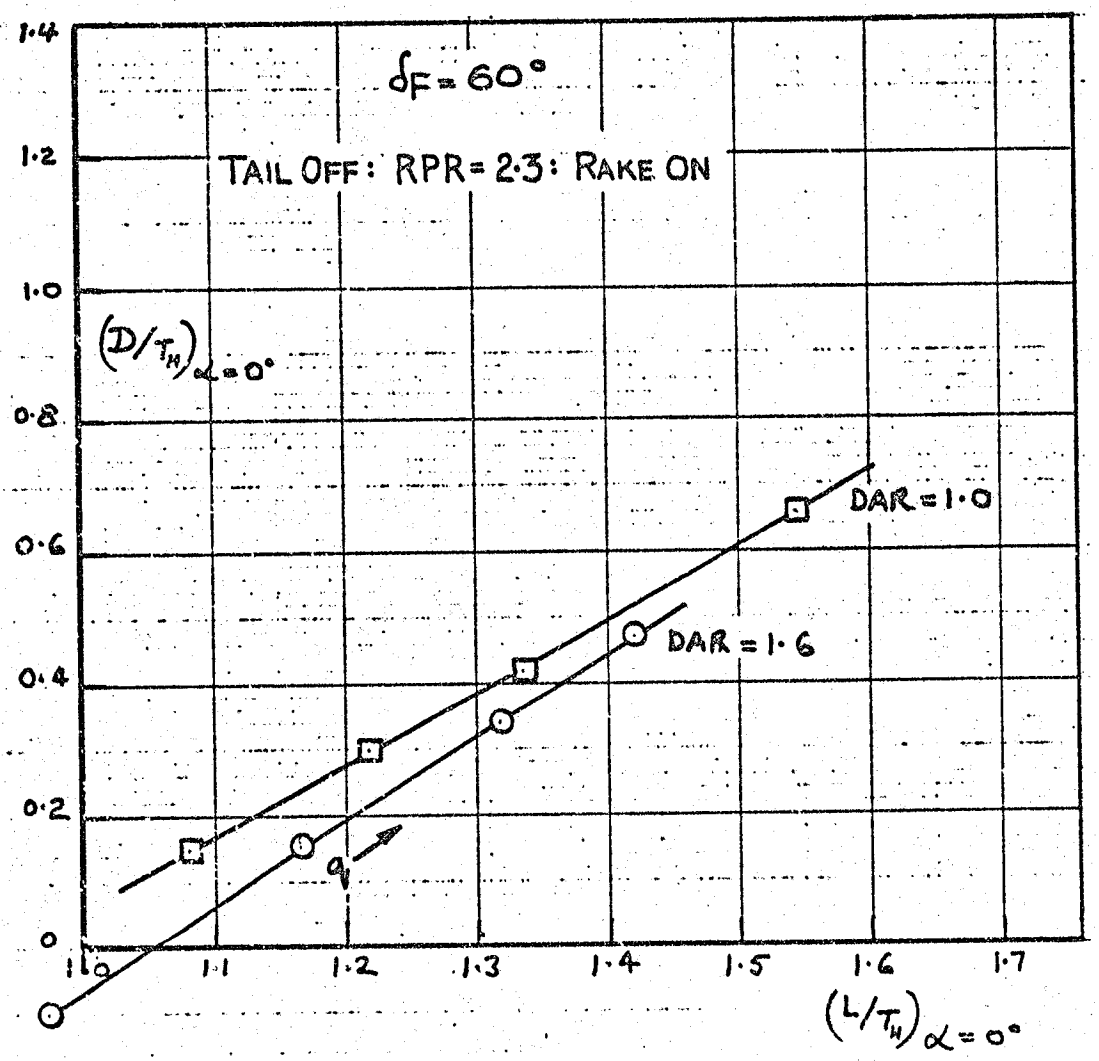

δ_F=60°: TAIL OFF: DAR = 1.0: 1/4 NOZZLES
BLANKED OFF: RAKE ON

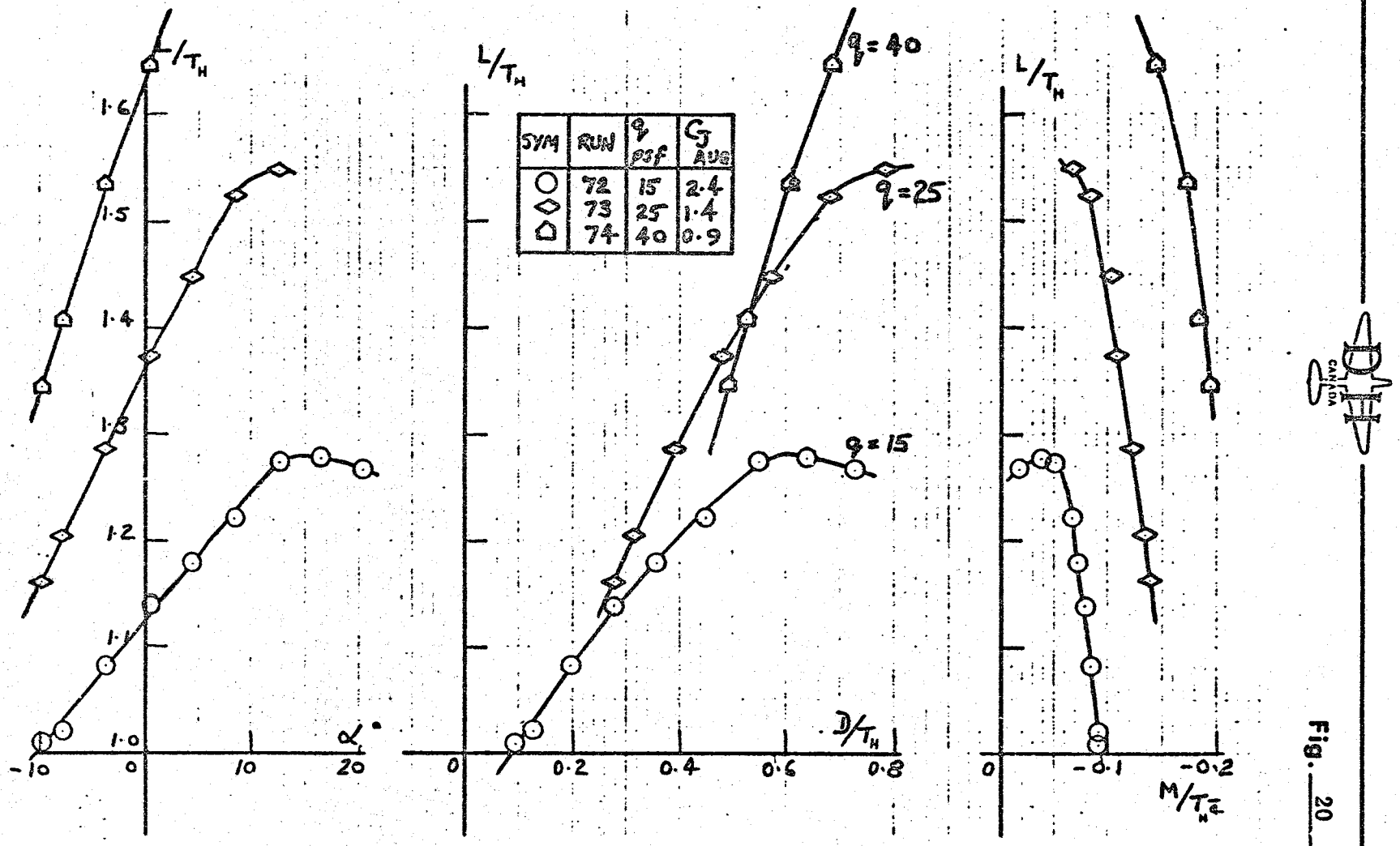

Fig. 20

δ_F=60°: TAIL OFF: DAR = 1.0: RPR = 2.3:
1/2 NOZZLES BLANKED OFF: RAKE ON

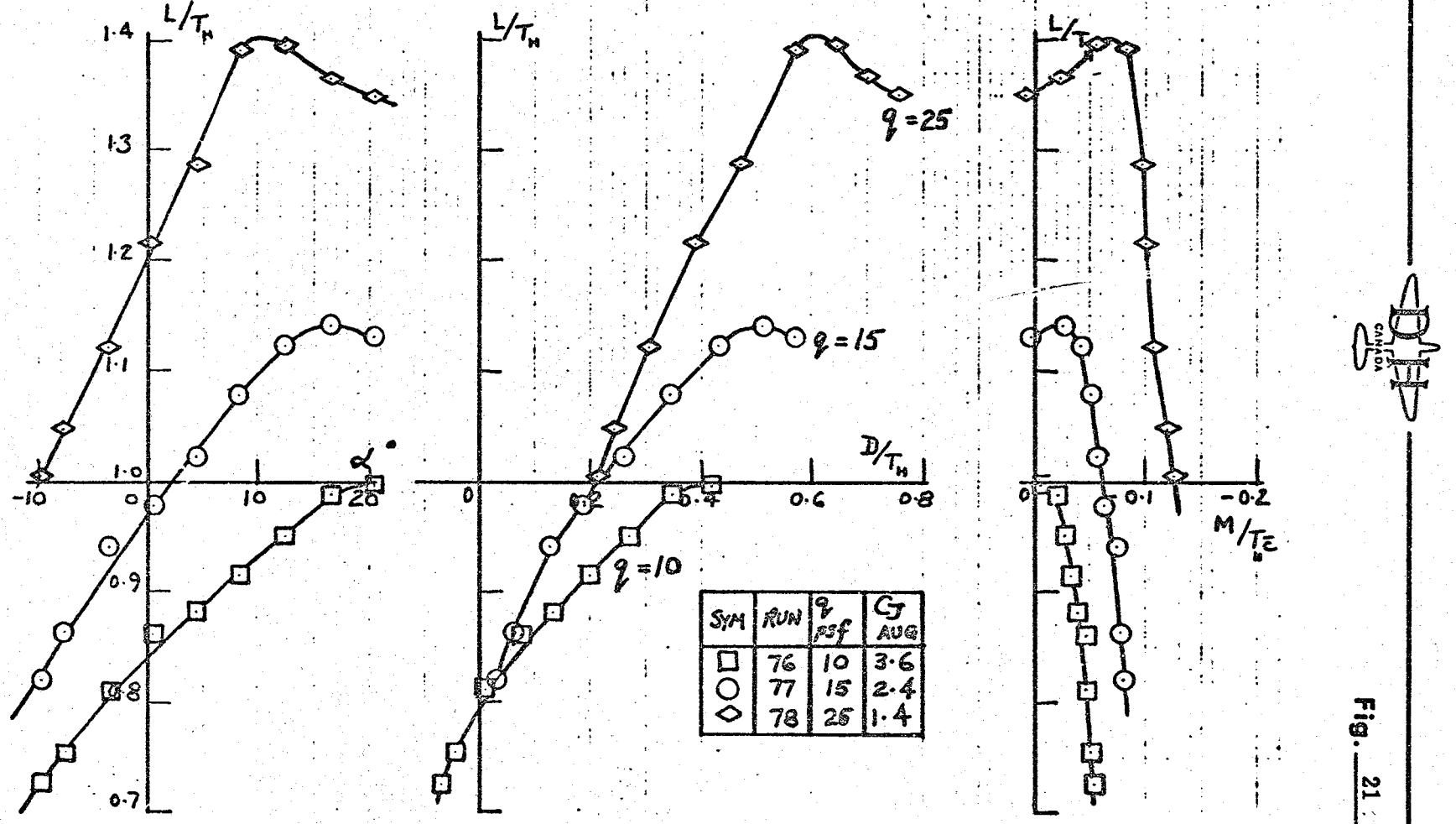

SYM	RUN	q psf	CJ AUG
□	76	10	3·6
○	77	15	2·4
◇	78	25	1·4

Fig. 21

$\delta_F = 30^0$: TAIL OFF: DAR = 1.0: RPR = 2.3: 1/2 NOZZLES BLANKED-OFF: RAKE OFF

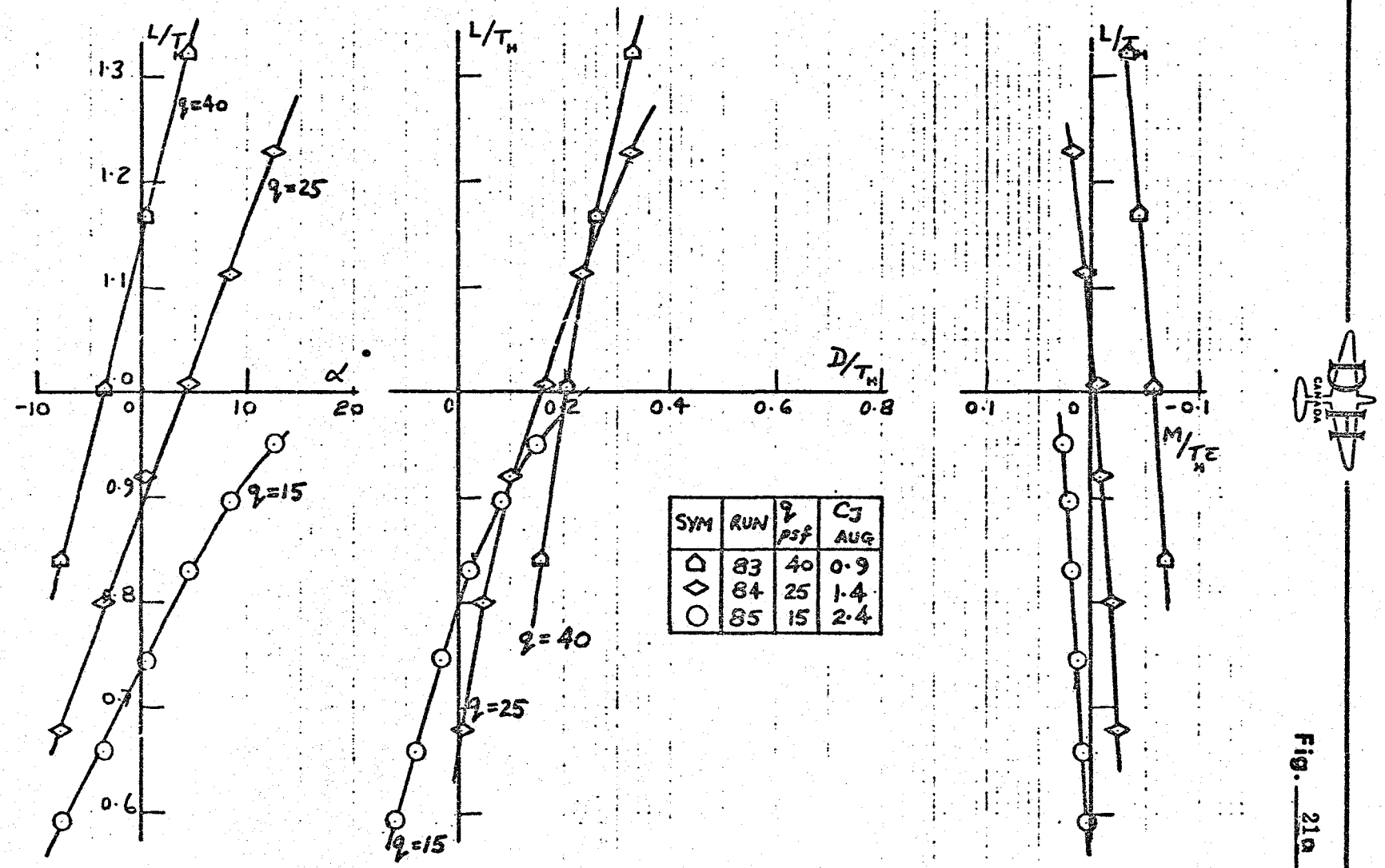

Fig. 21a

$\delta_F = 0^\circ$: TAIL OFF: DAR = 1.0: RPR = 2.3: 1/2 NOZZLES BLANKED OFF: RAKE OFF

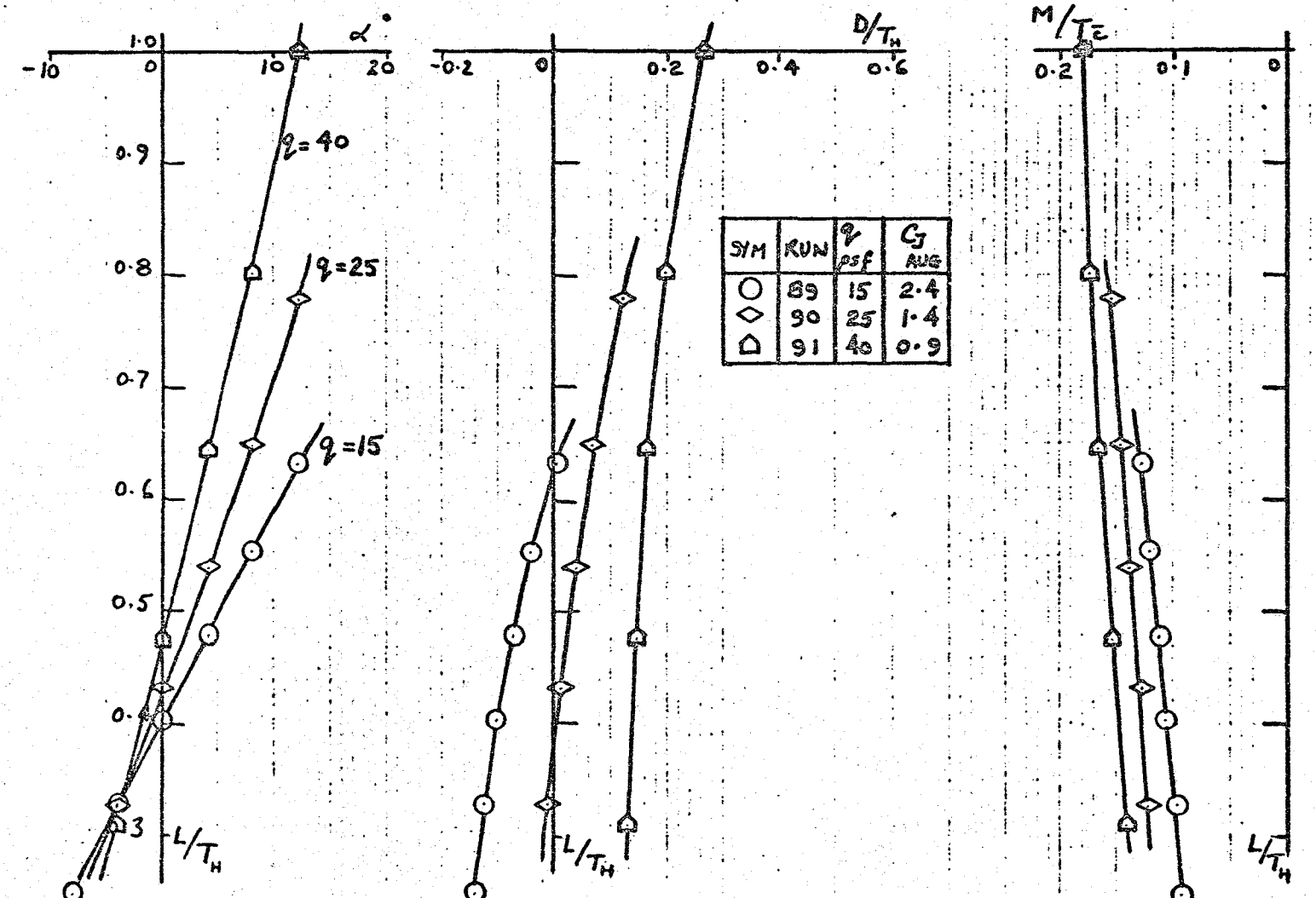

SYM	RUN	q psf	CJ AUG
○	89	15	2·4
◇	90	25	1·4
△	91	40	0·9

Fig. 21b

Fig. 22

EFFECT OF BLANKING NOZZLES ON L/T_H VS D/T_H

$\delta_F = 60°$: DAR = 1·0

NPR = 2·3 : RAKE ON

$q \approx 10$ psf

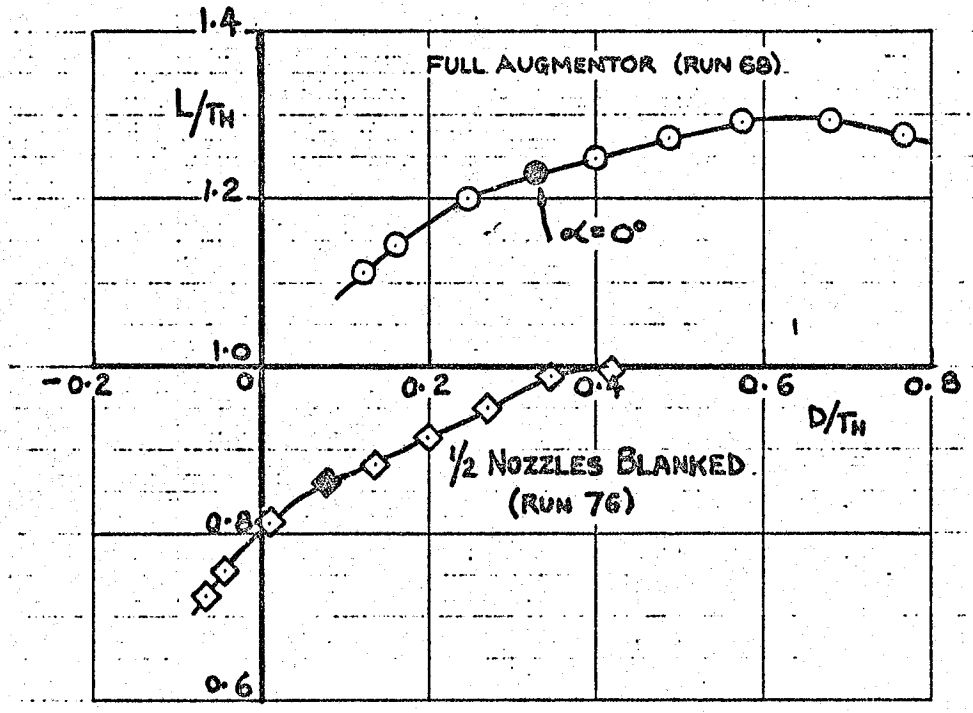

Fig. 22a

EFFECT OF BLANKING NOZZLES ON L/T_H vs D/T_H

$\delta_F = 60°$: DAR = 1.0

NPR = 2.3 : RAKE ON

$q \approx 15$ psf

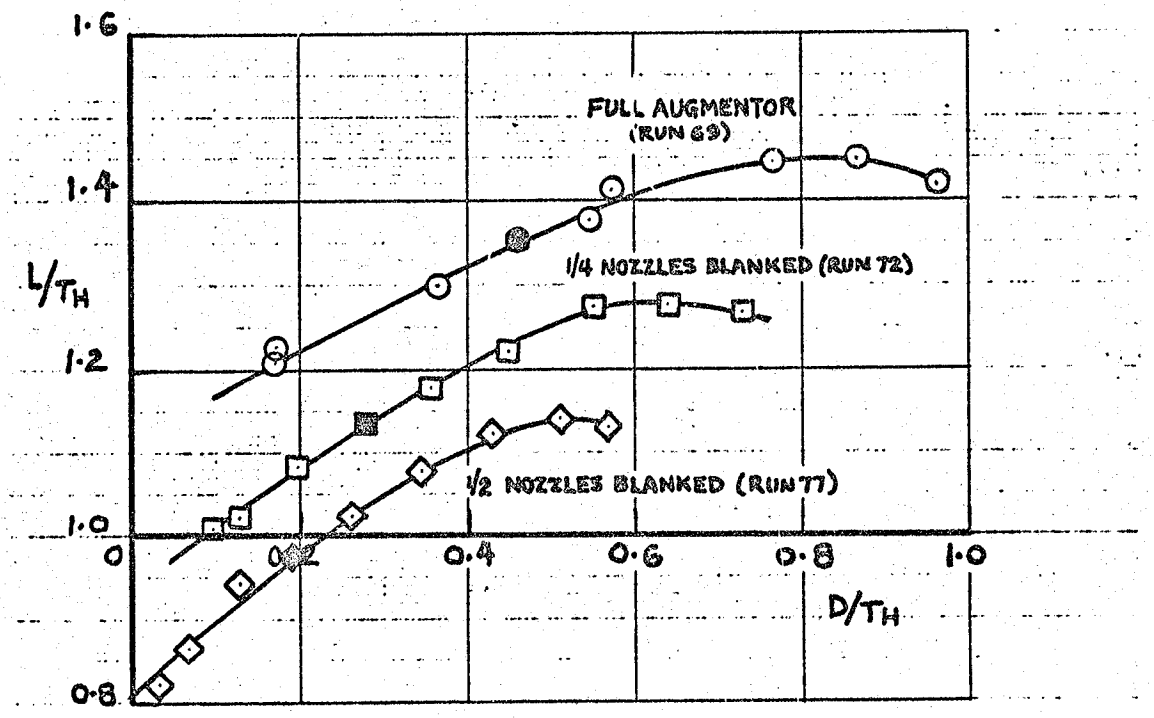

Fig. 22b

EFFECT OF BLANKING NOZZLES ON L/T_H vs D/T_H

$\delta_F = 60°$: DAR = 1·0

NPR = 2·3 : RAKE ON

$q \approx 25$ psf

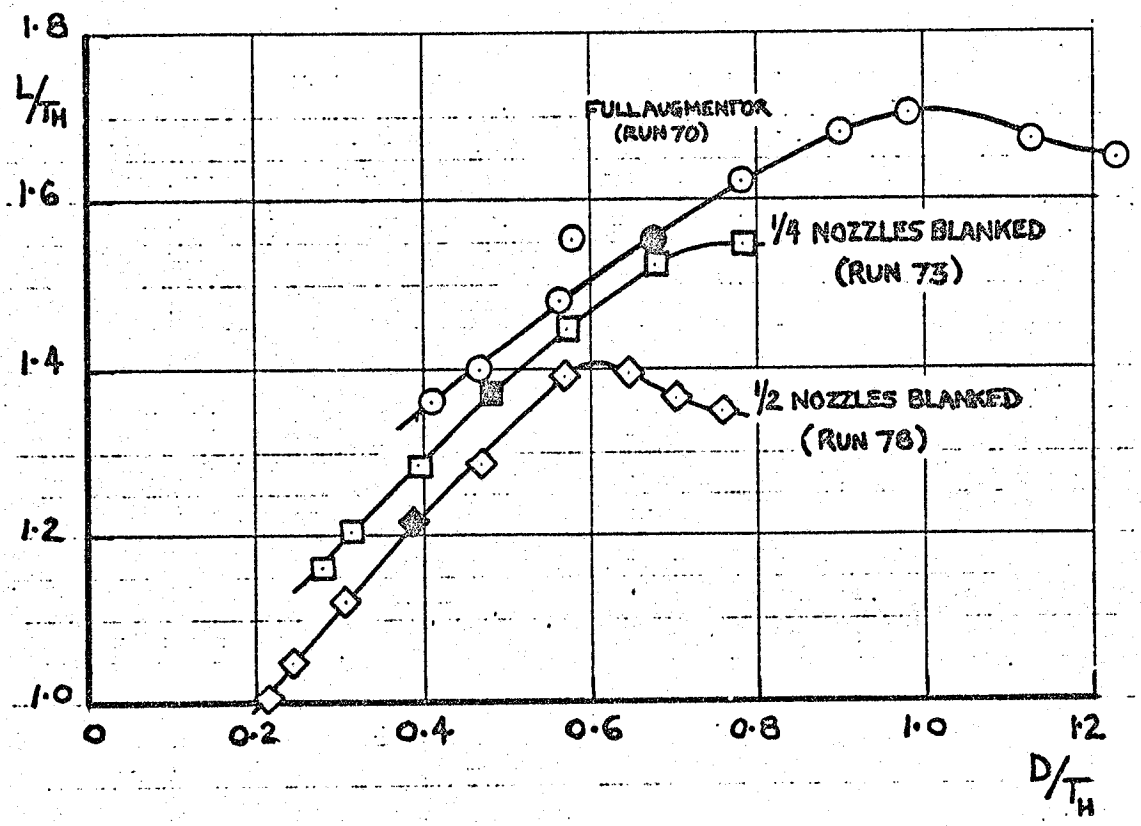

EFFECT OF THRUST TRANSFER ON ACCELERATION

δ_F=60°: α = 0°: RPR = 2.3: TAIL OFF: RAKE ON: DAR = 1.0

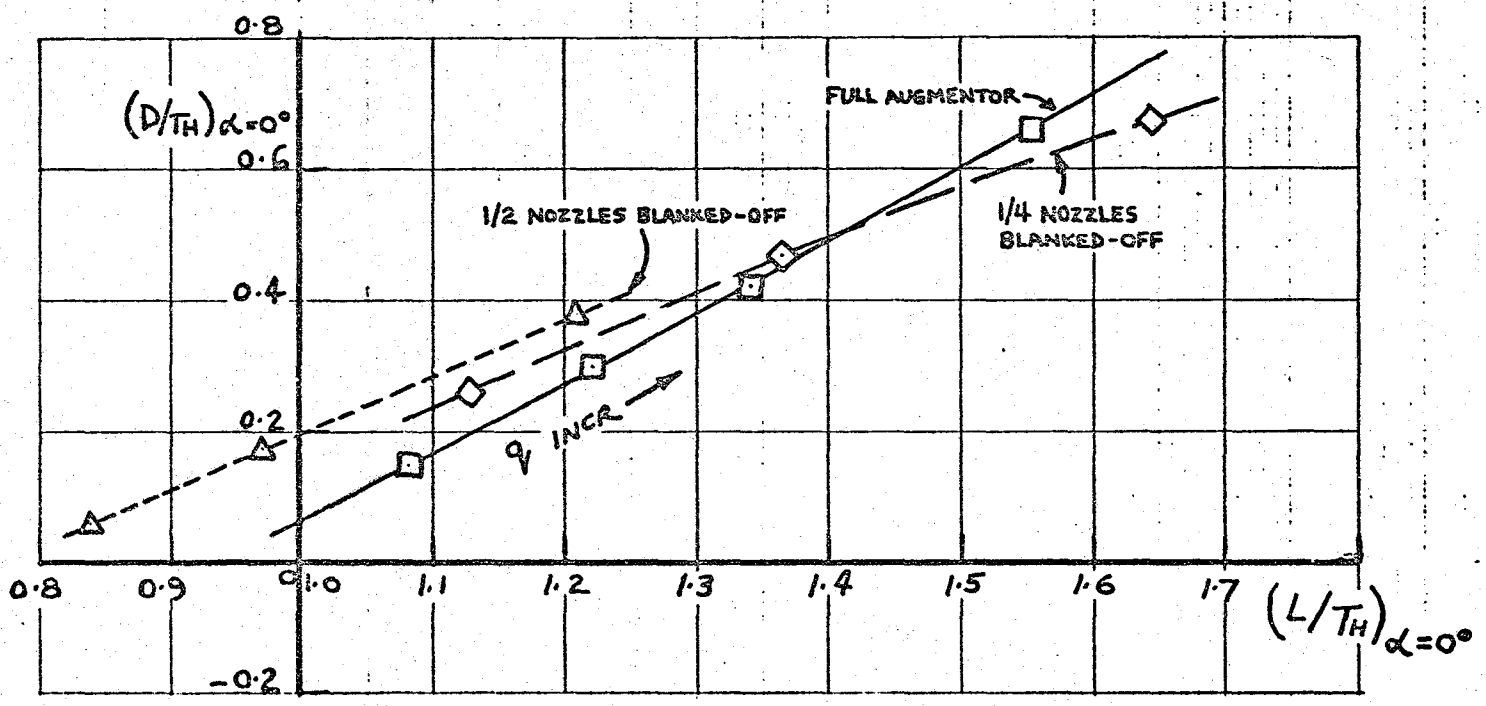

Fig. 23

Fig. 24

EFFECT OF BLANKING NOZZLES ON L/T_H vs D/T_H

AT q = 40 psf: δ_F=30°: TAIL OFF: DAR = 1.0 RPR = 2.3: RAKE OFF

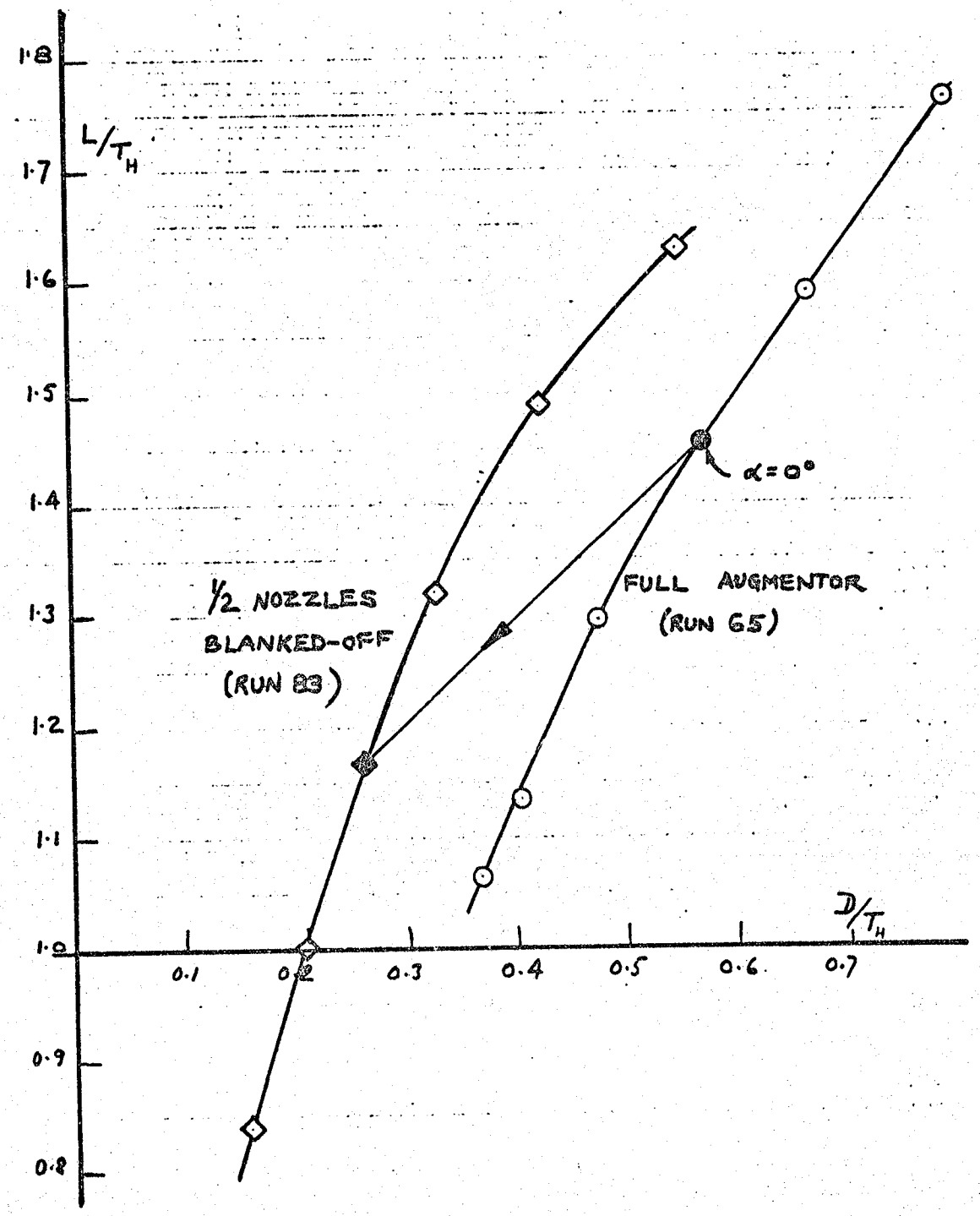

EFFECT OF THRUST TRANSFER ON DRAG

$\delta_F = 30°$: RPR = 2·3

TAIL OFF : RAKE OFF

DAR = 1·0

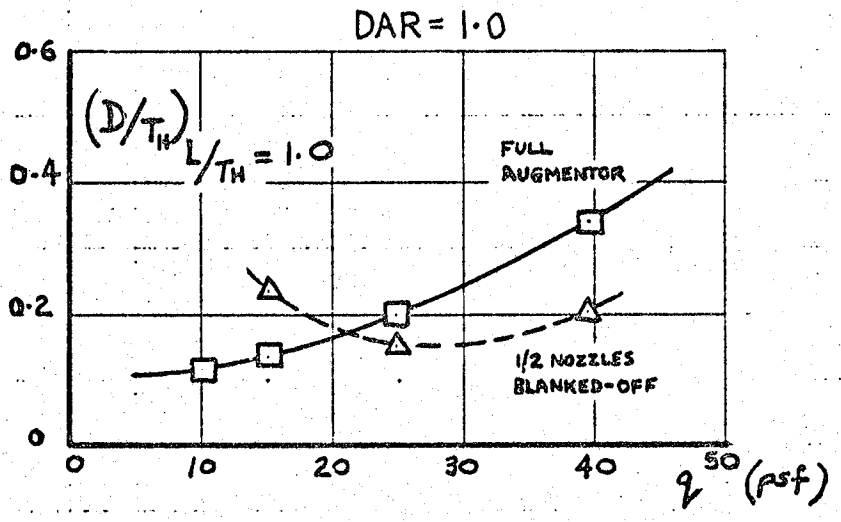

Fig. 26

EFFECT OF BLANKING NOZZLES ON AUGMENTOR

EXIT RAKE MASS FLOW AT $q = 0$ DAR = 1.0

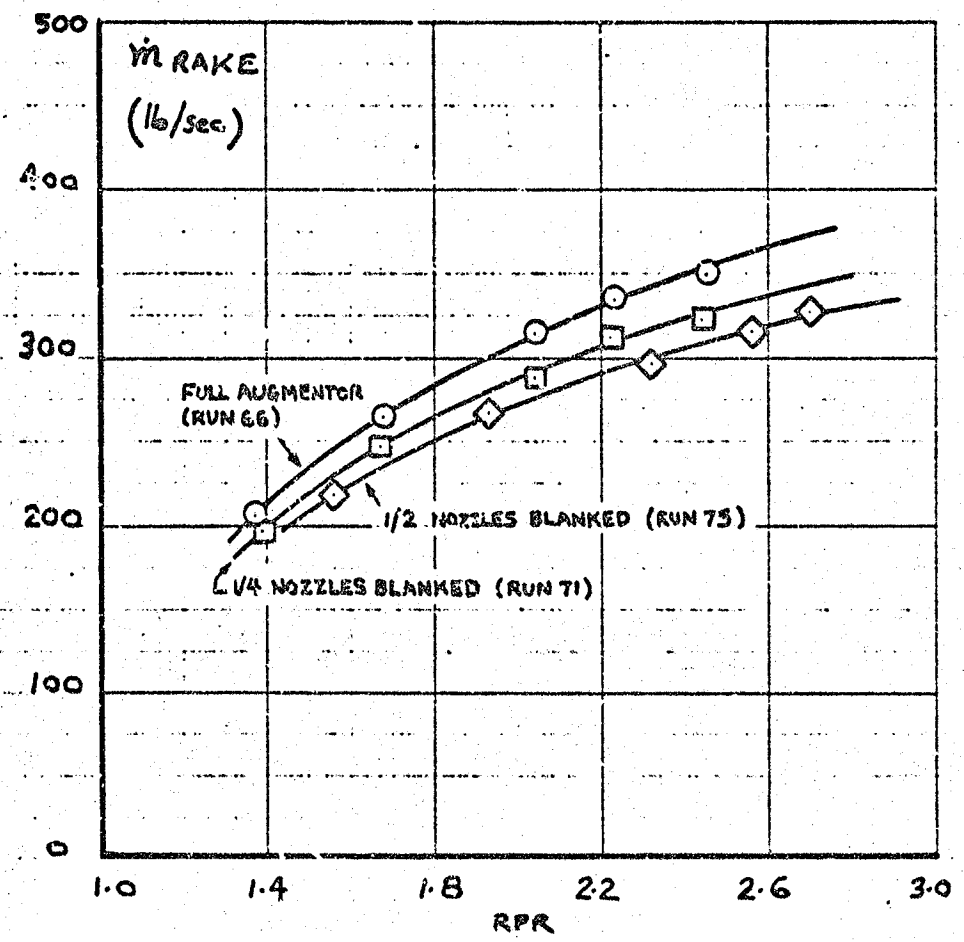

Fig. 27

EFFECTIVE LIFT COEFFICIENT $\delta_F = 0^0$

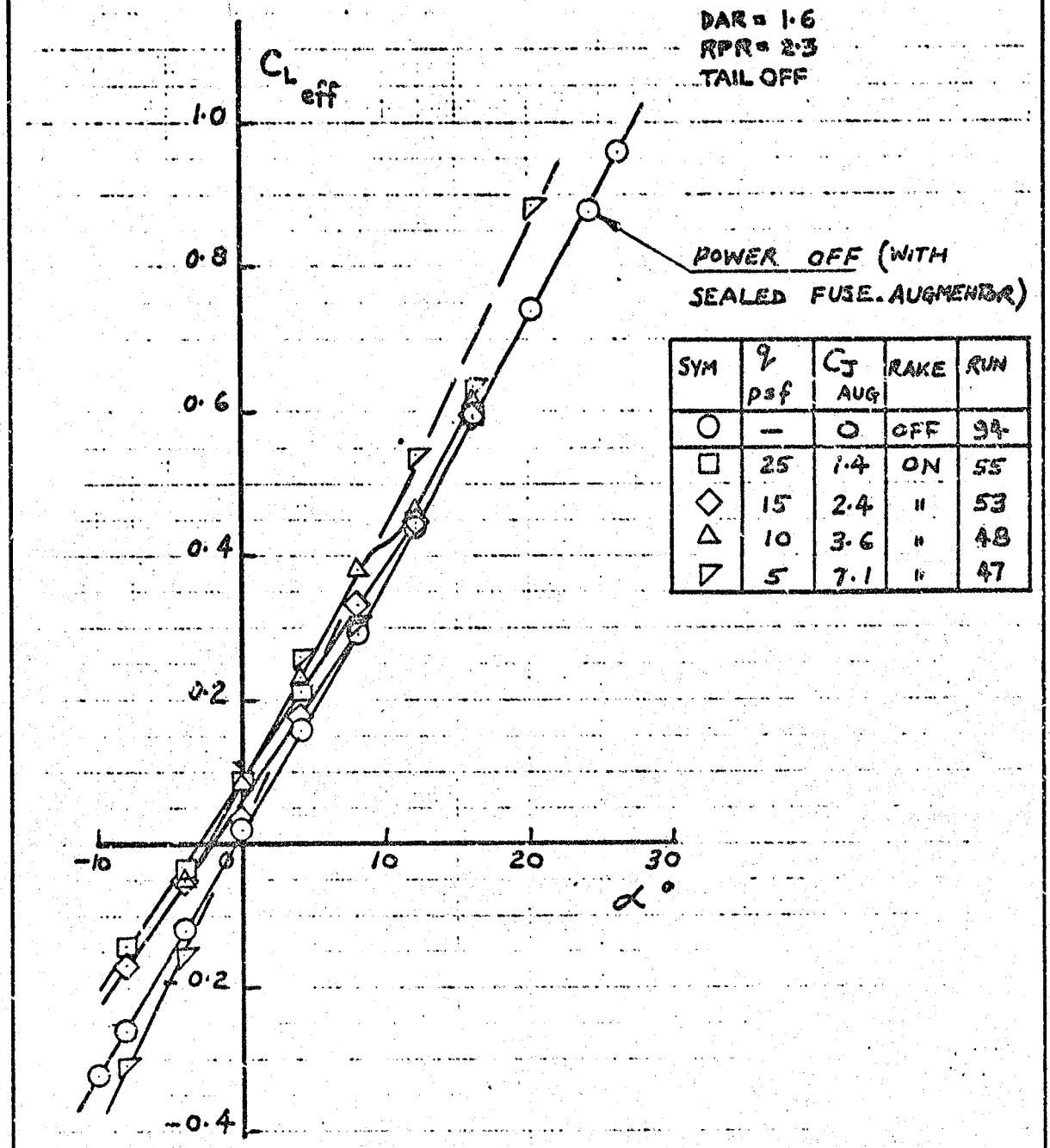

SYM	q psf	C_J AUG	RAKE	RUN
○	—	0	OFF	94
□	25	1.4	ON	55
◇	15	2.4	"	53
△	10	3.6	"	48
▽	5	7.1	"	47

Fig. 27(a)

EFFECTIVE LIFT COEFFICIENT AT $\delta_F = 30^\circ$

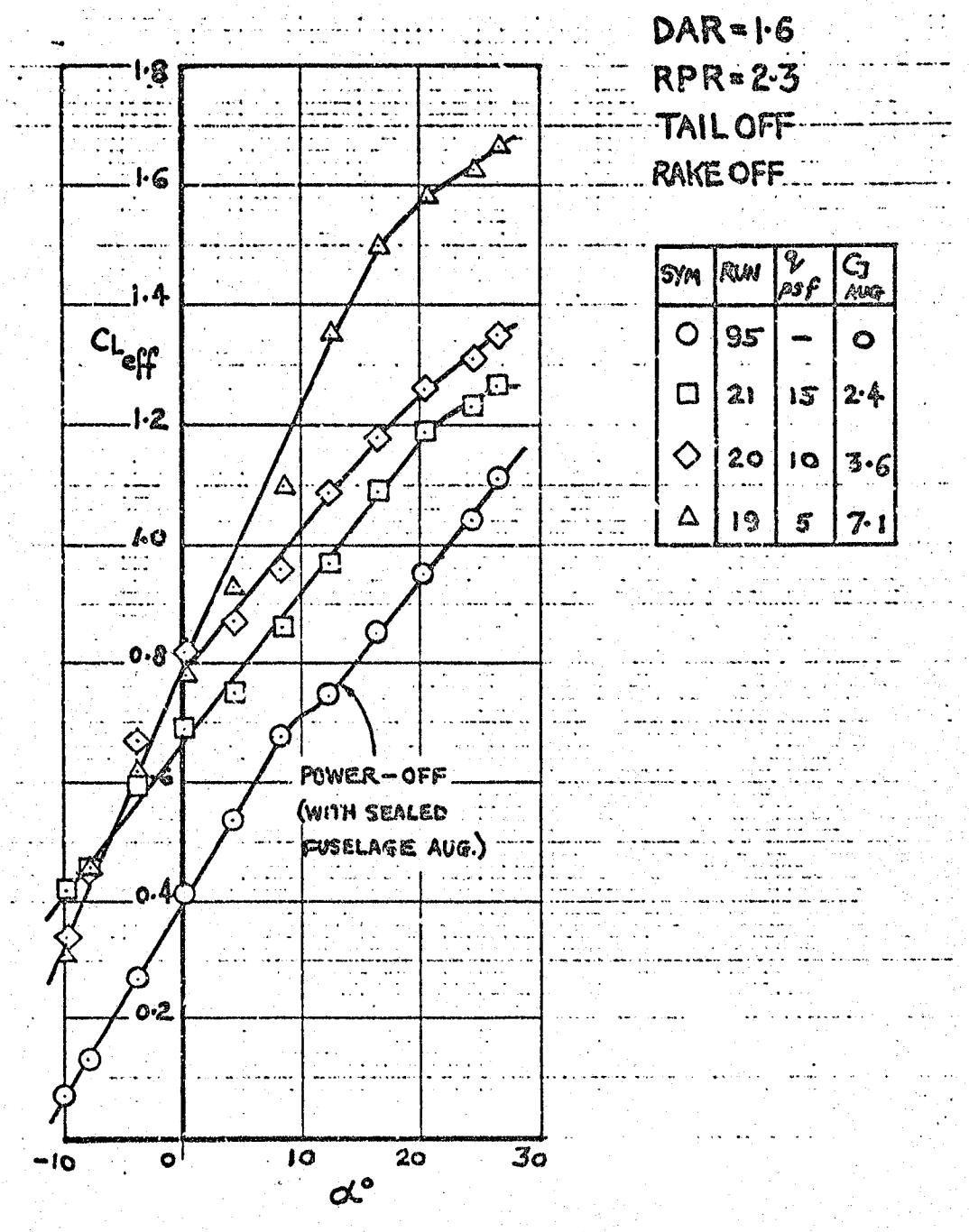

Fig. 27(b)

EFFECTIVE LIFT COEFFICIENT AT $\delta_F = 60^\circ$

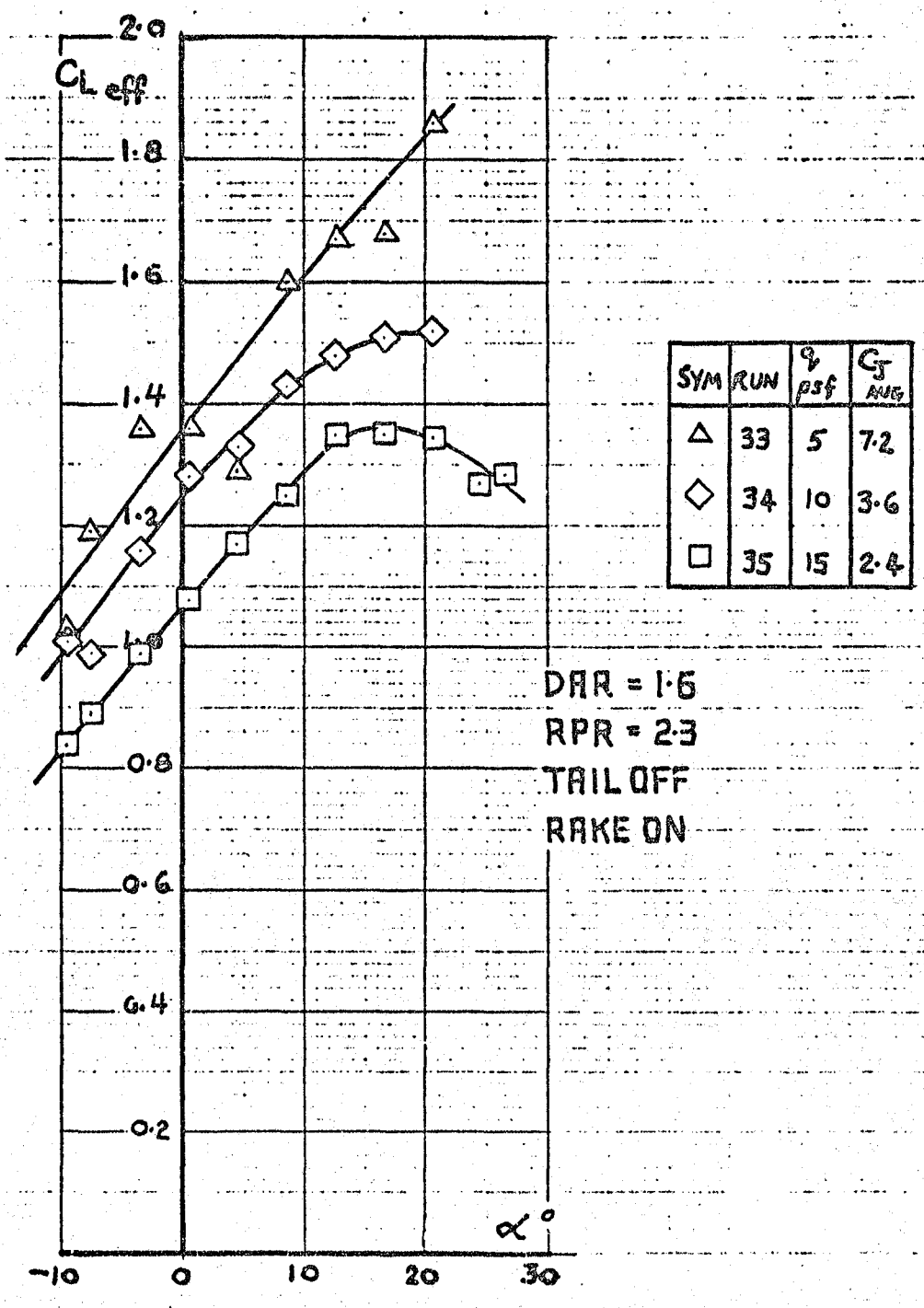

Fig. 28

EFFECT OF FLAP ANGLE ON $C_{L_{eff}}$ AT $\alpha = 0^\circ$

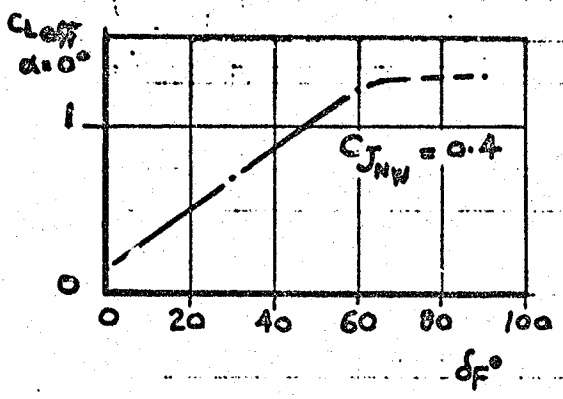

DAR = 1.6

SYM	δ_F	q psf	RUN	RAKE
○	0	25	54	ON
□	30	10 25	27 28	ON
◇	60	10	36	ON
△	90	5 10	13 14	OFF

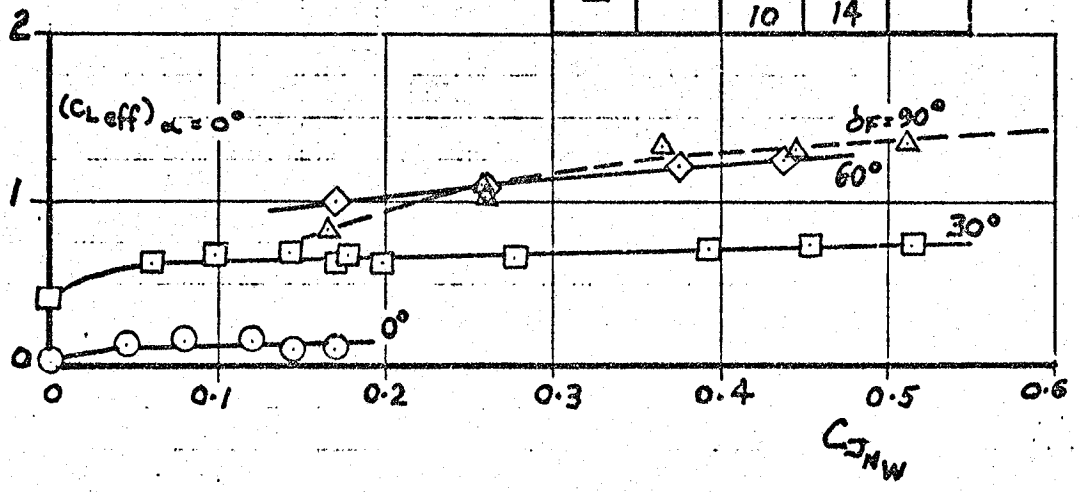

Fig. 29

CONFIGURATION EFFECTS ON EFFECTIVE LIFT

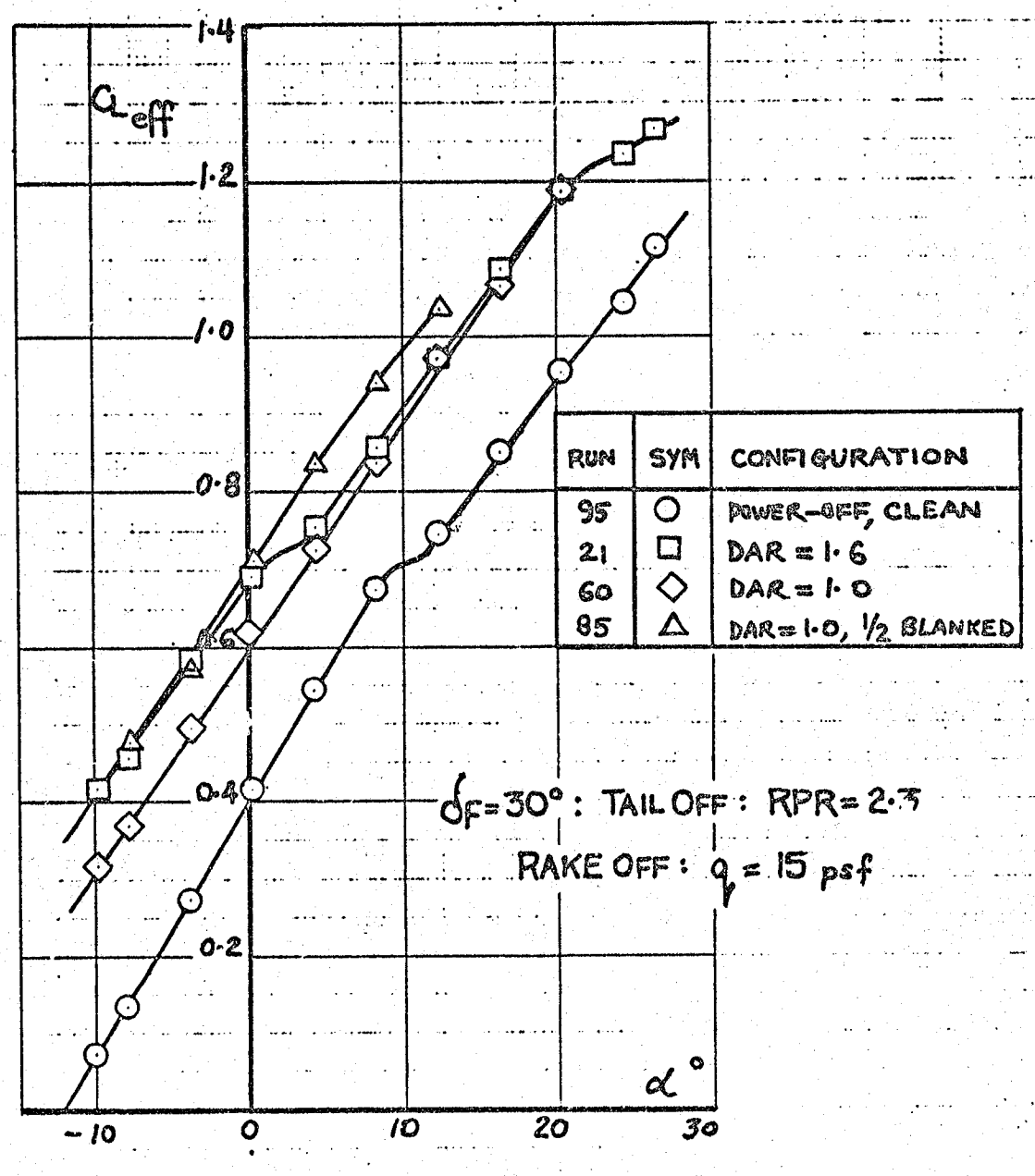

EFFECTIVE DRAG COEFFICIENT, $\delta_F = 0^o$

SYM	RUN	q psf	C_J AUG	RAKE
○	94	—	0	OFF
□	55	25	1.4	ON
◇	53	15	2.4	"
△	48	10	3.6	"
▽	47	5	7.1	"

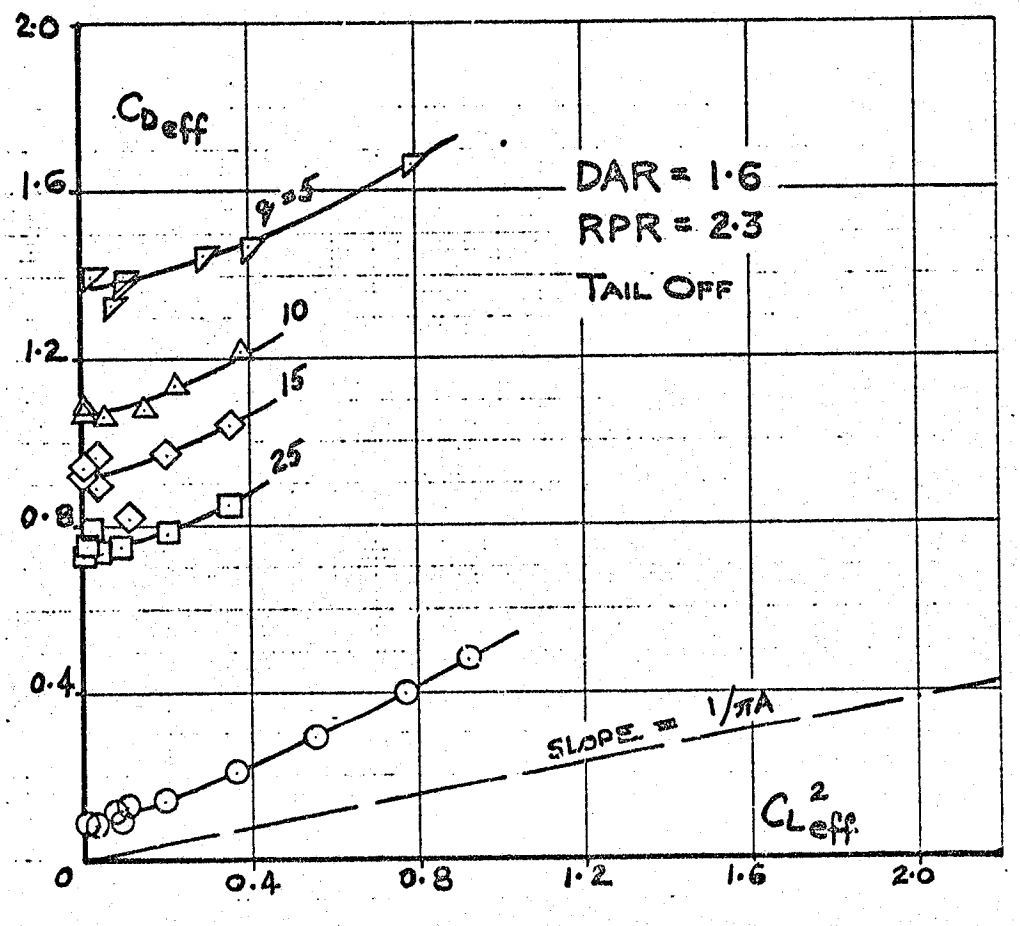

Fig. 30(a)

EFFECTIVE DRAG COEFFICIENT, $\delta_F = 30^\circ$

DAR = 1.6: RPR = 2.3: RAKE OFF: TAIL OFF

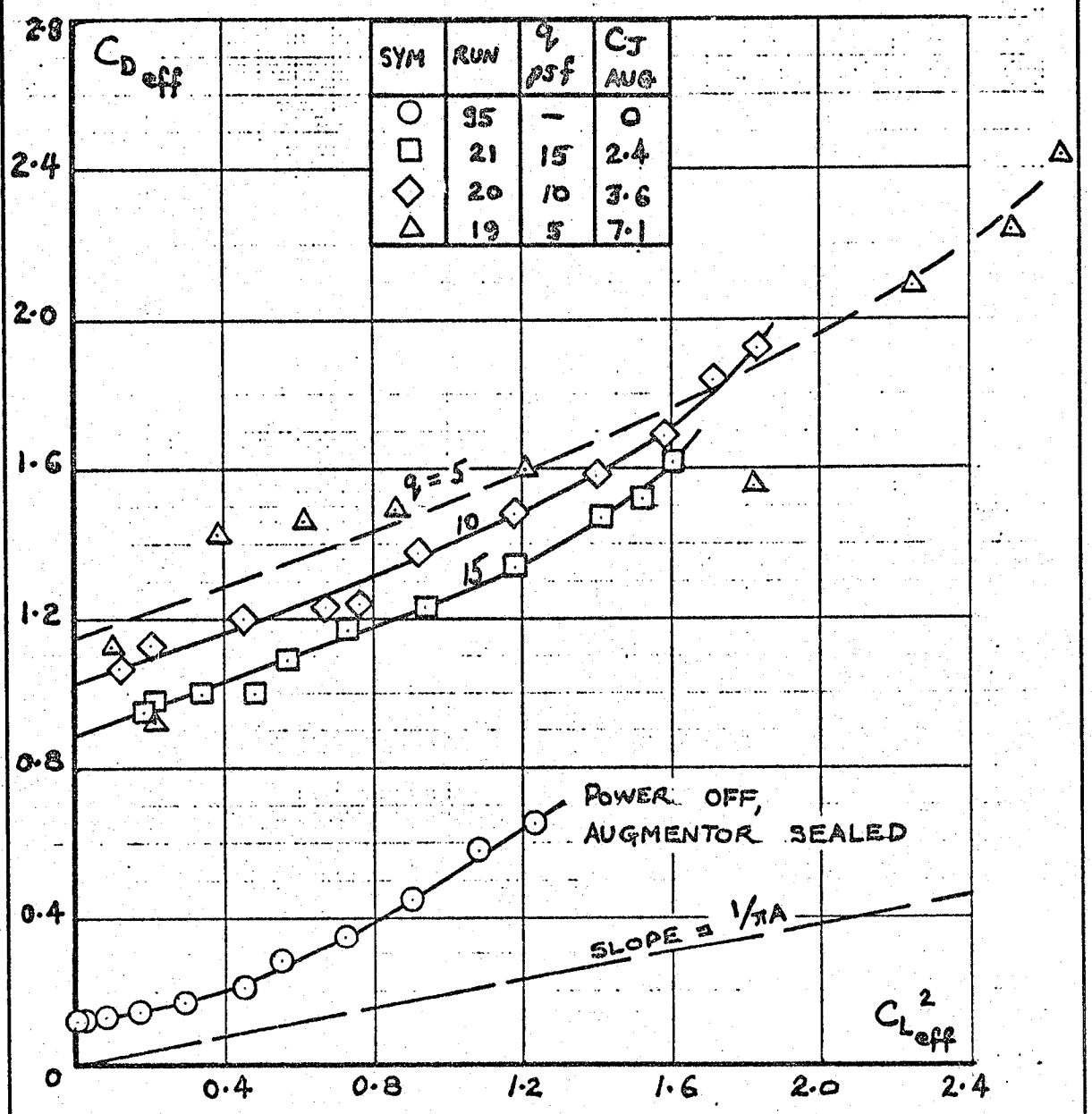

Fig. 30(b)

EFFECTIVE DRAG COEFFICIENT, $\delta_F = 60^0$

DAR = 1.6: RPR = 2.3: TAIL OFF: RAKE ON

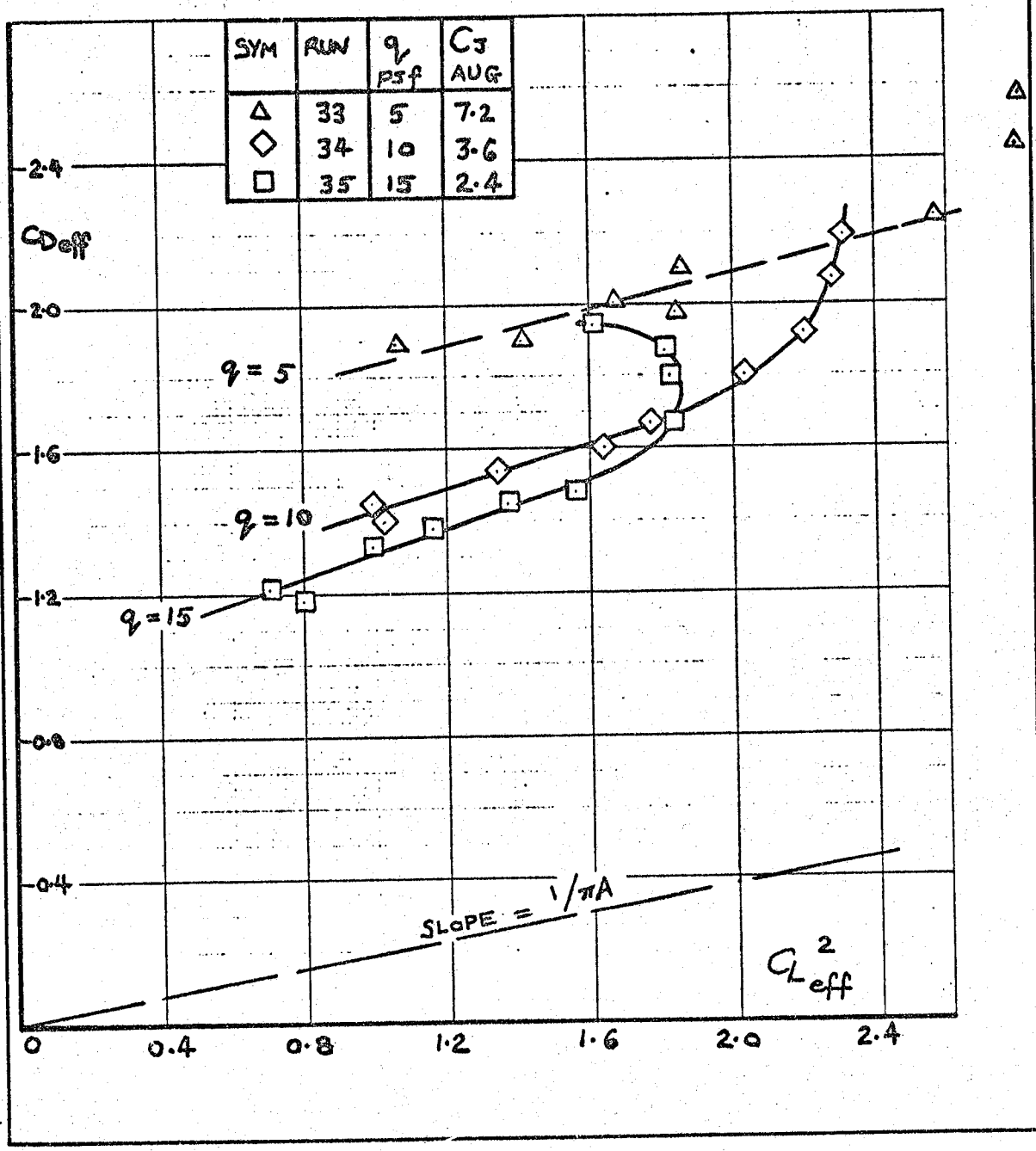

Fig. 31

EFFECT OF FLAP ANGLE ON $C_{D_{eff}}$ vs $C_{L^2_{eff}}$

$q = 15$ psf; RPR = 2.3; $C_{J_{AUG}} \approx 2.4$

DAR = 1.6 ; TAIL OFF

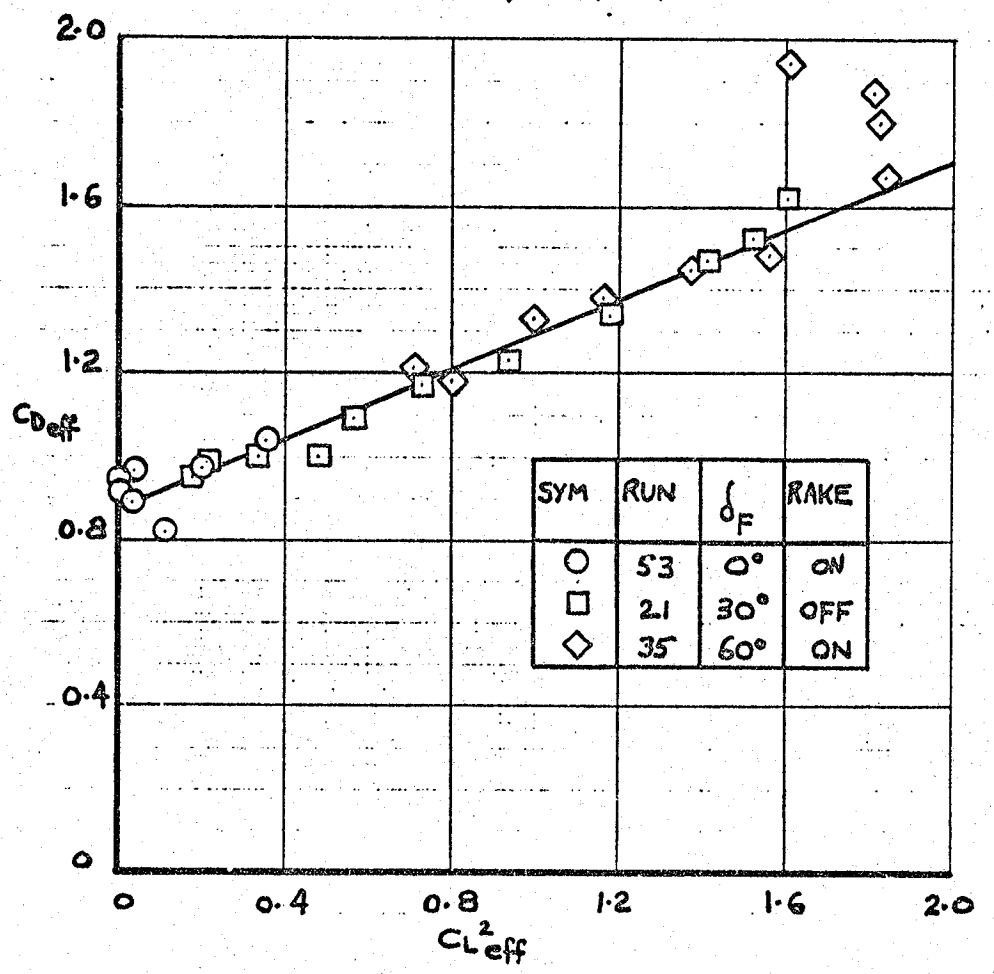

DRAG COMPONENTS, $\delta_F = 0^0$, $\alpha = 0^0$, RPR = 2.3

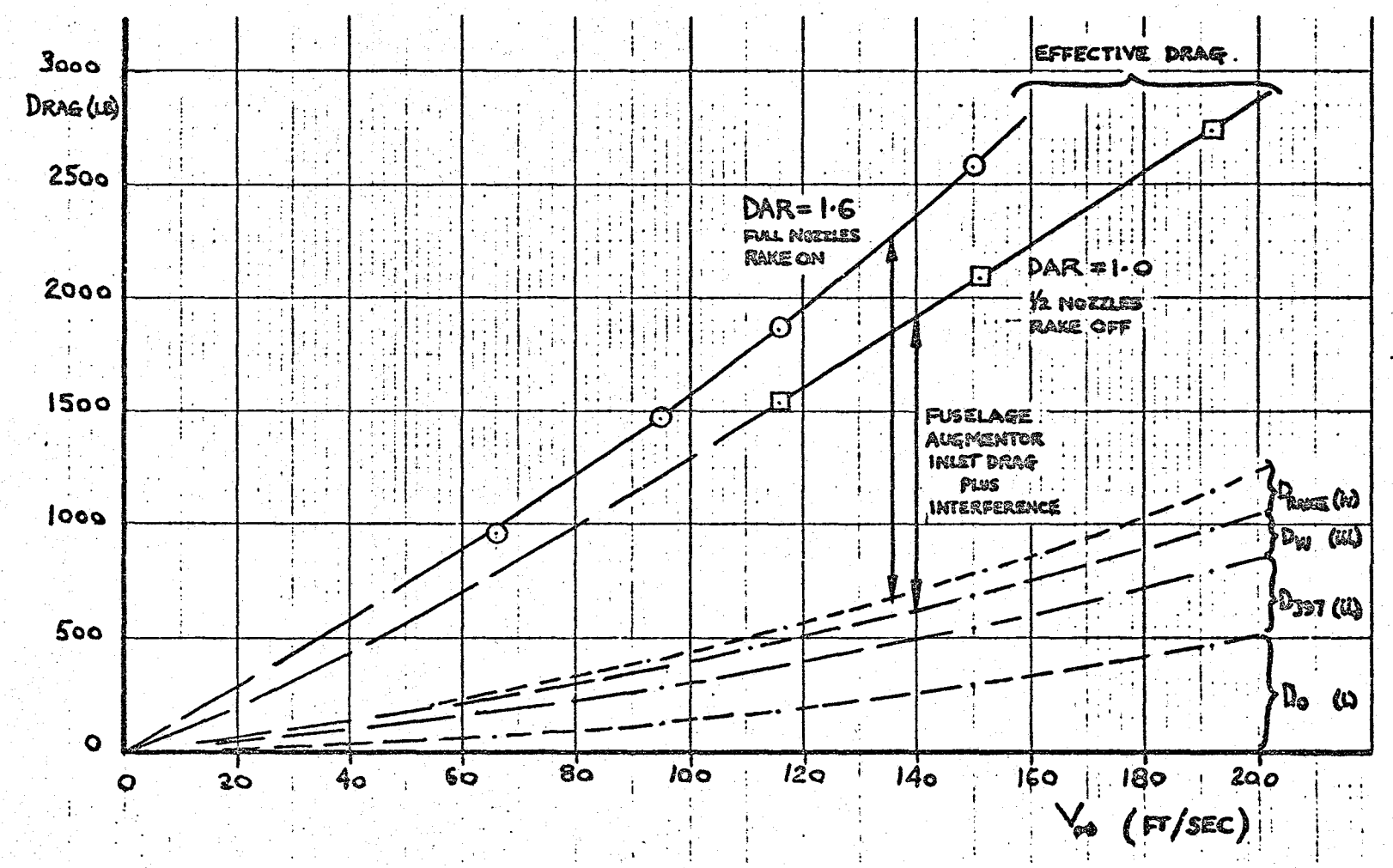

Fig. 32

Fig. 33

DERIVED FUSELAGE AUGMENTOR INLET FLOWS

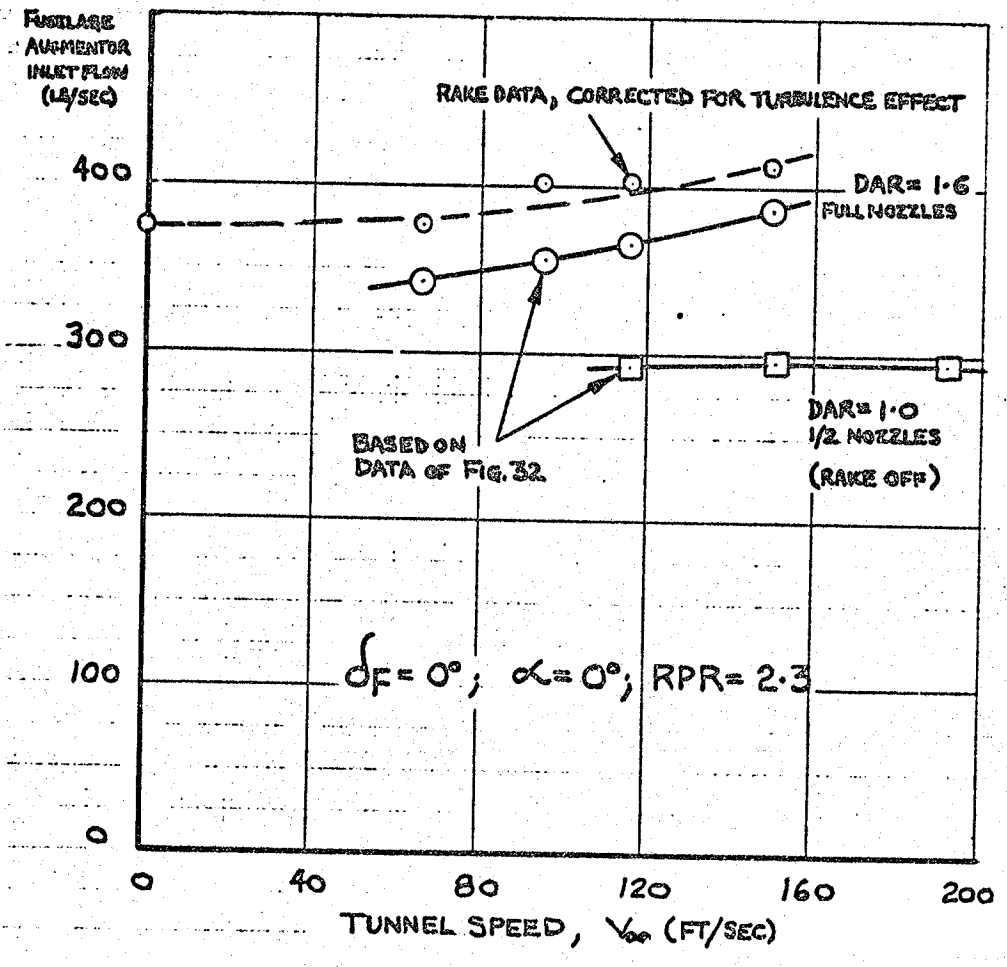

Fig. 34

MEASURED AND DERIVED AUGMENTOR INLET FLOW, $\delta_F = 0^\circ$

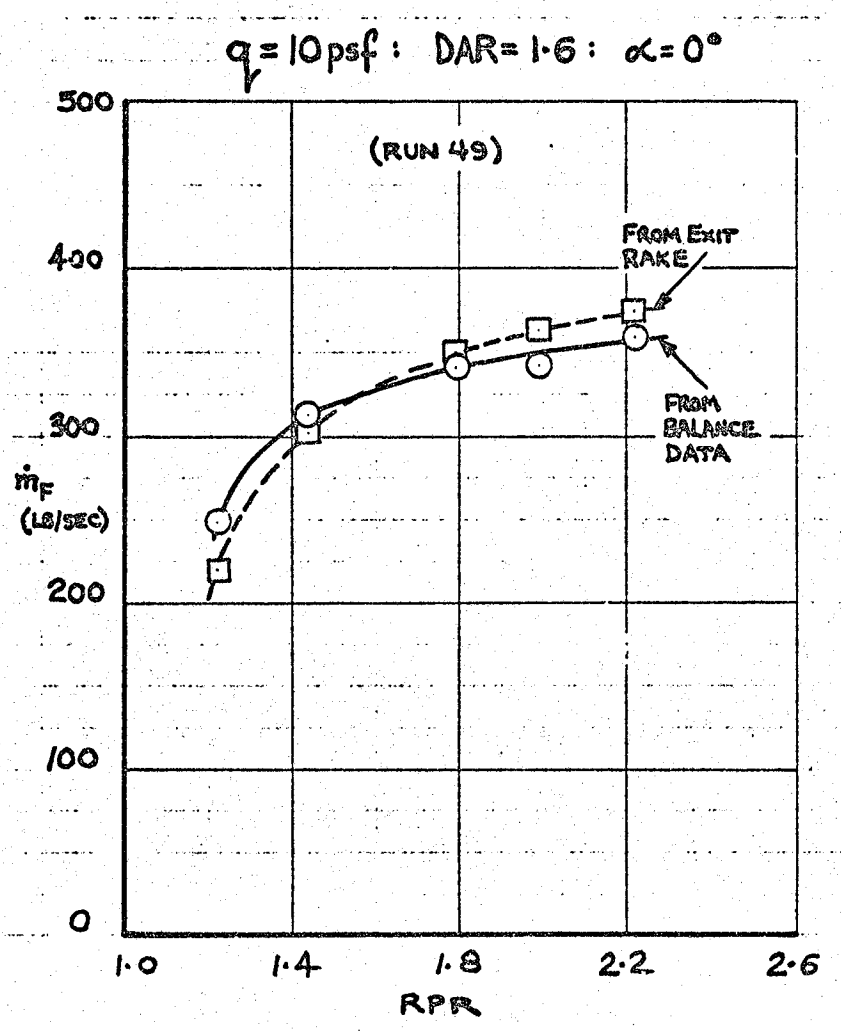

Fig. 34(a)

MEASURED AND DERIVED AUGMENTOR INLET FLOW, $\delta_F = 0^\circ$

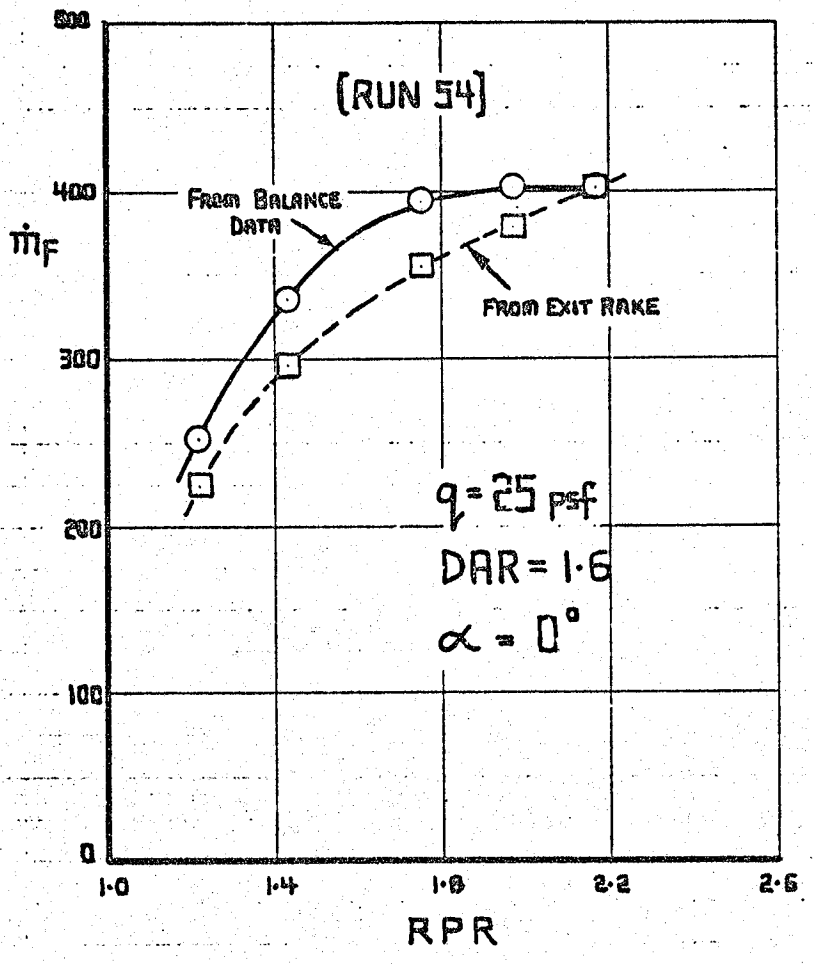

Fig. 35

PITCHING MOMENT INDUCED BY FUSELAGE

AUGMENTOR INFLOW

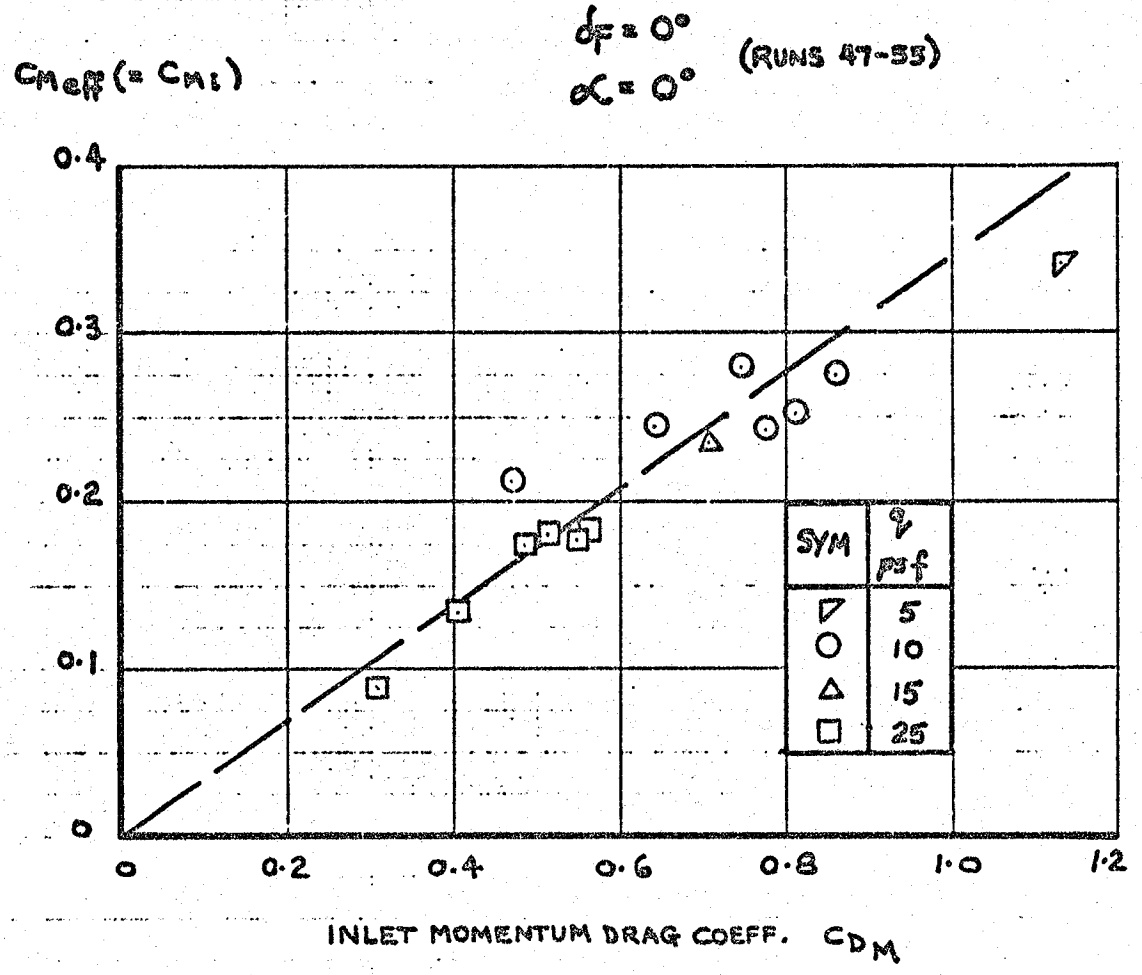

EFFECT OF FLAP ANGLE ON $C_{M_{eff}}$ AT $\alpha = 0^\circ$

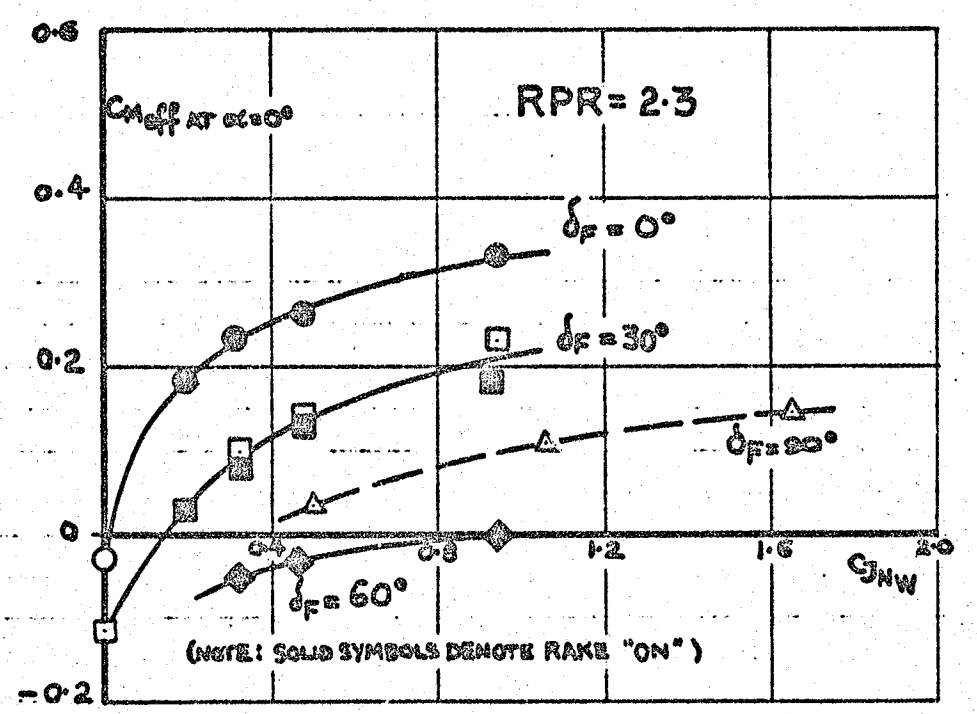

Fig. 37

$C_{M_{eff}}$ vs α: RPR = 2.3

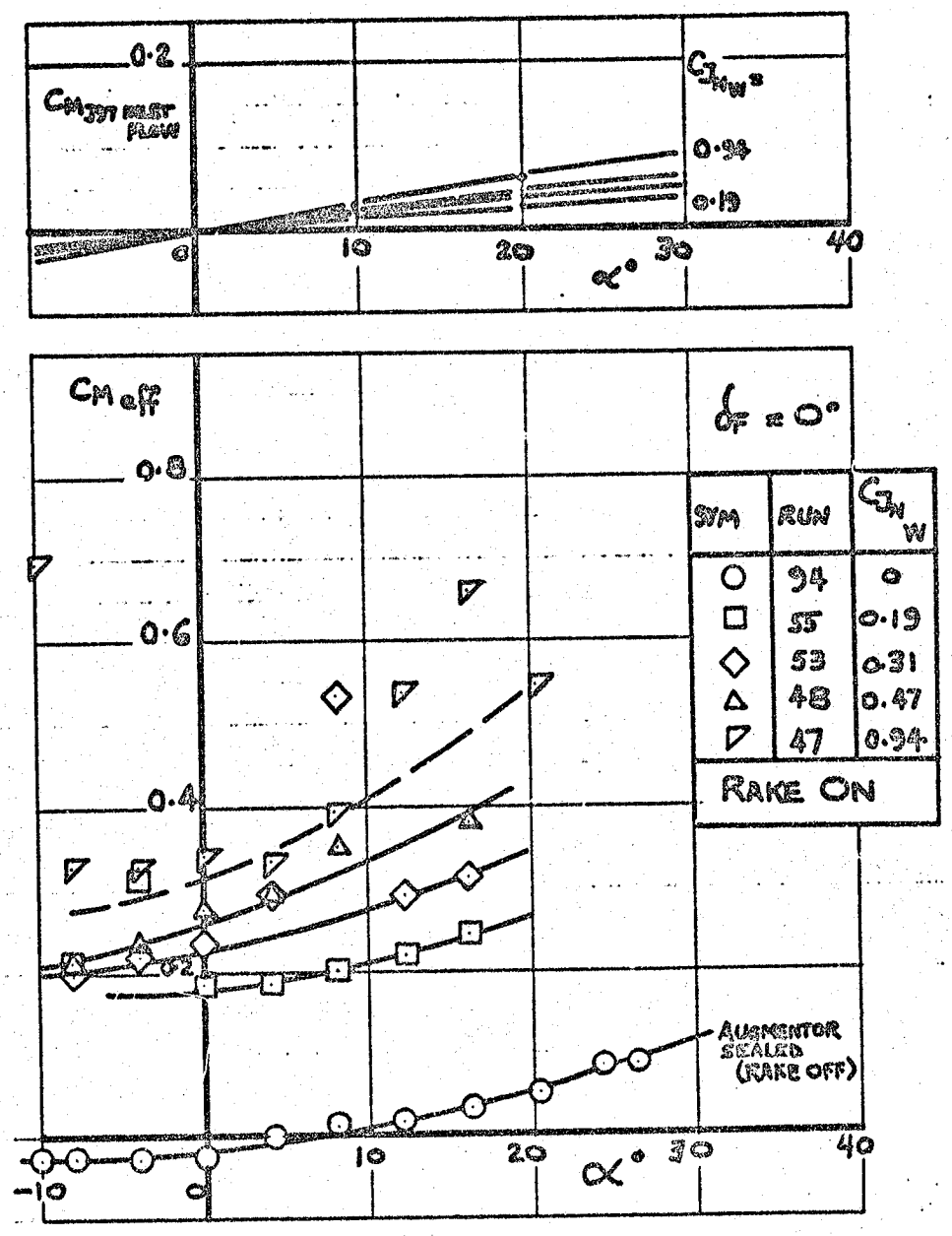

Fig. 37(a)

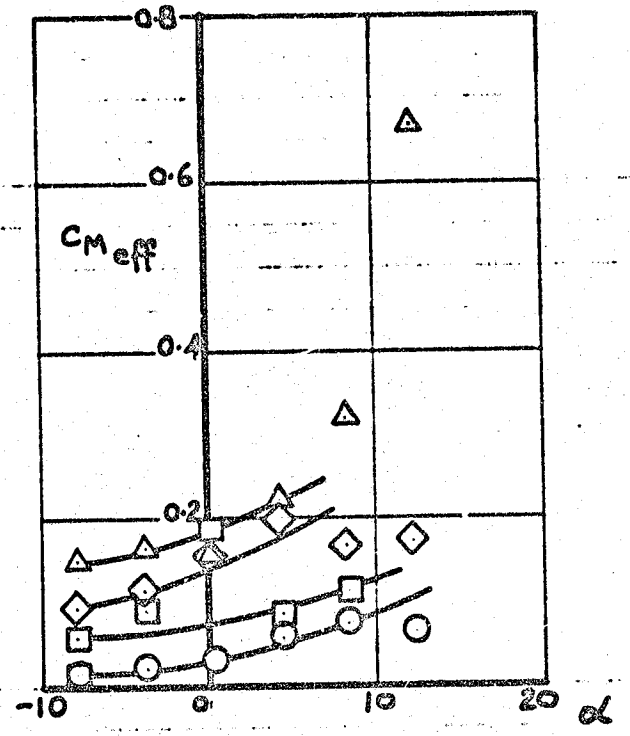

$\delta_f = 30°$

SYM	RUN	$C_{J_{N_W}}$
○	26	0·19
□	25	0·32
◇	24	0·47
△	23	0·93

RAKE ON

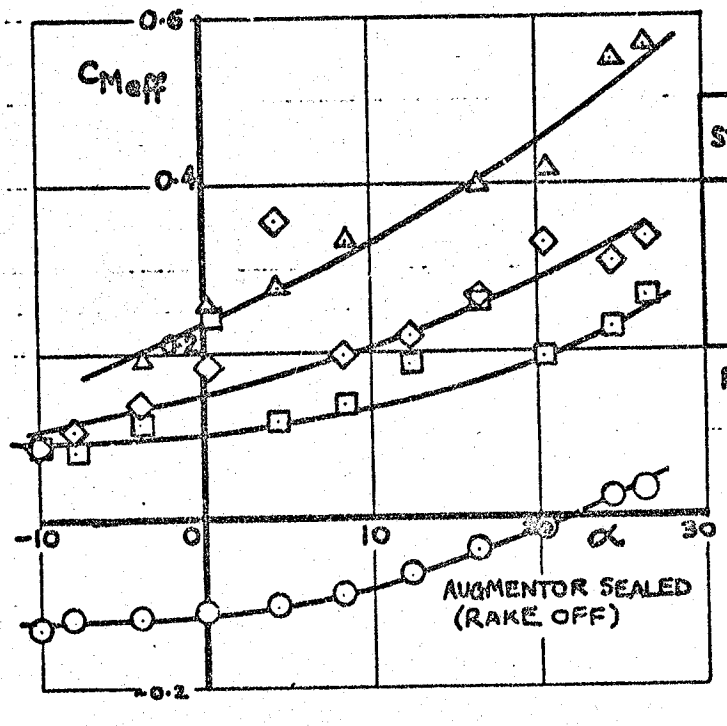

$\delta_f = 30°$

SYM	RUN	$C_{J_{N_W}}$
○	95	0
□	21	0·32
◇	20	0·47
△	19	0·94

RAKE OFF

Fig. 37(b)

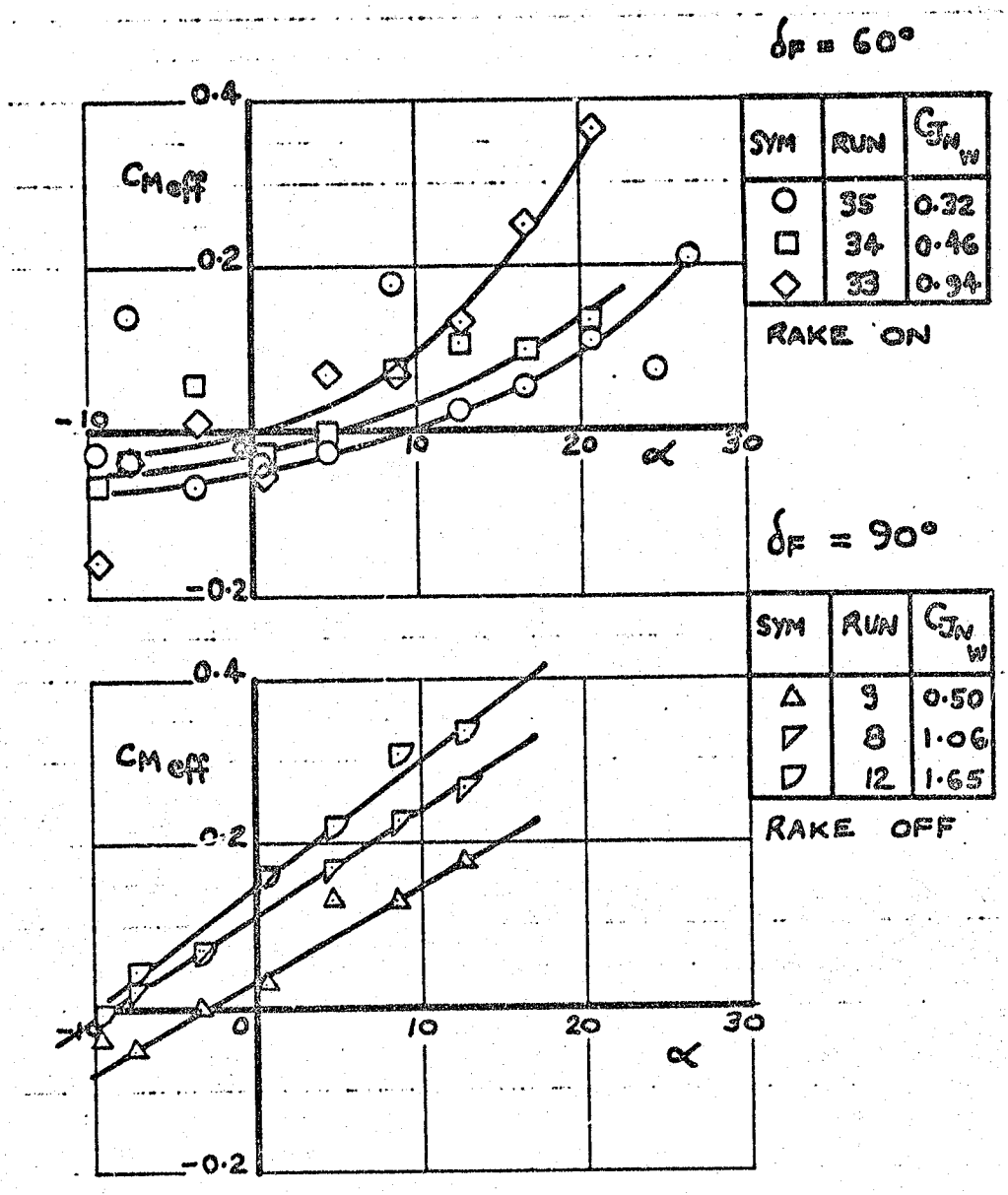
$\delta_F = 60°$
$C_{M_{eff}}$
0.4
0.2
-0.2
-10
0
10
20
30
α
SYM | RUN | $C_{J_{N_W}}$
○ | 35 | 0.32
□ | 34 | 0.46
◇ | 33 | 0.94
RAKE ON
$\delta_F = 90°$
$C_{M_{eff}}$
0.4
0.2
-0.2
-10
0
10
20
30
α
SYM | RUN | $C_{J_{N_W}}$
△ | 9 | 0.50
▽ | 8 | 1.06
▽ | 12 | 1.65
RAKE OFF

q = 15 psf

SYM	RUN	CONFIGURATION
○	69	FULL AUGMENTOR
□	72	¼ FRONT NOZZ. BLANKED
△	77	½ ALTERNATE NOZZ.

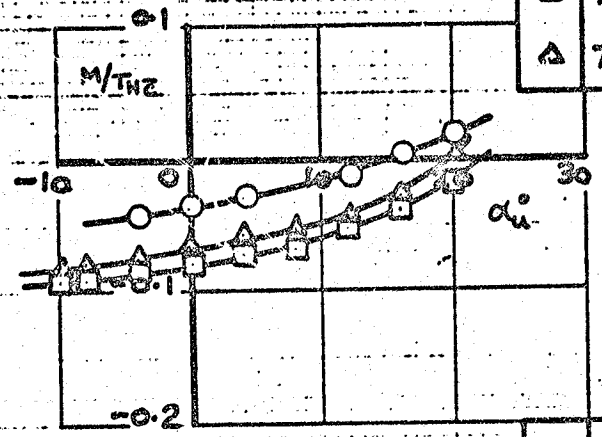

q = 25 psf

SYM	RUN	CONFIGURATION
○	70	FULL AUGMENTOR
□	73	¼ FRONT NOZZ. BLANKED
△	78	½ ALTERNATE NOZZLES

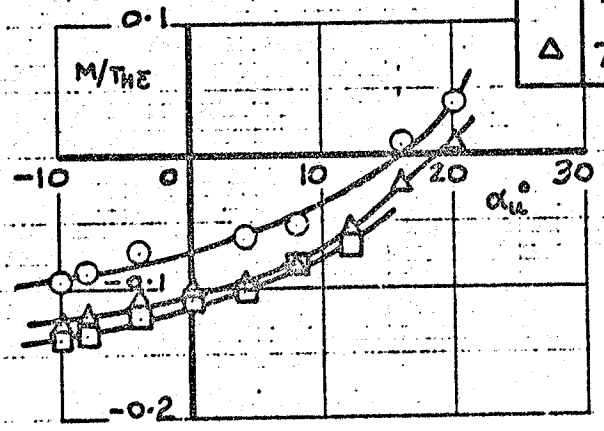

EFFECT OF FUSELAGE AUGMENTOR NOZZLE CONFIGURATION ON PITCHING MOMENT: δ_F=60°, TAIL OFF, RAKE ON

DAR = 1.0

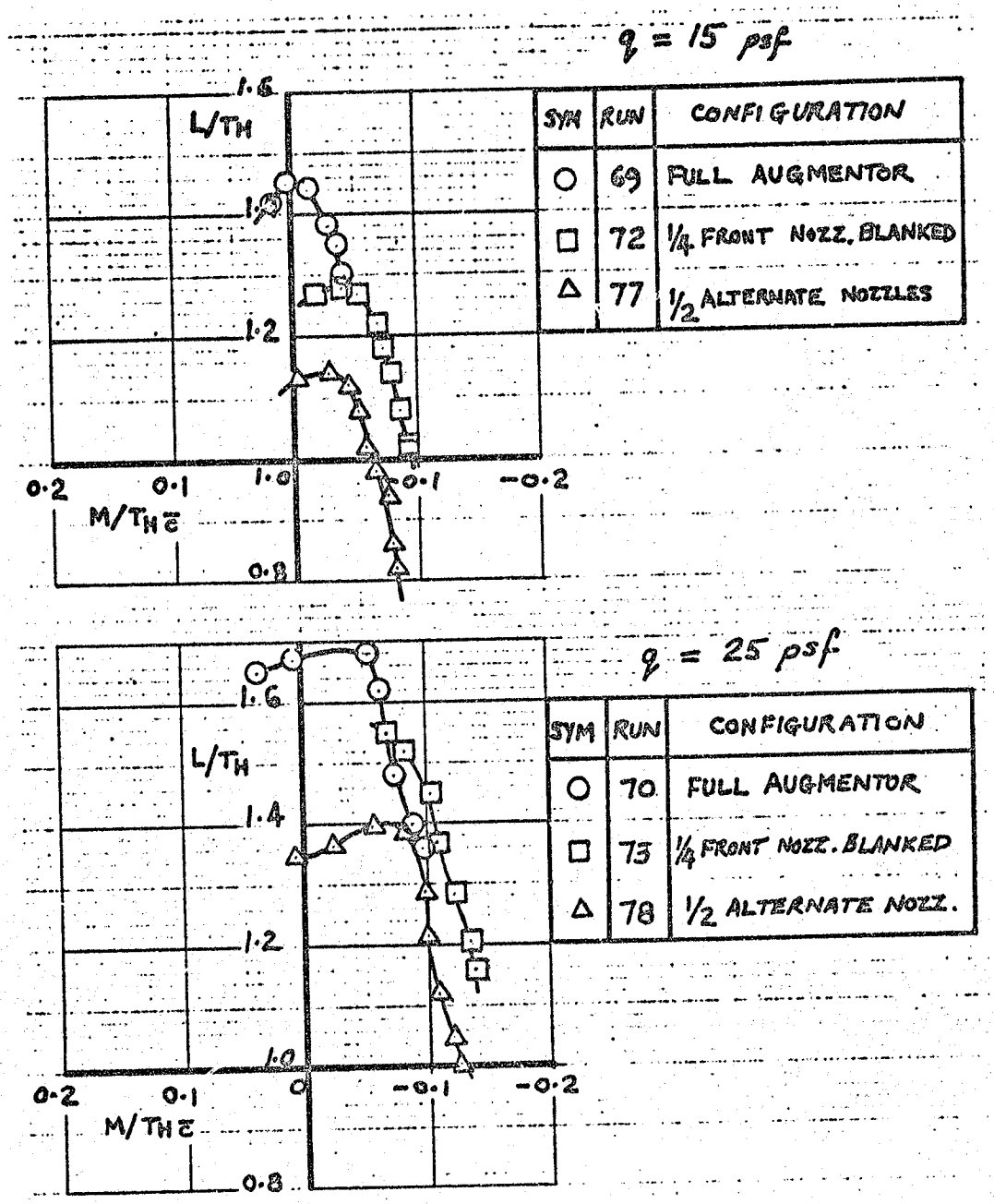

EFFECT OF FUSELAGE AUGMENTOR NOZZLE CONFIGURATION ON PITCHING MOMENT: δ_F=60°: TAIL OFF: RAKE ON: DAR = 1.0

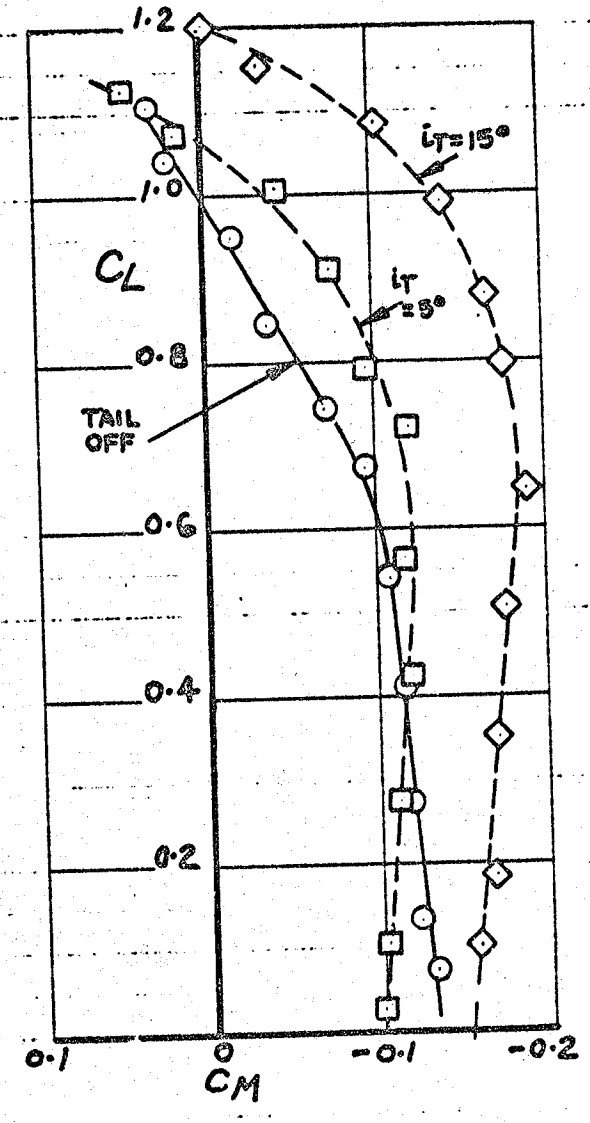

PITCHING MOMENT DUE TO TAIL: POWER-OFF: δ_F=30°

(FUSELAGE AUGMENTOR CLOSED-UP)

Fig. 41

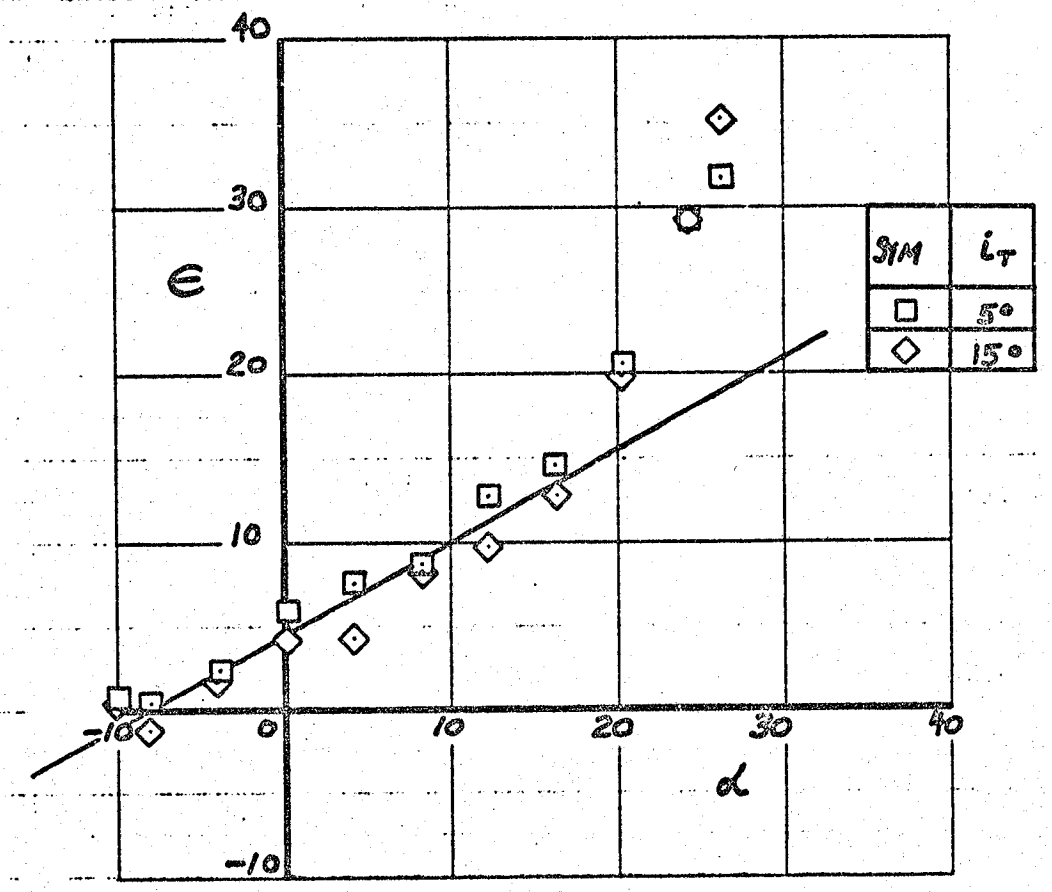

DOWNWASH, POWER-OFF; $\delta_F = 30^\circ$

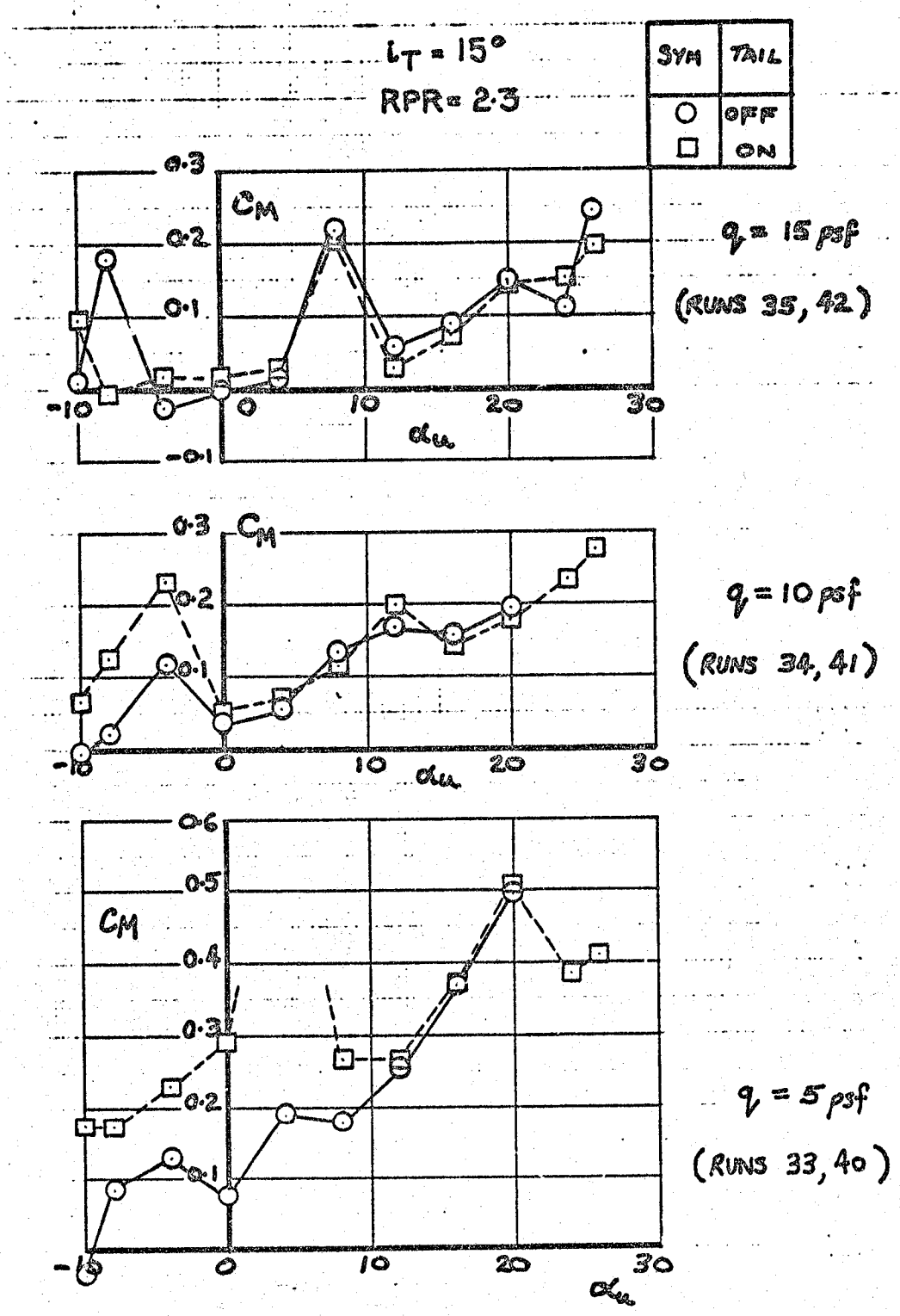

EFFECT OF TAIL, POWER ON AT δ_F=60°

Fig. 43

DOWNWASH, POWER-ON AT $\delta_F = 60^\circ$

RPR = 2·3

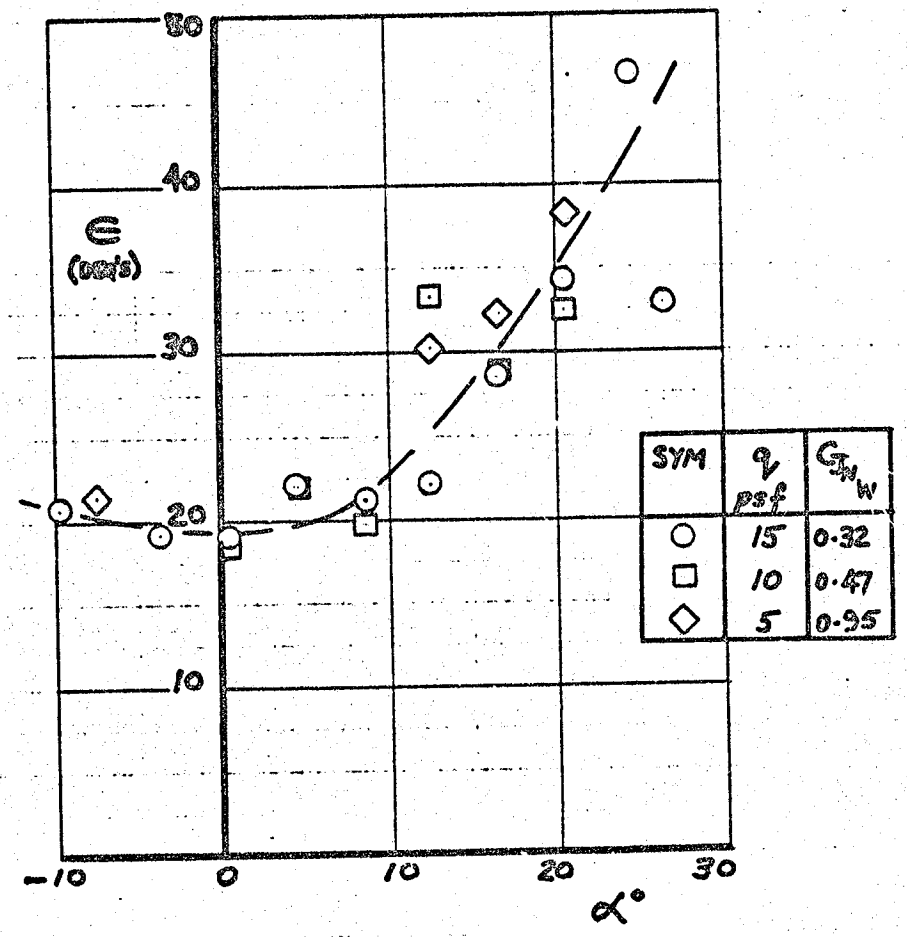

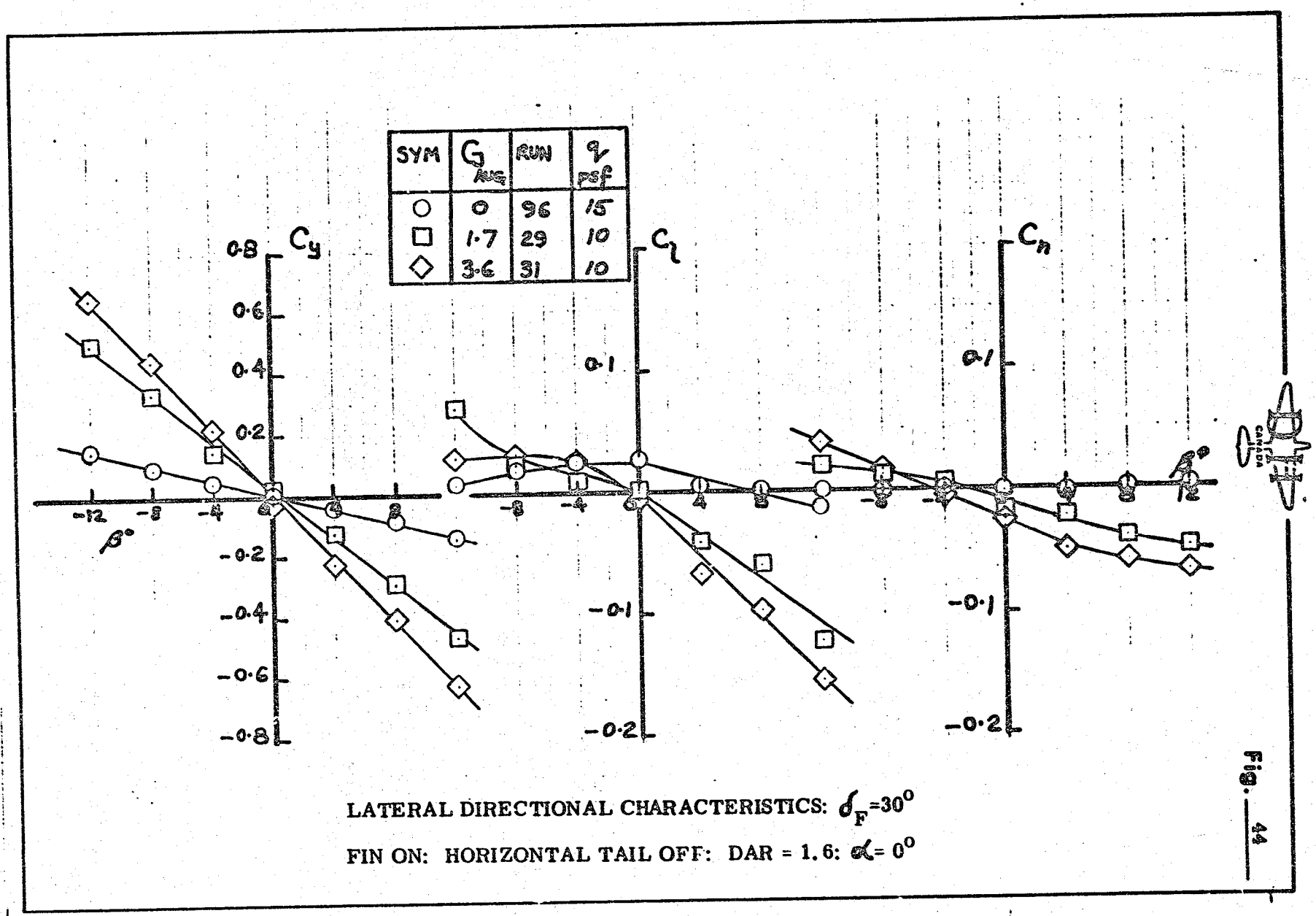

LATERAL DIRECTIONAL CHARACTERISTICS: $\delta_F = 30^\circ$

FIN ON: HORIZONTAL TAIL OFF: DAR = 1.6: $\alpha = 0^\circ$

Fig. 44

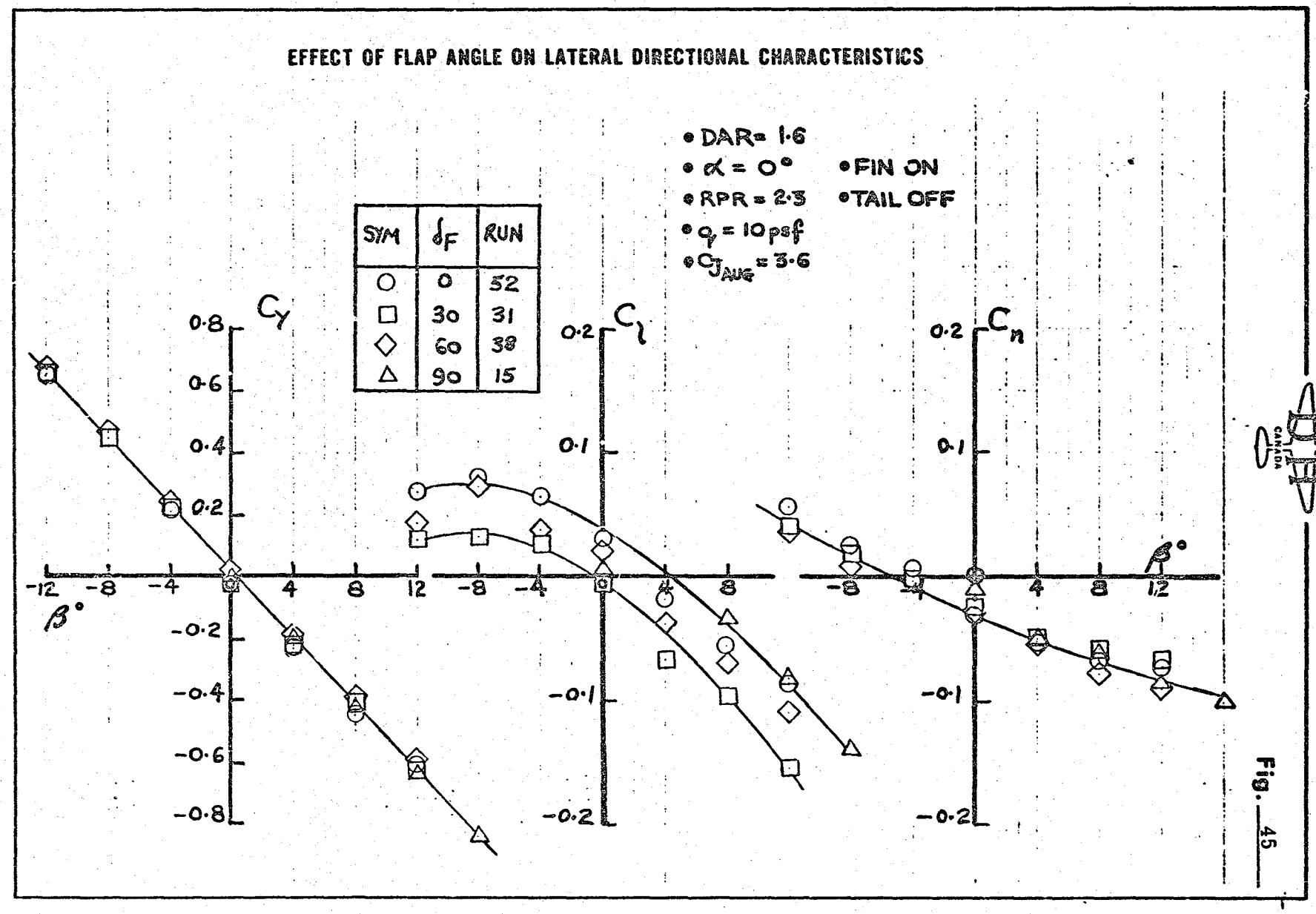
EFFECT OF FLAP ANGLE ON LATERAL DIRECTIONAL CHARACTERISTICS
• DAR = 1.6
• α = 0°
• RPR = 2.3
• q_f = 10 psf
• $C_{J_{AVG}}$ = 3.6
• FIN ON
• TAIL OFF
SYM | δ_F | RUN
○ | 0 | 52
□ | 30 | 31
◇ | 60 | 38
△ | 90 | 15
C_Y
C_l
C_n
β°
α°
0.8
0.6
0.4
0.2
-0.2
-0.4
-0.6
-0.8
0.2
0.1
-0.1
-0.2
-12
-8
-4
4
8
12
CANADA

Fig. 45

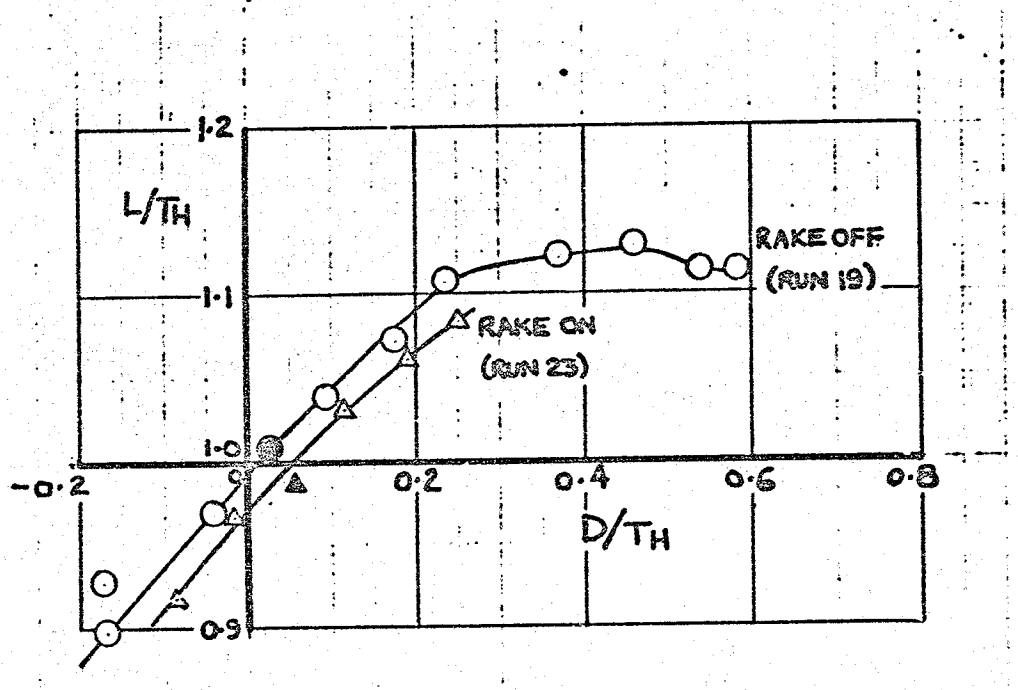

EFFECT OF RAKE ON L/T_H, D/T_H AT $q = 5$ psf

$\delta_F = 30^\circ$: DAR = 1.6: RPR = 2.3

Fig. 46

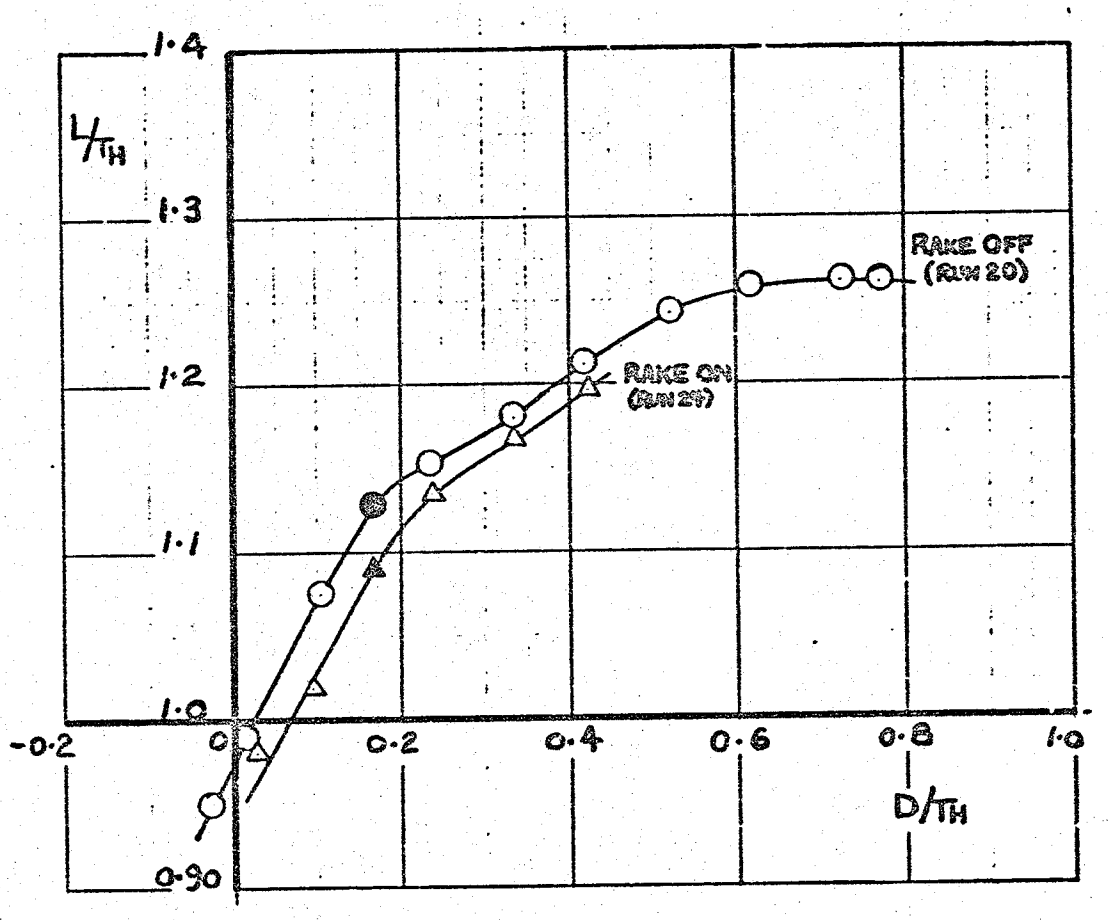

EFFECT OF RAKE ON L/T_H, D/T_H AT $q = 10$ psf

$\delta_F = 30^\circ$: DAR = 1.6: RPR = 2.3

Fig. 46(a)

Fig. 46(b)

EFFECT OF RAKE ON L/T_H, D/T_H AT $q = 15$ psf

$\delta_F = 30°$; DAR = 1·6 ; RPR = 2·3

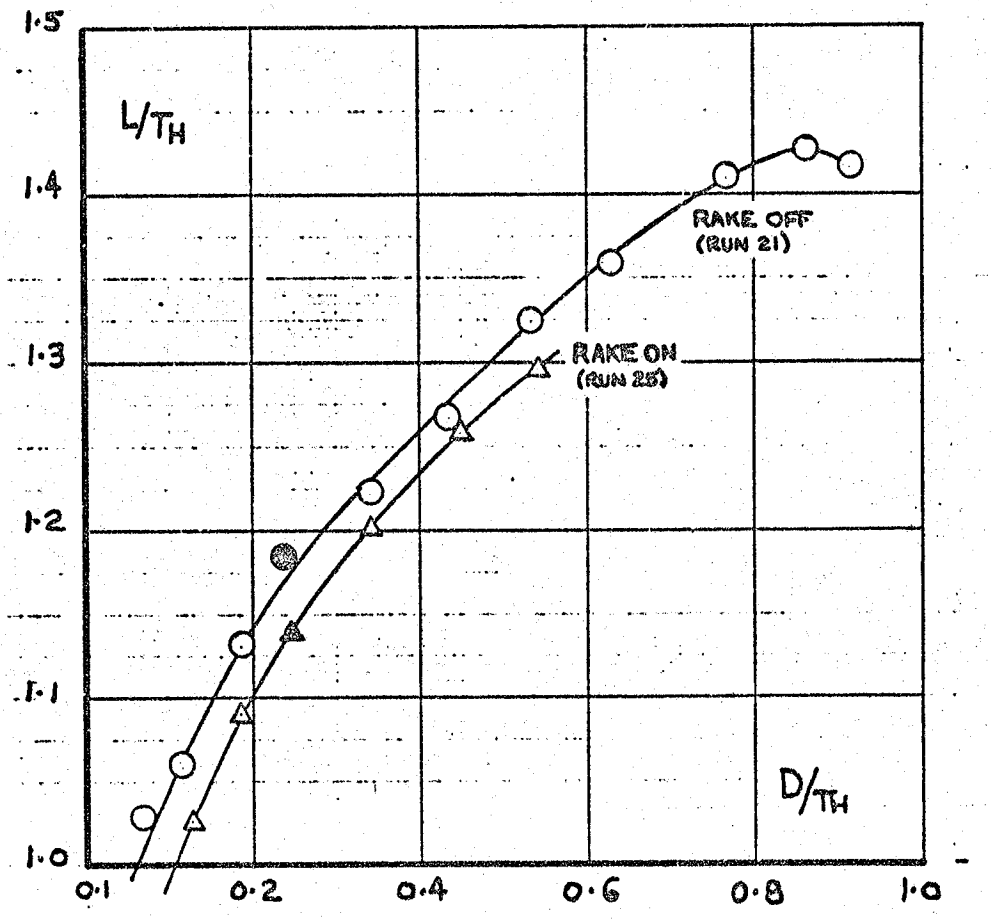

Fig. 46(e)

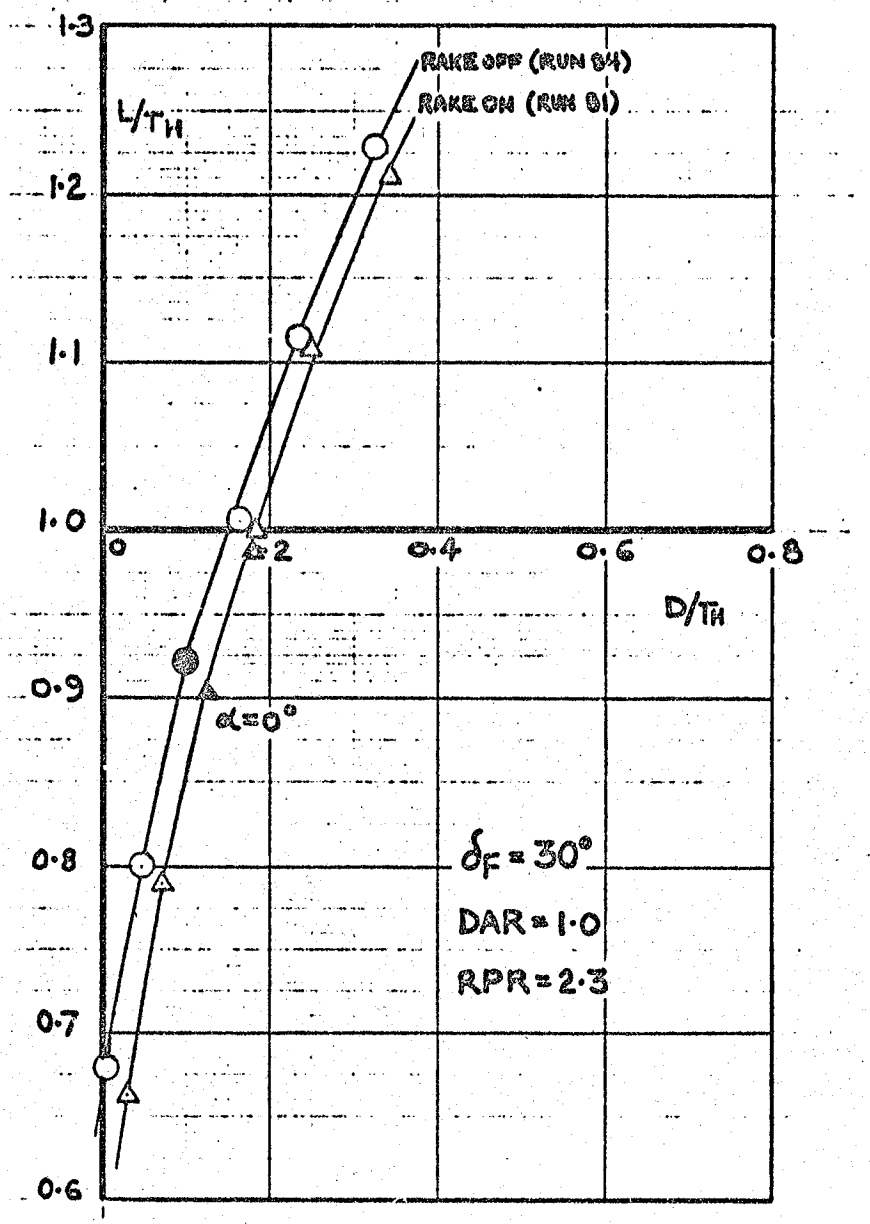

EFFECT OF RAKE ON L/T_H, D/T_H AT $q = 25\ psf$

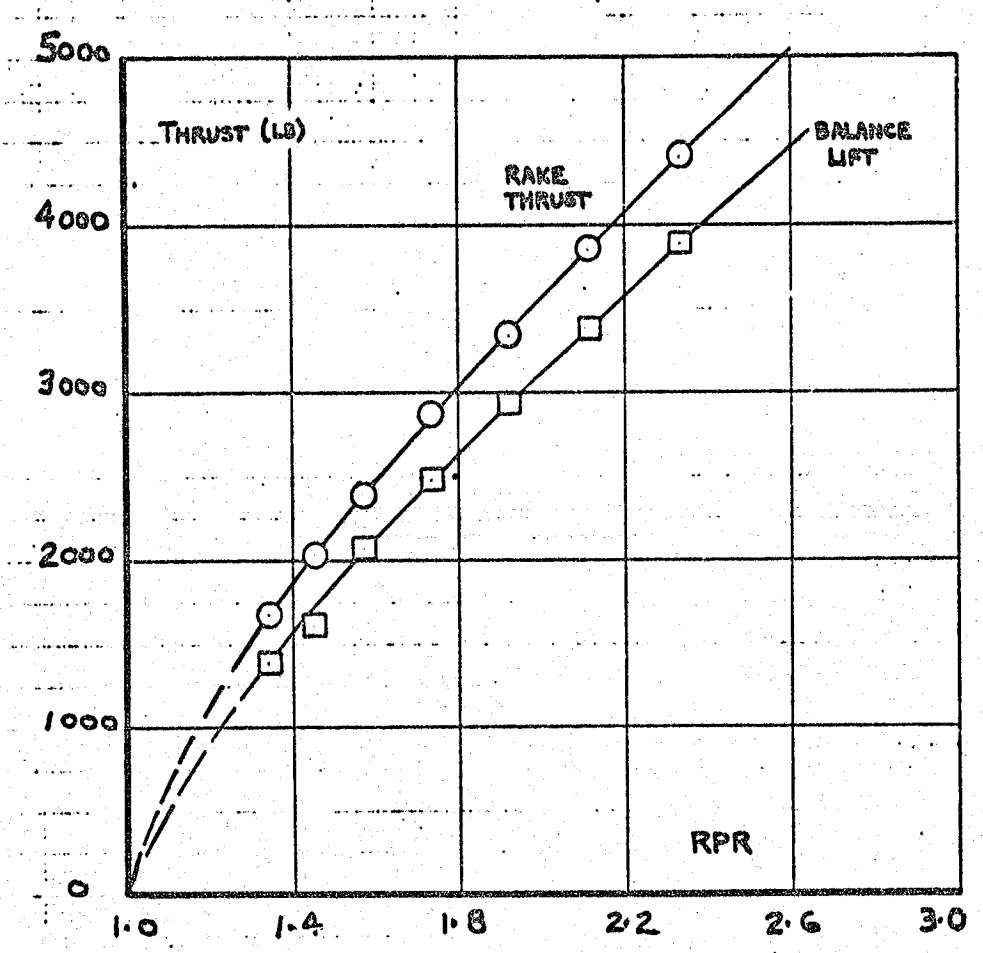

COMPARISON OF RAKE THRUST WITH BALANCE LIFT

$q = 0$: $\delta_F = 0^\circ$: DAR = 1.6 (RUN 46)

Fig. 48

LONGITUDINAL DISTRIBUTION OF THRUST

BY RAKE MEASUREMENT,

FUSELAGE AUGMENTOR: DAR = 1.6

q = 0 (RUN 46)

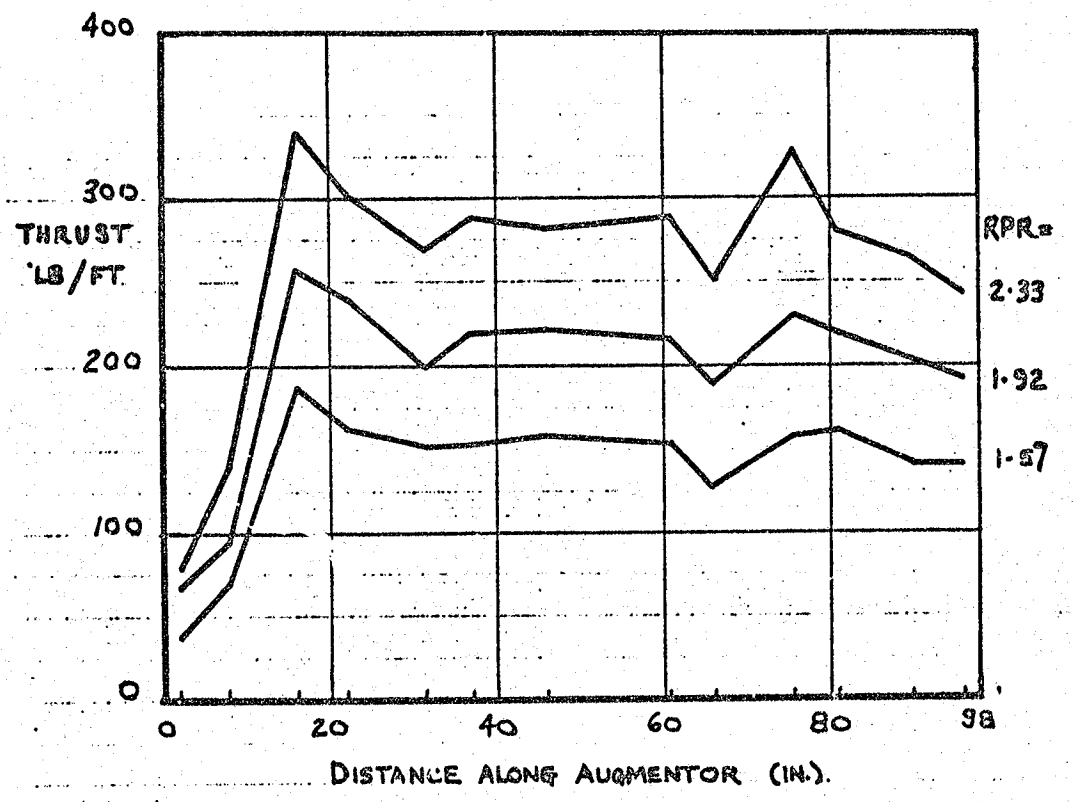

EFFECT OF FORWARD SPEED ON AUGMENTOR EXIT

THRUST DISTRIBUTION: DAR = 1.6: RPR = 2.3: $\alpha = 0^{\circ}$

$\delta_F = 0^{\circ}$

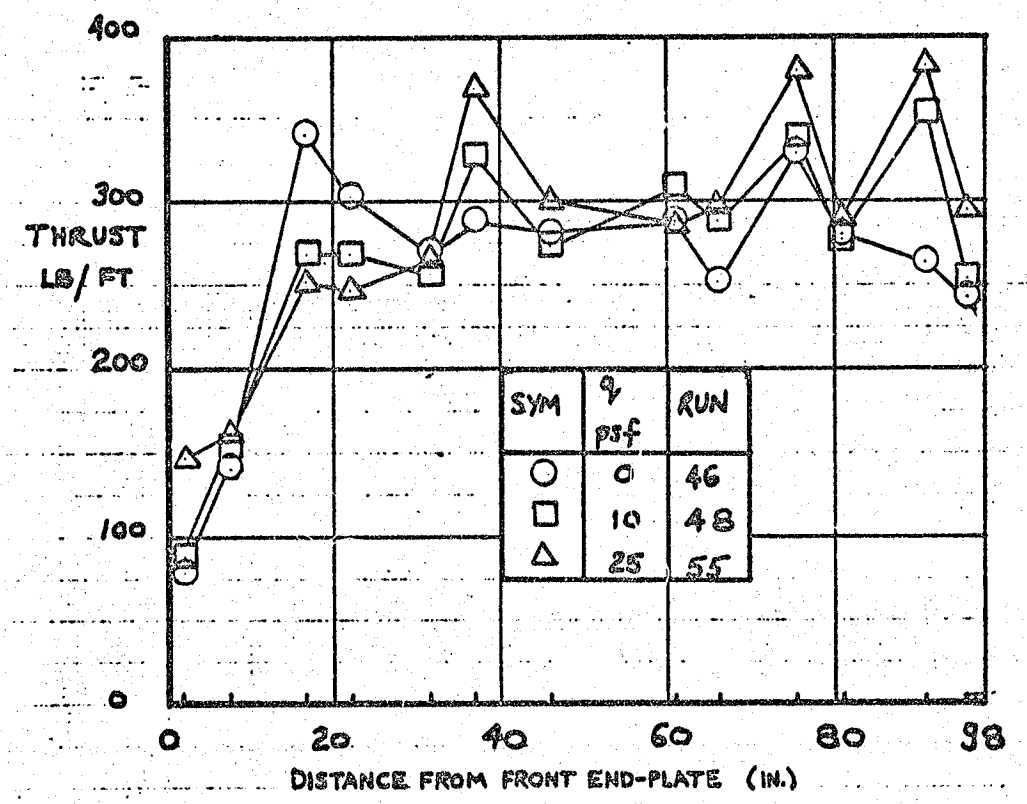

EFFECT OF FORWARD SPEED ON FUSELAGE AUGMENTOR EXIT VELOCITY DISTRIBUTION

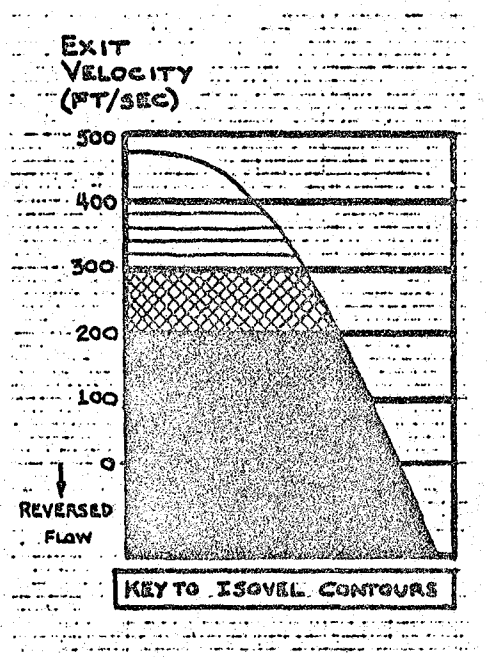

DAR = 1·6

RPR = 2·33

$\alpha = 0°$

$\delta_F = 0°$

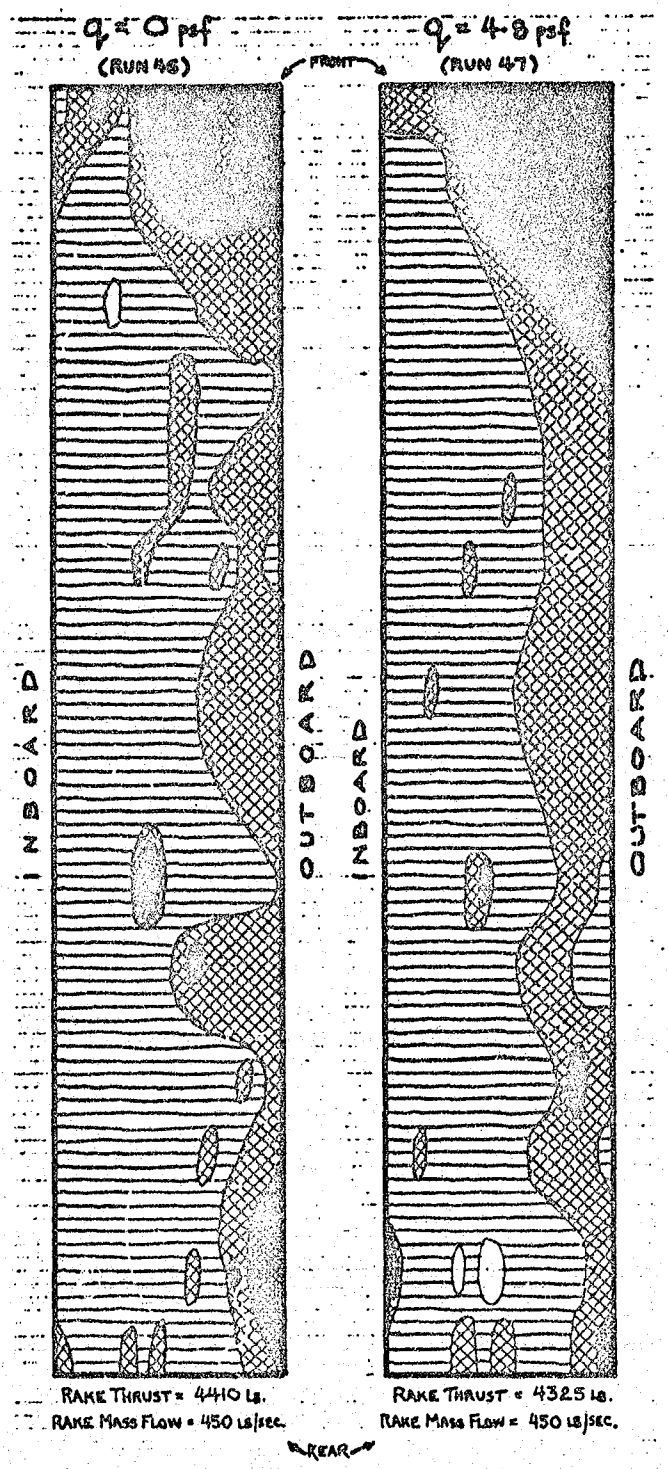

(LEFT AUGMENTOR VIEWED FROM BELOW)

Fig. 50(a)

DAR=1.6; α=0°; δ_F=0°; RPR=2.3

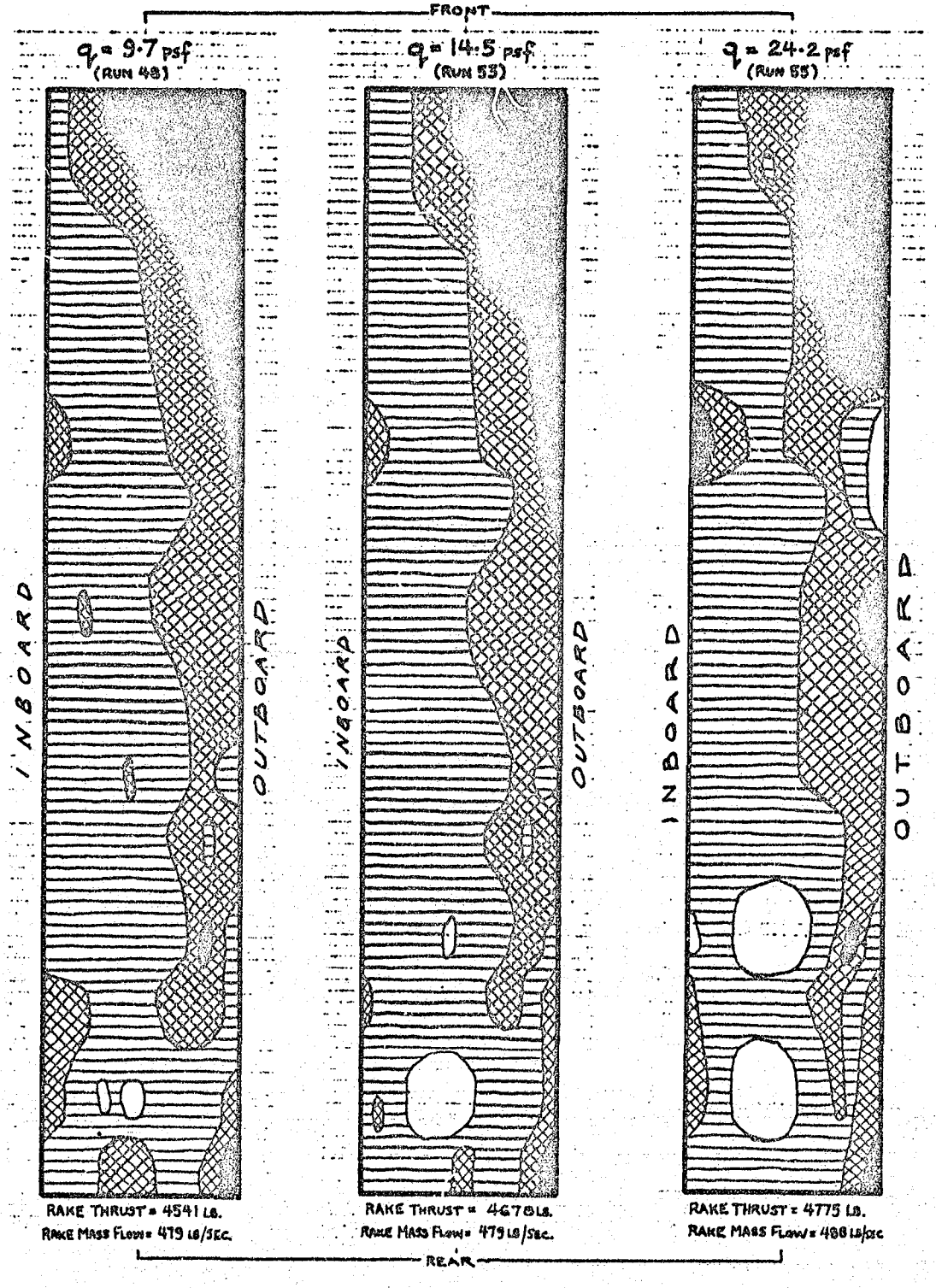

(LEFT AUGMENTOR VIEWED FROM BELOW)

EFFECT OF FORWARD SPEED ON RAKE THRUST AND MASS FLOW

$\alpha = 0°$ DAR = 1·6 RPR = 2·3

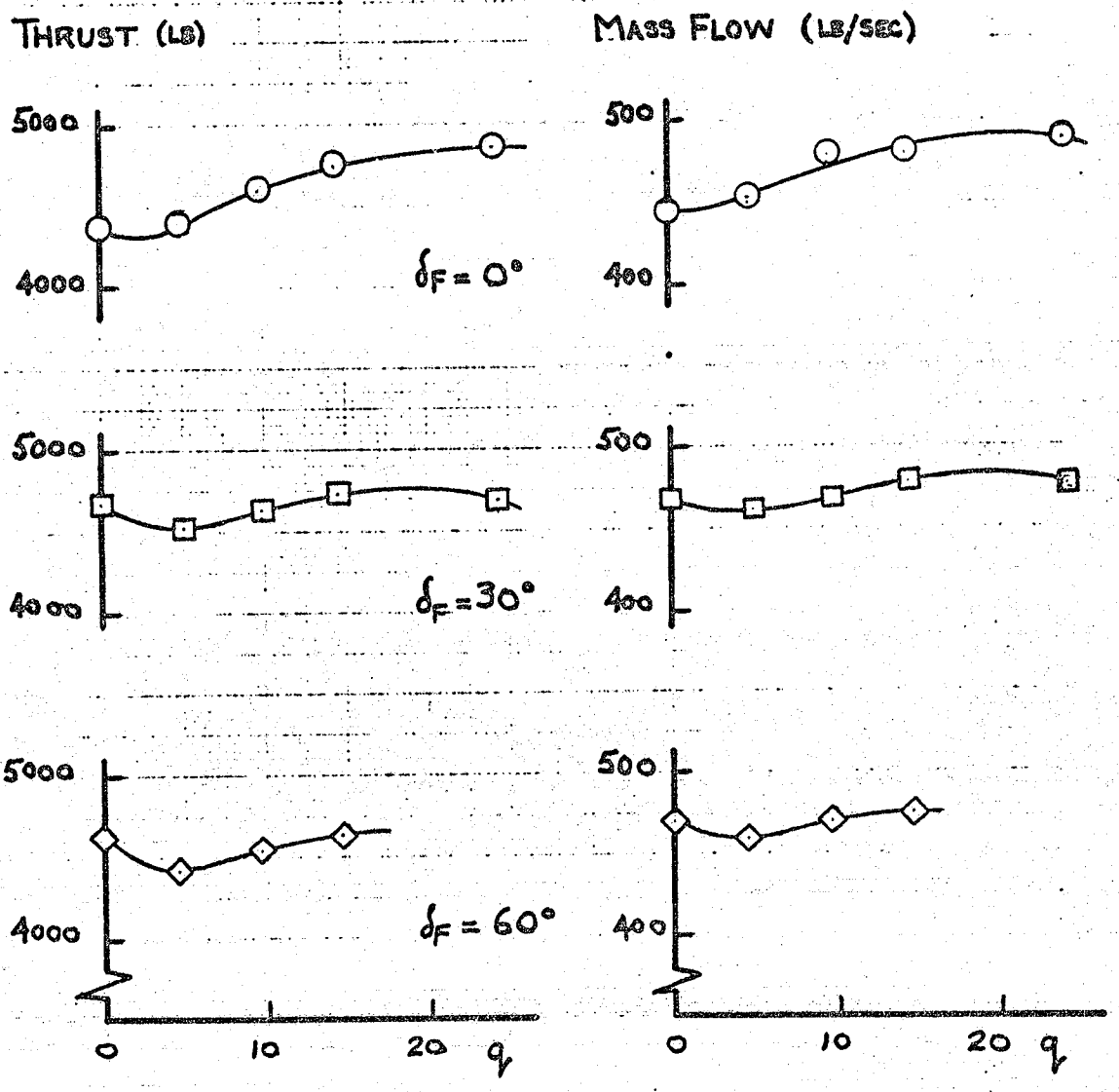

EFFECT OF ANGLE OF ATTACK ON RAKE THRUST

$\delta_F = 0°$; DAR = 1·6 ; RPR = 2·3

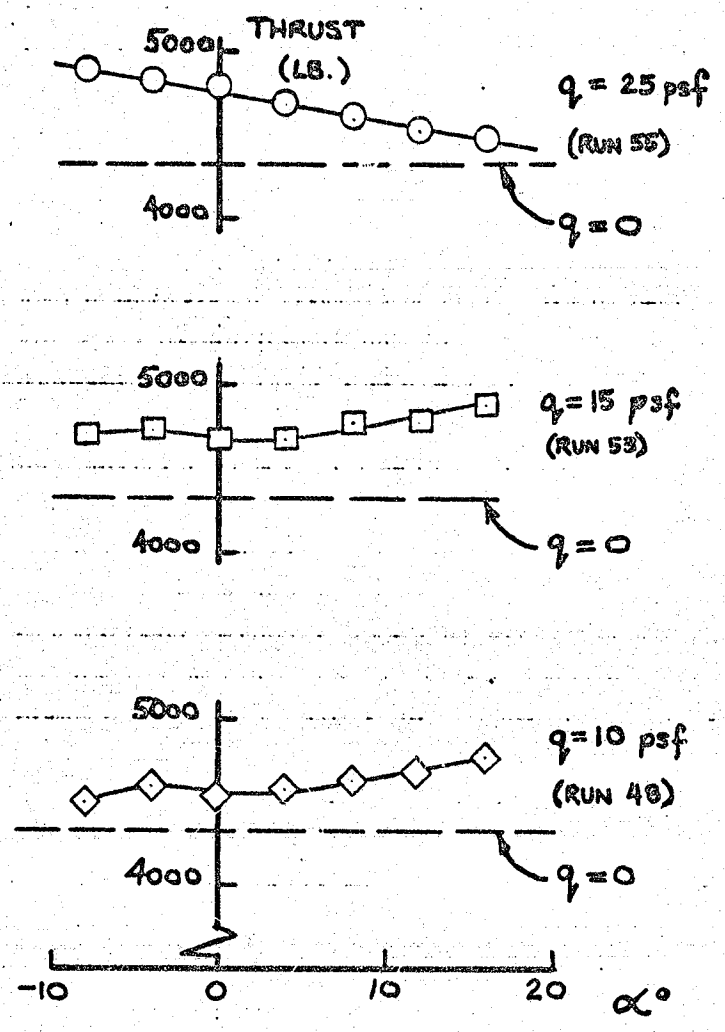

Fig. 53

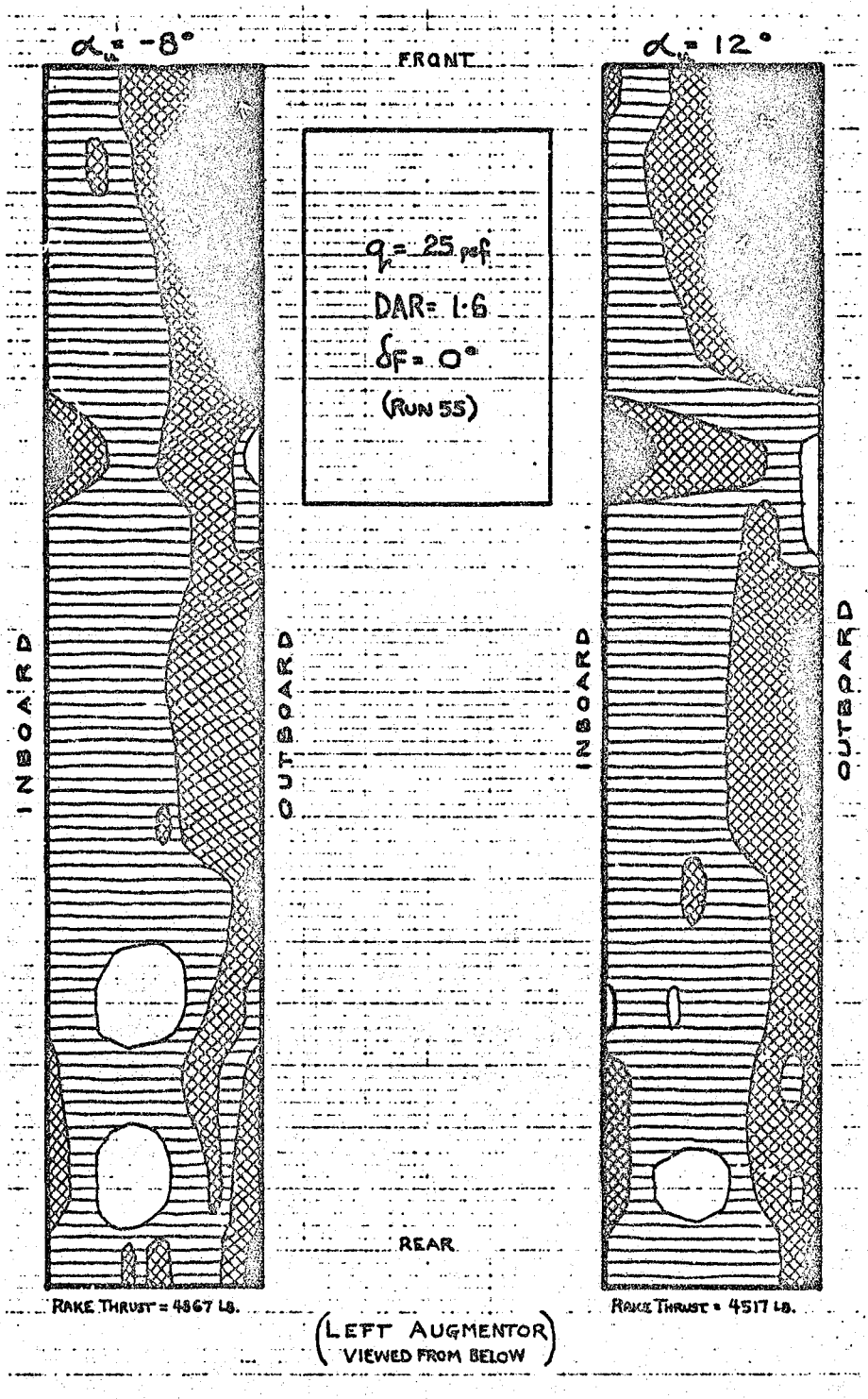

EFFECT OF ANGLE OF ATTACK ON FUSELAGE AUGMENTOR EXIT VELOCITY DISTRIBUTION

Fig. 54

EFFECT OF FORWARD SPEED ON FUSELAGE AUGMENTOR EXIT RAKE THRUST

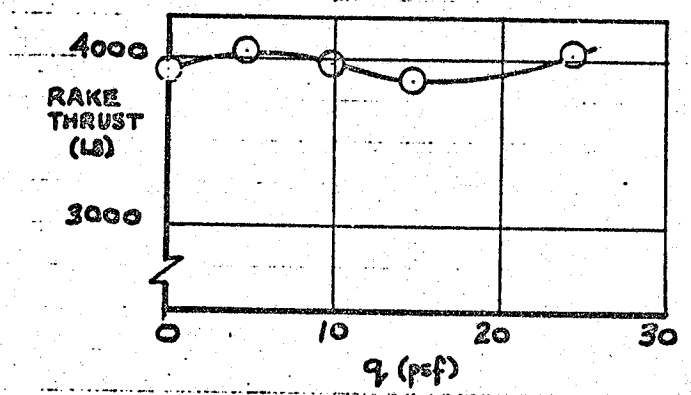

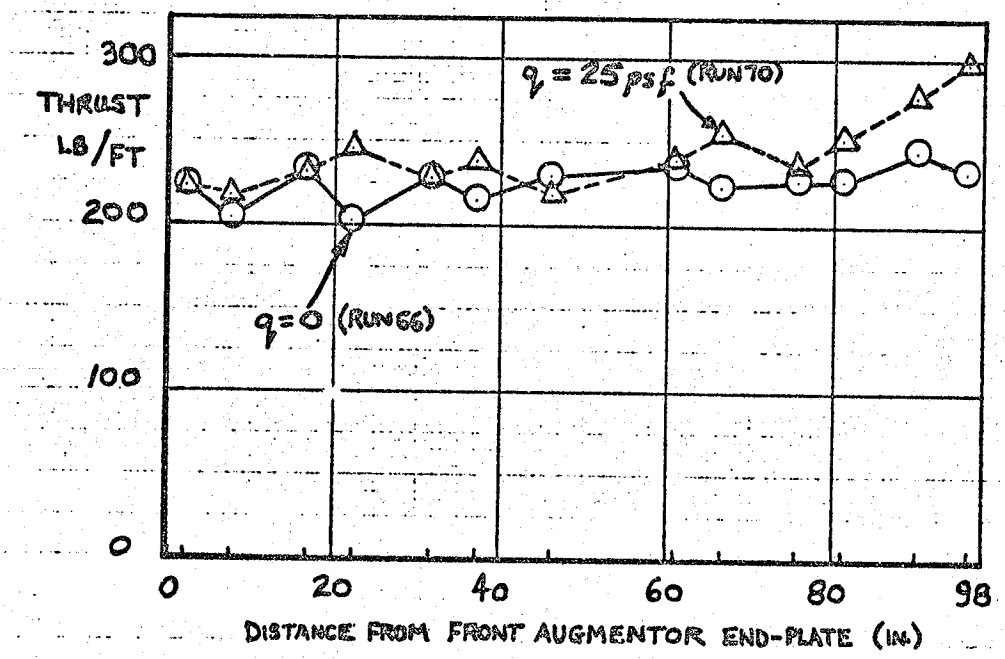

Fig. 55

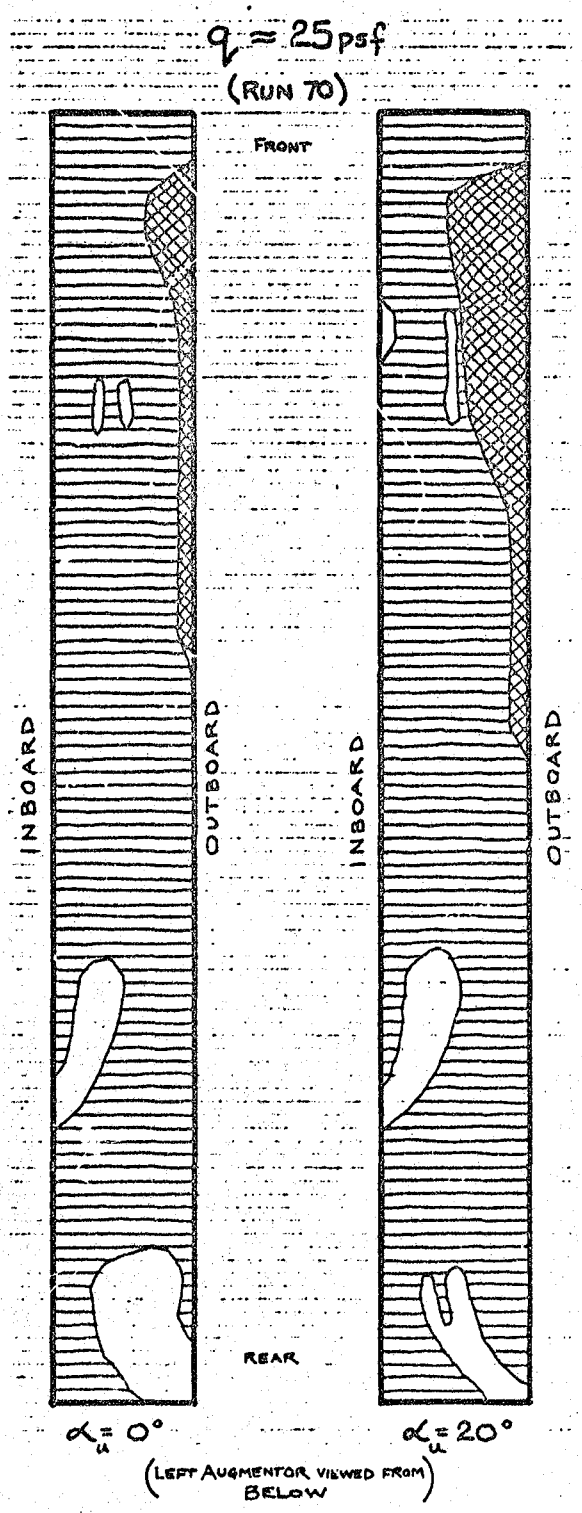

FUSELAGE AUGMENTOR EXIT VELOCITY CONTOURS: DAR = 1.0

END

DATE

FILMED

SEP 19 1980